Rat organic cation transporter 1 (rOCT1): investigation of conformational changes and ligand binding

Dissertation zur Erlangung des

naturwissenschaftlichen Doktorgrades

der Bayerischen Julius-Maximilians-Universität Würzburg

vorgelegt von

Dmitry Gorbunov

aus Tokmak, Kyrgyzstan, UdSSR

Würzburg, 2008

Eingereicht am: .....

Mitglieder der Promotionskommission:

Vorsitzender: .....

Gutachter : ... .Prof. Dr. Hermann Koepsell

Gutachter:.....Prof. Dr. Rainer Hedrich

Tag des Promotionskolloquiums: .....

Doktorurkunde ausgehändigt am: .....

TABLE OF CONTENTS

1. Introduction

1.1. The SLC22 family of membrane transporters

Polyspecific organic cation transporter rOCT1 from rat kidney was identified in our laboratory in 1994 (Gründemann et al., 1994). Subsequent expression cloning of further family members revealed that rOCT1 was the first prototypical member of a new transporter family, the solute carrier family 22 (SLC22).

SLC22 is a large family of organic ion transporters that belongs to the major facilitator superfamily (MFS) (Koepsell et al., 2003). MFS is one of the two largest groups of membrane transporters comprising uniporters, symporters, and antiporters from mammals, lower eukaryotes, bacteria, and plants (Pao et al., 1998); another large superfamily is the ABC (ATP-binding cassette) superfamily comprised of primary active transporters driven by phosphate-bond hydrolysis of ATP (Schinkel and Jonker, 2003). Transporters are grouped according to phylogeny and function similarity (primary or secondary active transporters, facilitative diffusers, etc) (Saier M., 2000).

Most transporters of SLC22 are polyspecific, i.e. they translocate multiple substrates of different sizes and with different molecular structures, and various ligands can act as inhibitors; at that, the transporters exhibit large variations in affinity and transport efficiency for different compounds (Anzai et al., 2006; Koepsell et al., 2007; Nigam et al., 2007; Rizwan and Burckhardt, 2007). Since many of these transporters are highly expressed in intestine, liver and kidney, the SLC22 family plays a pivotal role in absorption and excretion of drugs, xenobiotics, and endogeneous compounds (Wright and Dantzler, 2004; Koepsell, 2004; Sekine et al., 2006; Koepsell et al., 2007). They also play a role in the maintenance of homeostasis in brain, lung, heart, and other organs (Zwart et al., 2001; Schneider et al., 2005; Lips et al., 2007; Taubert et al., 2007).

The name of the family *"SLC22"* originates from the official gene symbol assigned by the "Human Genome Nomenclature Committee" (Koepsell et al., 2003; Koepsell and Endou, 2004). Traditionally, functionally characterized mammalian transporters have been divided into three subgroups according to the preferential substrate selectivity and phylogenetic similarity (Koepsell et al., 2003; Koepsell and Endou, 2004; Burckhardt and Wolff, 2000). The first subgroup, the passive diffusion organic cation transporters (OCTs), consists of OCT1 (SLC22A1), OCT2 (SLC22A2) and OCT3 (SLC22A3). Transporters of the second subgroup, the organic cation/zwitterion transporters (OCTNs), operate as Na^+-

independent transporters of organic cations or Na^+-zwitterion cotransporters. This subgroup consists of Na^+-ergothioneine cotransporter OCTN1 (SLC22A4) which is also capable to transport carnitine and may be a proton-organic cation exchanger; Na^+-carnitine cotransporter OCTN2 (SLC22A5) that can also operate as Na^+ independent transporter for organic cations; a mouse-specific transporter mOCTN3 (mouse Slc22a21), and carnitine and cation transporter OCT6 or CT2 (SLC22A16). The subgroup of organic anion transporters (OATs) contains OAT1-3 (SLC22A6-8), human OAT4 (SLC22A11), urate transporter URAT1 (SLC22A12), rodent OAT5 (Slc22a19) and OAT6 (Slc22a20); most OATs operate as anion exchangers which couple efflux of intracellular dicarboxilates (e.g. α-ketoglutarate, lactate) with uptake of organic anions into the cell.

A number of potential members of the family including invertebrate (fly and worm) homologs were isolated by comprehensive search through gene databases (Eraly et al., 2004; Jacobsson et al., 2007). In vertebrates, similarity between orthologs is higher than between paralogs, whereas there is considerable difference between vertebrate and invertebrate homologs at both proteine sequence and gene structure levels. It was suggested that OCT, OCTN, and OAT genes emerged after the divergence of vertebrates and invertebrates (Eraly et al., 2004).

Phylogenetic analysis of known mammalian members shows that transporters are clustered into six subgroups: three of them are OCTs, OCTNs and OATs, and others have yet unknown substrate specificities (Fig. 1) (Jacobsson et al., 2007). Considering that closely related transporters also demonstrate at least partially overlapping substrate specificities, uncharacterized members that cluster with transporters of established biochemistry can be organic cation or anion transporters.

In general, genes encoding SLC22 members of the same subgroup are localized on the same chromosome; in particular, those that are most phylogenetically related are localized on the same chromosomal band: in human, OCT1-3 are localized on chromosome 6q25.3, OCTN1-2 on 5q23.3, and OATs mainly on 11q12.3-11q13.1 (Koepsell et al., 2003; Eraly et al., 2003). It has been shown that majority of genes of the SLC22 members occur in pairs, or cluster with such a pair (Eraly et al., 2003). The phenomenon of transporter gene pairing is relatively specific to vertebrate Slc22 family; it is suggested that such pairing can facilitate coregulation (Eraly et al., 2004).

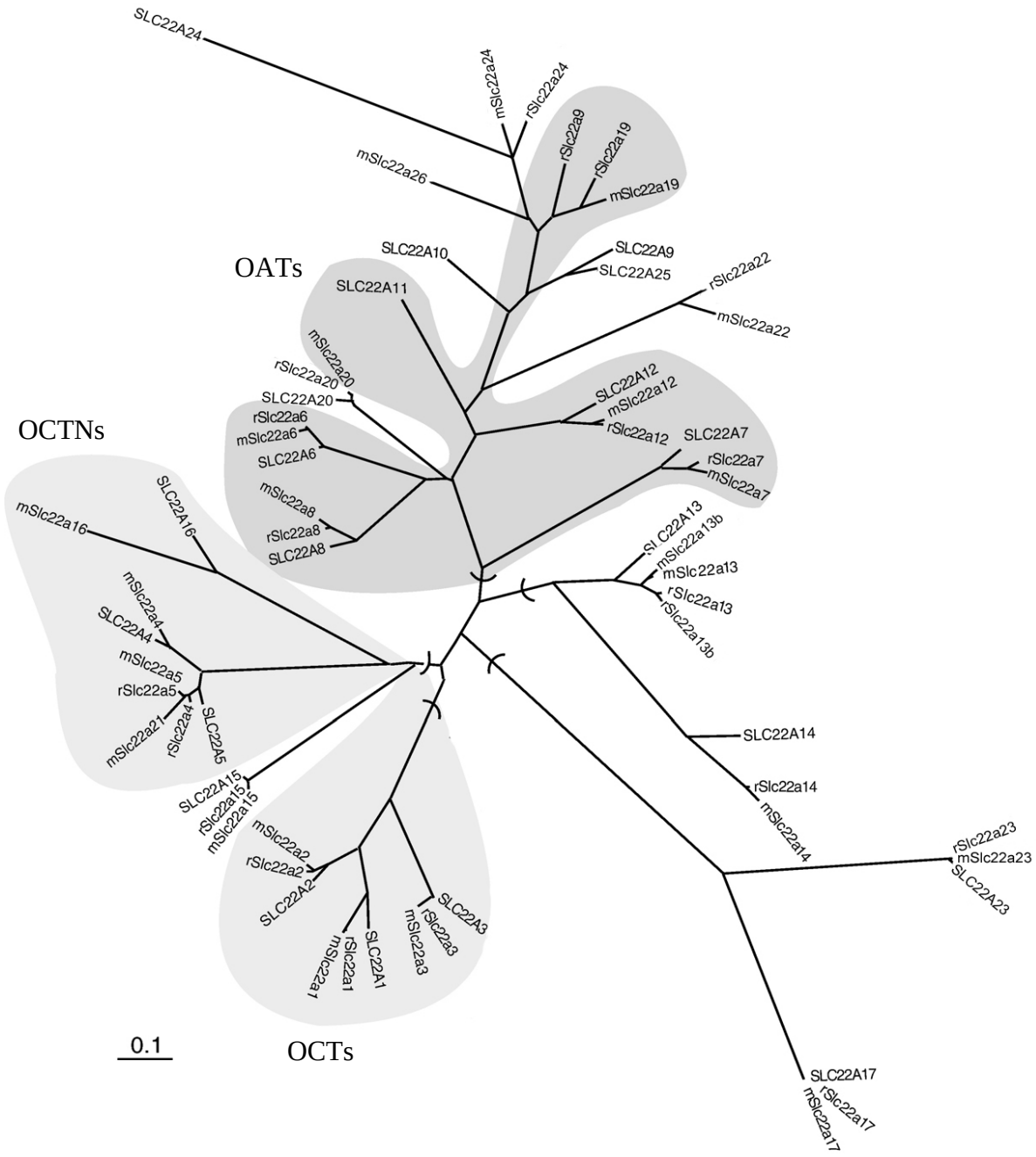

Figure 1. Phylogenetic tree of known human, mouse, and rat SLC22 members (*adapted from: Jacobsson et al., 2007*). Distance along the branches is inversely related to the degree of sequence identity. The prefixes *m* and *r* correspond to mouse and rat members. Members of the SLC22 family with known ligands are marked with shadings, anion transporters with dark gray and cation transporters with light gray.

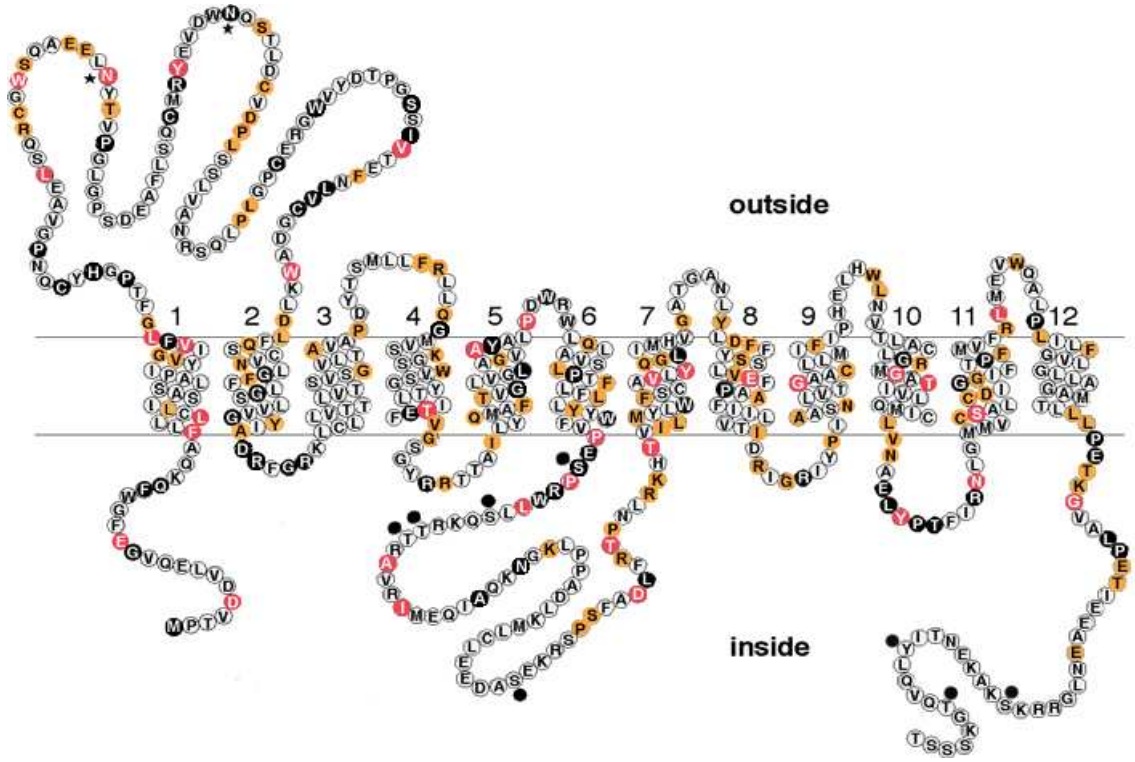

Figure 2. The rat organic cation transporter rOCT1: amino acid sequence and predicted secondary structure. Amino acids (a.a.) that are conserved in particular subfamilies of the SLC22 transporter family are color-coded as follows: black, a.a. conserved in all members of the SLC22 family; red, a.a. conserved only in the mammalian organic cation transporters OCT1/OCT2/OCT3 and OCTN1/OCTN2/mOCTN3; orange, a.a. conserved only in the electrogenic mammalian cation transporters OCT1/OCT2/OCT3. Consensus phosphorylation and N-glycosylation sites are indicated with black circles or asterisks, respectively.

Transporters of the SLC22 family have a similar predicted membrane topology (Fig. 2 and Fig. 3). With the exception of splice variants (Zhang et al., 1997; Urakami et al., 2002; Bahn et al., 2004) and some potential proteins identified through search in gene databases (Jacobsson et al., 2007), these transporters are approximately 550 amino acids long and consist of 12 transmembrane α-helices (TMHs), an intracellular N-terminus, a long glycosylated extracellular loop between TMHs 1 and 2, a long intracellular loop with consensus phosphorylation sites between TMHs 6 and 7, and an intracellular C-terminus (Gründemann et al., 1994; Meyer-Wentrup et al., 1998; Tanaka et al., 2004; Ciarimboli and

Schlatter, 2005; Zhou et al., 2005; Pelis et al., 2006; Hong M., 2007; Zhou and You, 2007; Keller et al., 2008).

1.2. Expression and function of OCTs

Polyspecific organic cation transporters of the SLC22 family play an important role in secretion and reabsorption of organic cations, and particularly xenobiotics, in kidney and liver (Koepsell et al., 2003; Wright and Dantzler, 2004; Wright, 2005; Koepsell et al., 2007). In other organs, OCTs and OCTNs are supposed to be involved into the transport of neurotransmitters and metabolites (Schömig et al., 2007; Amphoux et al., 2005; Lips et al., 2005). OCTs play an essential role in maintenance of homeostasis in the body since a variety of structurally different organic cations can act as transported substrates or nontransported inhibitors (Schömig et al., 2006; Koepsell et al., 2007).

OCT1 exhibits a broad tissue distribution; it is expressed in epithelial cells and in some neurons (Koepsell et al., 2007). Human OCT1 is most strongly expressed in the liver (Gorboulev et al., 1997; Zhang et al., 1997), whereas rodent OCT1 is strongly expressed in liver, kidney, and small intestine (Meyer-Wentrup et al., 1998; Karbach et al., 2000; Sugawara-Yokoo et al., 2000; Chen et al., 2001). In human and rodents OCT1 was also detected in skin, airway epithelia, skeletal muscles, heart, brain, in tumor cells, and basophilic granulocytes (Hayer-Zillingen et al., 2002; Slitt et al., 2002; Choudhuri et al., 2003; Augustine et al., 2005; Lips et al., 2005; Müller et al., 2005; Koepsell et al., 2007). Mouse OCT1 was found in the basolateral membrane of enterocytes (Chen et al., 2001), rat OCT1 was located to the basolateral membrane of epithelial cells in the S1 and S2 segments of proximal tubules (Karbach et al., 2000; Sugawara-Yokoo et al., 2000). At variance, in the trachea and bronchi of human, rat and mouse, OCT1 is located in the luminal membrane of epithelial cells (Lips et al., 2005; Kummer et al., 2006).

OCT2 is most strongly expressed in kidney (Okuda et al., 1996; Gorboulev et al., 1997). Similar to OCT1, OCT2 is expressed in epithelial cells and neurons but also in a variety of other organs including small intestine, lung, skin, and brain (Busch et al., 1998; Sweet et al., 2001; Slitt et al., 2002; Choudhuri et al., 2003; Augustine et al., 2005; Lips et al., 2005; Alnouti et al., 2006; Koepsell et al., 2007). In human kidney OCT2 is expressed in all three segments of proximal tubules (Motohashi et al., 2002), whereas in rat kidney OCT2 is located in the S2 and S3 segments (Karbach et al., 2000; Sugawara-Yokoo et al., 2000). Similar to OCT1, OCT2 was localized to the basolateral membrane of epithelial cells in renal

proximal tubules and small intestine and to the luminal membrane of epithelial cells in trachea and bronchi (Karbach et al., 2000; Sugawara-Yokoo et al., 2000; Motohashi et al., 2002; Lips et al., 2005).

The tissue expression pattern of OCT3 is very broad. At variance to OCT1 and OCT2, OCT3 is strongly expressed not only in epithelial cells and neurons but also in muscle cells and glial cells (Kristufek et al., 2002; Inauzi et al., 2003; Shang et al., 2003; Haag et al., 2004; Kummer et al., 2006; Seithel et al., 2006). In human, the strongest expression was found in skeletal muscle, liver, placenta and heart; however, OCT3 is also expressed in many other organs including kidney, intestine, brain, and placenta (Gründemann et al., 1998; Wu et al., 1998; Hayer-Zillingen et al., 2002; Müller et al., 2005; Wu et al., 2004; Sata et al., 2005). OCT3 protein was localized to the basolateral membrane of the trophoblast in placenta (Sata et al., 2005), and to the luminal membranes of bronchial epithelial cells and small intestinal enterocytes (Lips et al., 2005; Müller et al., 2005).

1.3. Substrate translocation mechanism and binding pocket of OCTs

OCTs translocate a variety of organic cations in an electrogenic manner. Electrogenicity of transport has been shown for the rat transporters rOCT1, rOCT2, and rOCT3 (Gründemann et al., 1994; Busch et al. 1996; Nagel et al. 1997; Kekuda et al. 1998; Okuda et al. 1999; Budimann et al., 2000; Arndt et al. 2001), for the human transporters hOCT1 and hOCT2 (Gorboulev et al. 1997; Busch et al. 1998; Dresser et al. 2000), and rabbit transporters rbOCT1 (Dresser et al., 2000). Transport of organic cations is not coupled to translocation of Na^+, Cl^-, or H^+; it is driven solely by membrane potential and concentration gradient of the organic cations (Busch et al. 1996; Gorboulev et al. 1997; Kekuda et al. 1998; Sweet and Pritchard, 1999; Budimann et al., 2000; Arndt et al., 2001; Keller et al., 2005; Schmitt and Koepsell, 2005; Keller et al, 2008). OCTs are able to translocate cations across the plasma membrane in either direction: in addition to cation influx, cation efflux has been demonstrated for rOCT1, rOCT2, hOCT2, rOCT3, and hOCT3 (Busch et al. 1996; Nagel et al. 1997; Busch et al., 1998; Kekuda et al. 1998; Budimann et al., 2000; Arndt et al., 2001; Lips et al., 2005; Keller et al., 2005).

Experimental data obtained for rOCT1 and rOCT2 suggest a carrier-type transport mechanism with binding site alternatively accessible to intra- or extracellular side. It was found that affinity for transported substrates as well as nontransported inhibitors can be different from intracellular or extracellular side, and point muations within presumed binding

pocket may have different effect on affinity at both sides of the membrane (Koepsell et al., 2003; Volk et al., 2003; C. Volk, V. Gorboulev, and H. Koepsell, unpublished data). Alternating access mechanism is supported by the demonstration of *trans*-stimulation of substrate uptake by translocated substrates for purified rOCT1 and rOCT2 reconstituted in liposomes (Keller et al., 2005; Keller et al., 2008). A carrier-type transport is also compatible with the steep temperature dependence of the substrate-induced currents in rOCT2 (Schmitt and Koepsell, 2005).

Intensive studies of ligand binding to OCTs have led to the development of the concept of a large binding pocket containing partially overlapping substrate binding sites (Koepsell et al., 2005). It explains observations of differential effect of mutations on affinities to different substrates and deviations from pure competitive interaction for some pairs of ligands (Koepsell et al., 2003; Koepsell et al., 2007). Furthermore, the same concept can be applied to explain different affinities toward some substrates or inhibitors in different subtypes of OCTs. However, it does not concern the substrate selectivity of transport. In a particularly interesting study of rOCT2, authors implemented a pore-like selectivity filter bearing negative charge ascribing to it the transport-governing function (Schmitt and Koepsell, 2005). In this term, transporter contains central cavity and vestibule, opening alternatively to each side of the membrane. Only ligands which are able to fit inside the central cavity are transported inasmuch as they do not hinder the transition to a conformation that lets them dissociate at the opposite membrane face. The narrowest part of the pore was estimated as ~4 Å, which fits to the size of known rOCT2 substrates (molecular mass below 200, diameter between ~2.5-4 Å) (Schmitt and Koepsell, 2005). Such model can also explain why mutations of selected amino acids located in the presumed binding pocket cause significant effect on affinity at one side of the membrane without any considerable effect at another side (C. Volk, V. Gorboulev, and H. Koepsell, unpublished data).

Systematic studies of interactions of various ligands with OCTs have led to generation of pharmacophores for hOCT1 (Bednarczyk et al., 2003; Moaddel et al., 2007), hOCT2 and rbOCT2 (Suhre et al., 2005). Importantly, these studies were performed by measuring inhibition of tetraethylammonium (TEA) uptake into stably transfected cells (Bednarczyk et al., 2003; Suhre et al., 2005), or displacement of 1-methyl-4-phenylpyridinium (MPP) bound to membranes prepared from stably transfected cells (Moaddel et al., 2007). Thus, these studies revealed determinants for binding leaving out the question how binding is linked to the transport. Besides, taking into account considerations of a large binding pocket and mechanism of transport, the developed pharmacophores rather

describe a hypothetical binding site with mixed properties of inward- and outward-oriented conformations. Nevertheless, despite the inherent uncertainties, the models provide an insight into the structural features of the binding pocket. In general, models share similar structure featuring a positive ion interaction site, a hydrogen-bond acceptor site (for hOCT1, two sites were suggested (Moaddel et al., 2007)), and a hydrophobic interaction site. The models suggest an importance of structural features in selected regions (e.g., at hydrogen-bond acceptor site) and the tolerance of the transporter binding site with respect to steric bulk in other regions (e.g., at hydrophobic site), although to a different extent for different transporters (Suhre et al., 2005). Considering these findings along with high sequence similarity between OCT orthologs (~90%) and marked difference between affinities of some compounds to different OCTs, it suggests that quite moderate differences in the amino acid residues composition of a protein can result in substantial changes in affinity of the respective transporters for some ligands, having no effect on the interaction with other ligands. It is also consistent with the idea of multiple but partially overlapping binding sites within one binding pocket.

These conclusions are corroborated by other experimental data. Mutational analysis revealed aspartate at position 475 in TMH 11 of rOCT1 as an important determinant of substrate binding (Gorboulev et al., 1999). Negative charge at this position is essential for active transporter since only substitution to glutamate was acceptable, although significantly reducing transport rate. The mutant D475E exhibited 4-15 times higher apparent affinities to N-methylnicotinamide and tetraalkylammonium compounds (choline, tetraethyl- , tetrabuthyl- , and tetrapenthylammonium), whereas affinity to MPP was not changed. Thus, this mutation changed the substrate selectivity of the transporter.

Aspartate at this position is conserved in OCTs, whereas OCTNs and OATs carry an arginine in this position. Point mutations of the arginine residues in the organic anion transporters OAT1 from flounder (fOAT1), OAT3 from rat (rOAT3), and hOAT1 that correspond to D475 in rOCT1 also produced specific functional changes (Feng et al. 2001; Wolff et al. 2001; Rizwan et al., 2007). In fOAT1, the mutation R478D decreased affinity and maximal transport rate for *para*-aminohippurate (PAH) and abolished interaction with glutarate (Wolff et al. 2001). Similarly, in hOAT1 replacement R466D but not R466K abolished interaction with glutarate, whereas substitution R466K significantly decreased transport of PAH (Rizwan et al., 2007). In rOAT3, the mutations R454D significantly reduced transport of the anions PAH, estrone sulfate, and ochratoxin A retaining ability to transport a weak base cimetidine (Feng et al. 2001). Interestingly, fractional protonation of cimetidine

(pKa 6.92) at physiological pH should be considerable; moreover, cimetidine was shown to be a substrate for OCTs, which efficiency of interaction with hOCT2 strongly depends on degree of ionization (Barendt and Wright, 2002). Thus, it is possible that cimetidine is transported by R464D mutant in nonprotonated form and/or protonated form, whereas wildtype rOAT3 accepts mainly (or solely) nonprotonated cimetidine.

Other data suggest that TMH 8 may also belong to the substrate binding pocket in transporters of the SLC22 family. The mutation of conserved in OATs lysine 370 in rOAT3 to alanine (amino acid residue which is located at corresponding position in OCT1-2) changed substrate selectivity: for example, uptake of PAH, estrone sulfate, and ochratoxin A was reduced to a considerably higher extent than the uptake of cimetidine (Feng et al. 2001). Moreover, double mutant K370A/R454D of rOAT3 could transport not only cimetidine but also an organic cation MPP. An effective inhibition of MPP or cimetedin uptake in the double mutant could be induced by bulky organic cations and anions (TBuA, verapamil, estrone sulfate) but not by small organic ions (tetramethylammonium, TEA, choline, PAH). It suggests that the mutations have strongest effect on the interaction of the transporter with small organic ions where ionic interactions should be predominant, whereas bulkier organic cations and anions might interact with transporter due to hydrophobic and/or hydrogen-bond interactions. Thus, conserved aspartate of TMH 11 in OCTs, arginine of TMH 11 and lysine of TMH 8 in OATs, may serve to recognize a positive or negative organic ion. Whether and how these amino acid residues are involved into the translocation through the membrane is not clear.

Experimental data suggest that TMH 10 is also involved into the binding. When L447 and G448 of rOCT1 were replaced by corresponding amino acids of rOCT2, L447Y and G448E, respectively, K_i of corticosterone for inhibition of TEA uptake increased more than 10 times and resembled the value for rOCT2 (Gorboulev et al., 2005). The involvement of amino acid at position 448 in binding is supported by the study of rabbit OCT1 and OCT2, which showed that exchange G448E in OCT1 also shifted transporter properties to OCT2-specific phenotype (Zhang et al., 2005). However, those experiments could not distinguish between inhibition from extra- or intracellular side. Recent data from our laboratory show that mutation at position 448 has extremely distinct effect on affinity of corticosterone from different sides of the membrane, increasing K_i value 26-fold for intracellular corticosterone, while leaving it unchanged from extracellular side. In contrast, substitution L447Y increased K_i from both extra- and intracellular sides 2.5- and 5.6-fold, respectively (C. Volk, V.

Gorboulev, and H. Koepsell, unpublished data). These findings support suggested structure of the binding pocket and alternating-access mechanism.

Finally, data from our laboratory suggest an involvement of TMH 4 in substrate recognition (Popp et al., 2005). Eighteen amino acids in the fourth transmembrane helix of rOCT1 were mutated. Among them, replacements of conserved in OCTs residues W218Y and Y222L increased affinity for both TEA and MPP, whereas the T226A mutant (threonine at this position is conserved in OCTs) had a higher affinity only for MPP.

The experimental data of mutational analysis support structural models of OCTs. Homology modeling of rOCT1 (Popp et al., 2005) and rbOCT2 (Zhang et al., 2005) were performed using as template crystal structure of LacY (Abramson et al., 2003) or GlpT (Huang et al., 2003), respectively, in inward-open conformations. Both models are very similar (Zhang et al., 2005). Indeed, homology modeling of MFS transporters is not pure speculative since crystallization of several members of the MFS superfamily showed very strict structural similarity between transporters despite moderate or low sequence similarity, different substrate specificities and mechanisms of function (uniporters, antiporters, cotransporters, or echangers) (Vardy et al., 2004; Lemieux M., 2007). The models show a large cleft formed by eight transmembrane helices; amino acid residues that have been assigned to the substrate binding region are located within the cleft (Fig. 3). The size of the cleft supports the idea of partially overlapping binding sites and suggests that more than one ligand molecule can bind to the transporter.

Two conserved cysteines of hOCT2, C474 and C451, were shown to be accessible for thiol-specific covalent modifiers applied from extracellular side (Pelis et al., 2006b; Pelis et al., 2007). According to the models, C474 is located in the middle of TMH 11 (next to D475) facing the cleft that is in agreement with accessibility of the cysteine for quite bulky maleimide-PEO-biotine. The covalent modification was inhibited by saturating concentrations of substrates or inhibitors. The data support the model and importance of TMH 11 for substrate recognition. At variance, C451 is located at the intracellular end of TMH 10, and was accessible to small $HgCl_2$ or MTSEA-biotine but not to maleimide-PEO-biotine, although rate of modification was apparently lower than in the case of C474. Interestingly, MTSEA-biotine is not only smaller than maleimide-PEO-biotine but also carries partial positive charge on MTSEA-moiety at physiological pH (Stauffer and Karlin, 1994). Thus, it is possible that it can accommodate to the substrate binding pocket of the transporter, stabilizing an inward-open conformation or some intermediate conformation when C451 becomes accessible to the reagent. The data suggest that C451 can be a part of the binding pocket. Indeed, recent data

from our laboratory indicate that C451 is critical for affinity to choline in rOCT1 and rOCT2 (Sturm et al., 2007).

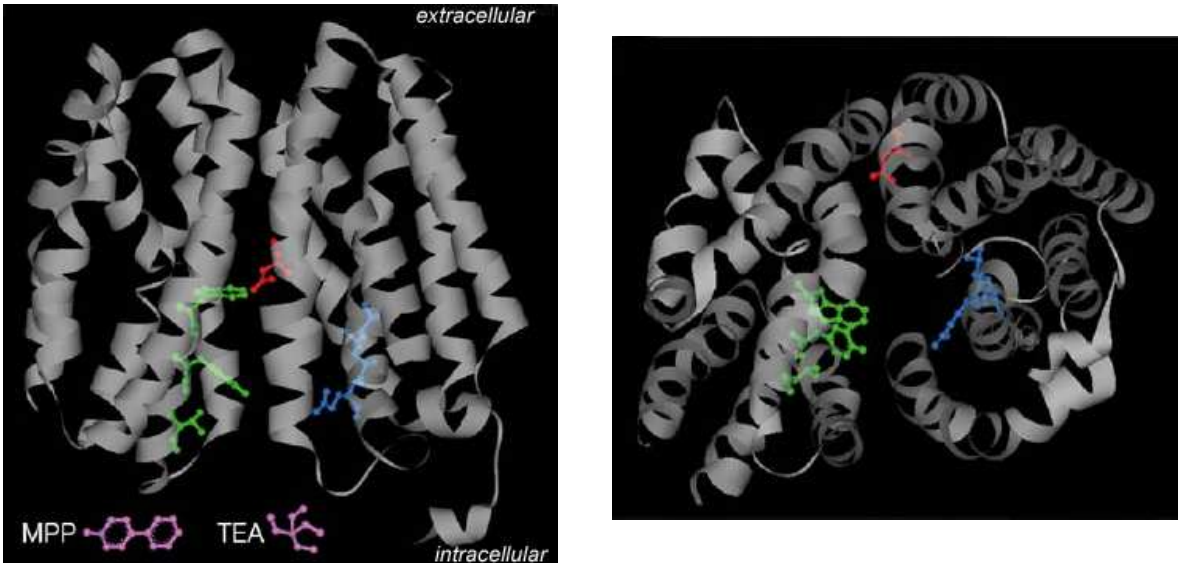

Figure 3. Model of the inward-facing conformation of rOCT1. Ribbon representations of the structural model of rOCT1 are presented. Long loops between TMHs 1-2 (extracellular) and TMHs 6-7 (intracellular) are not included into the model (Popp et al., 2005). ***Left panel***, side view; ***right panel***, view from intracellular. Amino acids that have been localized to the substrate binding region are depicted. Tryptophan 218, tyrosine 222, and threonine 226 of the TMH 4 are colored in green, alanine 443, leucine 447, and glutamine 448 of the TMH 10 are blue, and aspartate 475 of the TMH 11 is shown in red. The molecular structures of TEA and MPP are shown at the same scale.

Aims of the study

Biochemical and biophysical studies of organic cation transporters (OCTs) of the SLC22 family have revealed some important determinants of the binding pocket and suggested that these transporters employ alternating access as transport mechanism. However, the transport cycle and underlying conformational changes are still unsettled subjects. One of the reasons is low electrogenicity of the conformational changes in OCTs which make difficult to apply traditional electrophysiological approaches to study conformational changes in membrane transporters and channels. However, this problem can be overcome by use of conditionally sensitive optical or paramagnetic probes.

The aim of this study was to investigate conformational changes in rat OCT1. Our approach included site-directed labeling of the rat OCT1 with environmentally sensitive fluorophore tetramethylrhodamine-6-maleimide upon expression in Xenopus oocytes. After formation of a fluorescent sensor, it was used to monitor conformational changes of the transporter upon transport relevant conditions in living cells.

2. Materials and Methods

2.1. Materials

2.1.1. Chemicals

If not otherwise stated, all standard laboratory chemicals were of p.a. grade and purchased from AppliChem (Darmstadt, Germany), Fluka (Neu-Ulm, Germany), Merck (Darmstadt, Germany), Sigma-Aldrich (Taufkirchen, Germany), Roth (Karlsruhe, Germany), Serva (Heidelberg, Germany). Tetramethylrhodamine-6-maleimide was from Molecular Probes (Eugene, OR, USA).

2.1.2. Radioactive compounds

The following radiochemicals were purchased from Biotrend (Cologne, Germany): [^{14}C]-Tetraethylammonium bromide, specific activity 55mCi/mmol; [^{3}H]-1-Methyl-4-phenylpyridinium iodide, specific activity 85 Ci/mmol.

2.1.3. Enzymes, commercial buffers, molecular weight markers

Collagenase was from Sigma-Aldrich (Taufkirchen, Germany). *MluI* restriction endonuclease, R+ restriction buffer (10 mM Tris-HCl pH 8.5, 10 mM $MgCl_2$, 100 mM KCl, 0.1 mg/ml BSA), 10kb DNA-Ladder and RNA-Ladder were from Fermentas (St. Leon-Rot, Germany).

2.1.4. Kits

HiSpeed Midi Kit was purchased from Qiagen (Hilden, Germany). “mMESSAGE mMACHINE^{TM}” SP6 kit was from Ambion (Hundingdon, UK).

2.1.5. Bacterial strains

E.coli strain *DH10B* from Gibco BRL (Eggenstein, Germany) was used for selection and amplification of plasmids.

2.2. Methods

2.2.1. Molecular biology methods

2.2.1.1. Construction of vectors for expression of rat OCT1 mutants

Vectors encoding rat OCT1 and its mutants were generated by Dr. V. Gorboulev. All mutants were made on the basis of wild-type rOCT1 or a mutant 10ΔC (Sturm et al., 2007). In the latter construct, 10 of total 16 natural cysteine residues were replaced as follow: C26A, C155A, C417A, C322S, C358A, C418A, C437S, C451M, C470A, and C474A; six cysteines located in the large extracellular loop are crucial for the transporter and cannot be removed (Sturm et al., 2007). Single point mutations were introduced by use of polymerase chain reaction applying the overlap extension method (Ho et al., 1989). Mutants were cloned into the vector pRSSP (Busch et al., 1996) and PCR-derived parts of the mutant constructs were sequenced.

2.2.1.2. Preparation of cDNA

2.2.1.2.1. Analytical isolation of plasmid DNA

Individual colonies were picked and incubated in 1.5 ml of LB medium containing ampicillin 50 mg/l and grown overnight at 37^0C. Cells were precipitated by centrifugation and subjected to alkaline lysis with SDS. Bacterial DNA was separated from proteins by precipitation with isopropanol. Obtained clones were sequenced to approve the presence of mutation(s).

2.2.1.2.2. Preparative purification of plasmid DNA

Isolation of plasmid from *E. coli* was carried out using solutions and protocol of Qiagen. 50 ml overnight bacterial cultures were taken for plasmid isolation using the Hispeed Midi plasmid isolation kit (Qiagen, Hilden, Germany) according to the manufacturer's protocol.

2.2.1.2.3. Measurement of DNA concentration by spectrophotometry

DNA concentration was measured by absorbance at 260 nm using spectrophotometer Ultraspec3 (Pharmacia, Freiburg, Germany). Extinction coefficient of 0.05 mg/ml was used for calculations. Purity of DNA was estimated from the ratio of absorbancies

at 260 nm and 280 nm. The sample was considered to be free of protein contamination if the ratio was 1.7 - 2.0.

2.2.1.2.4. DNA gel electrophoresis

Samples containing 0.1 µg DNA were diluted in 4-fold gel-loading buffer (30% Glycerin, 0.25% Bromphenolblue) and subjected on 1% agarose gel containing 0.3 µg/ml ethidium bromide running in TAE buffer (40 mM Tris-Acetate, 1 mM EDTA, pH 8.0). Electrophoresis was run for 1 hour at 5 V/cm. DNA bands were visualized by illumination in UV light.

2.2.1.2.5. Linearization of plasmid

Linearization was carried out according to restrictase supplier's instructions (Fermentas, St. Leon-Rot, Germany). 10µg of plasmid DNA were digested with 15 units of restriction endonuclease *MluI* in 50 µl of R+ buffer (Fermentas) overnight at 37^0C. The completion of the digestion was controlled by the agarose gel electrophoresis. DNA was isolated by phenol/chloroform extraction and dissolved in 10 µl of RNase-free water. Concentration of DNA was determined by spectrophotometry.

2.2.1.2.6. Phenol/chloroform extraction of DNA

Extraction was carried out according to (Wallace D, 1987). 50 µl phenol/chloroform mixture (1:1 v/v) (Roth, Karlsruhe, Germany) was added to 10µg of DNA dissolved in 50µl of appropriate buffer. The tube was vortexed for 20 sec, centrifuged for 30 sec at room temperature at 10000g. The supernatant was decanted and DNA was precipitated by mixing with 3 volumes (150 µl) of ethanol and 1/10 volume (5 µl) of sodium acetate pH 5.0. Mixture was vortexed for 20 sec and kept at -20^0 C for 45 minutes. Afterwards, DNA was precipitated by centrifugation for 20 minutes at 4^0 C at 10000g. Supernatant was discarded; the pellet was washed with ice-cold 70% ethanol and centrifuged for 10 minutes at 4^0 C at 10000g. DNA pellet was air-dried and dissolved in 10 µl of RNase-free water (Ambion, Hundingdon, UK).

2.2.1.3. Preparation of cRNA

2.2.1.3.1. cRNA synthesis

m7G(5´)ppp(5´)G-capped cRNAs were prepared using the "mMESSAGE mMACHINE™" SP6 kit (Ambion, Hundingdon, UK) according to manufacturer's protocol.

20µl of reaction mixture contained 1µg linear template DNA, mixture of triphosphonucleotides, cap analogue, reaction buffer, and RNA polymerase. Reaction was carried out for 2 hours at 37^0C. Then the mixture was treated with DNAse I to remove the template DNA. Reaction was stopped and mRNA was precipitated with 2.8 M LiCl. Quality of the reaction and yield of cRNA was determined by agarose gel electrophoresis.

2.2.1.3.2. RNA gel electrophoresis

1µl of water solution containing 0.25 - 1µg RNA was mixed with 3µl loading buffer (71.4 % DMSO, 1.43 M glyoxal, 50 µg/ml ethidium bromide) and heated for 1 hour at 50°C to destroy secondary structure of RNA (McMaster and Carmichael, 1977). Samples were loaded on 1% agarose gel running in BES–buffer (10 mM BES, pH 6.7 and 0.1 mM EDTA). Electrophoresis was run for 1.5 hours at 5 V/cm. RNA bands were visualized by illumination in UV light. Amount of RNA in sample was estimated by comparison to RNA-ladder bands of known concentrations.

2.2.2. Expression and analysis of rOCT1 and its mutants in *Xenopus laevis* oocytes

2.2.2.1. Preparation of oocytes of *Xenopus laevis*

Maintenance, surgery of frogs and handling of oocytes were performed according to standard procedures (for example, see Weber 1999; Wagner et al., 2000).

Frogs were anesthetized in solution containing tricaine methanesulfonate and $NaHCO_3$ (1 g/l of each). The surgical site of the skin was rinsed with disinfection spray before the surgical incision had been made. Through a short abdominal incision (1-2 cm in length), small pieces of ovary were removed and placed in Ori−buffer (5mM MOPS-Na, pH 7.4, 100mM NaCl, 2mM KCl, 2mM $CaCl_2$, 1mM $MgCl_2$) . Muscle layer and skin were closed separately using a monofilament absorbable silk suture (Vomel, Kronberg, Germany). Frogs were allowed to recover in a separate tank filled with water before being returned to a common pool.

Ovaries were cut in small pieces by means of sharp scissors. Afterwards oocytes were washed with Ori until the solution became clear. Washed oocytes were subjected to the treatment with collagenase (1 mg/ml, 540 units) for overnight at 16^0C to remove follicular layer. Alternatively, digestion was performed for 3 hours at room temperature in the solution containing 2 mg/ml collagenase (1080 units). Both procedures gave similar results.

To stop the treatment and to facilitate separation of the cells, oocytes were repeatedly washed with Ori-buffer without calcium. Then oocytes were placed into standard Ori solution supplemented with 50 mg/l gentamicin and stored at 16^0C.

2.2.2.2. Injection of cRNA into oocytes

Oocytes of stage V-VI showing evenly colored poles and a sharp border between both poles were selected for experiments. Oocytes at these stages are best-suited for experiments involving expression of exogenous proteins since they reach maximal translational capabilities (Taylor and Smith, 1985a; Taylor et al., 1985b).

Borosilicate glass capillaries GB100-8P (Science Products GmbH, Hogheim, Germany) were pulled out using the micropipette puller P30 (Sutter instruments Co, Novato, CA, USA). The tip of capillary was broken manually under microscope using fine tweezers. The injection capillary was filled with mineral oil (Sigma 400-5 Heavy Weight Oil; Sigma) and injection was performed using the nanoliter injection pump (WPI, Berlin, Germany). The injection volume was 50 nl containing 10 ng of the respective cRNA per oocyte. This amount of cRNA is saturating for synthesis of exogenous proteins providing maximal translational velocity (Manniatis et al., 1976; Taylor et al., 1985b).

After injection, oocytes were stored in 6-well plates (7−10 eggs per well) at 16ºC. Before measurements, oocytes were incubated for 2 - 4 days at 16^oC in Ori buffer supplemented with 50 mg/l gentamicin. Buffer was exchanged for fresh Ori solution daily.

2.2.2.3. Two electrodes voltage-clamp (TEVC)

Experiments were performed using a feedback amplifier TEC-05 (NPI Electronic, Tamm, Germany) controlled by software PULSE and X-CHART (HEKA Electronics, Lambrecht, Germany). Amplifier and personal computer communicated via an analog-digital converter (ITC-16; Instrutech, Port Washington, NY). For measurements of steady-state currents, signals were filtered at 20 Hz, and for measurements of membrane capacitance at 20 kHz using a four-pole Bessel filter.

Oocyte of *Xenopus laevis* was placed in a small (~300µl), custom-made Teflon chamber and impaled with microelectrodes that were filled with 3 M KCl and had final resistances of 0.5–2.0 MΩ (current electrode) or 1–3 MΩ (potential electrode). Microelectrodes were pooled from borosilicate glass capillars GB150F-8P (Science Products GmbH, Hogheim, Germany) using puller PIP5 (HEKA Electronics, Lambrecht, Germany).

Silver wires for microelectrodes and ground wires were chlorided in 2 M KCl using a chloriding apparatus ACL-01 (NPI Electronic, Tamm, Germany). The external voltage electrode (reference electrode) was a commercial liquid reference half cell (DRIREF-2; WPI, Berlin, Germany). The chamber could be superfused continuously through a gravity-fed system. For quick solution changes, solutions were pipetted directly into the chamber.

2.2.2.4. Cystein-specific labeling of *Xenopus* oocytes with tetramethylrhodamine-6-maleimide (TMR6M)

Labeling was performed with mutants of rOCT1(10ΔCys) in which individual amino acid residues were replaced by cysteine. Cysteine-specific fluorescence labeling for epifluorescence measurements was achieved by incubating oocytes expressing these mutants for 5 min at room temperature in Ori buffer containing 5 µM of TMR6M if not otherwise stated, followed by extensive washing in dye-free buffer. These conditions were optimal to achieve sufficient labeling yet to avoid unspecific dye incorporation (Geibel et al., 2003; Dempski et al., 2005).

2.2.2.5. Two electrodes voltage clamp-fluorometry (TEVC-fluorometry)

The setup for TEVC-fluorometry was built according to schema developed by groups of Isaakof and Bezanilla (Manuzzu et al., 1996; Cha et al., 1998; Geibel et al, 2003). The scheme of the setup is shown in Figure 4.

The voltage clamp and data acquisition hardware were essentially the same as described above. The software Clampex 8.0 (Axon Instruments, Foster City, CA) was employed for stimulation, data acquisition and signal averaging.

The recording chamber (RC-10; Warner Instruments, Hamden, CT) had a volume of ~400µl with a 0.5-mm-thick glass coverslip as its base, upon which the oocyte was positioned and mechanically stabilized by two microelectrodes. The chamber could be continuously superfused by a gravity-feed perfusion system that allowed up to 16 different solutions to be applied independently.

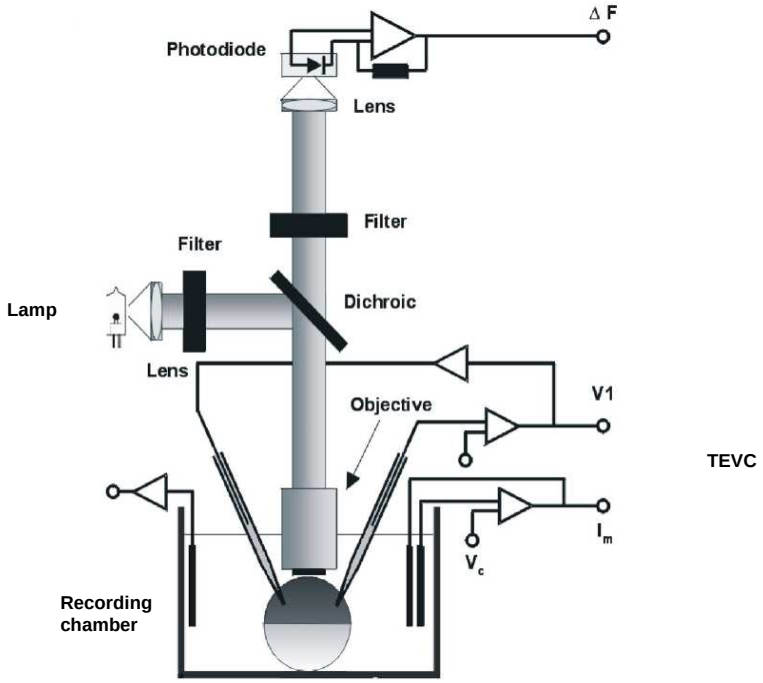

Figure 4. Scheme of the setup for two electrodes voltage clamp-fluorometry. Description is given in text.

The chamber was mounted on the stage of epifluorescence microscope Zeiss Axioskop 2FS equipped with 40X water-immerse objective (Carl Zeiss, Göttingen, Germany). Fluorescence was excited by a 100W halogen light source powered from a stabilized DC source. An electronic shutter VS252T1 (Uniblitz, Vincent Associates, Rochester, NY) was mounted between the light source and optical unit to avoid photobleaching when not recording. Excitation and emission wavelengths were nominally 535 and 605 nm, respectively, achieved using an XF33 filter set, which comprised a 535DF50 excitation filter, 570DRLP dichroic mirror, and 565EFLP emission filter (Omega Optical Inc, Brattleboro, VT). The excitation beam was focused on the oocyte via a 40X water immersion objective (numerical aperture 0.8). The ∞-focus emission beam was focused using a convex lens onto a photodiode PIN-020A (UDT Technologies, Torrance, CA) mounted to the camera output of the microscope. The signals from the photodiode were amplified with a patch-clamp amplifier EPC-5 (HEKA Electronics, Lambrecht, Germany). For measurements of stationary fluorescence signals were filtered at 20 Hz, and for measurements under voltage-step protocol at 2 kHz using a four-pole Bessel filter.

2.2.2.6. Fluorescence measurements by TEVC-fluorometry

Fluorescence changes (ΔF) of TMR6M-labelled oocytes were measured in response to changing substrate concentrations and/or membrane potential. ΔF were expressed as a percentage of the background fluorescence determined at holding potential V_{hold} = −50 mV.

In the voltage jump experiments, voltage-dependent fluorescence changes were investigated using a voltage-step protocol. Generally, the membrane voltage was stepped from V_{hold} = −50 mV to test potential ranging between −170 mV and +70 mV in 20 mV increment for a duration of 400 ms, and back to −50mV for 600 ms. To improve signal-to-noise ratio, signals were averaged over 3-5 runs. The duration of jumps was long enough to reach complete relaxation of the signals to steady values. Signas were acquired in normal Ori or in Ori containing organic cations – substrates or inhibitors of OCTs: choline, tetraethylammonium (TEA), 1-methyl-4-phenylpyridinium (MPP), and tetrabuthylammonium (TBuA).

The voltage-step protocol allowed following the time course of the voltage-induced fluorescence changes *F(t)*. For this analysis, fluorescence signals from the single cells or averaged signals across 4 - 10 cells were employed. Signals were fitted to exponential equation (Cha et al., 1997; 1998):

$$F(t) = \sum_{i=1}^{n} A_i \exp^{-t/\tau_i} + const \qquad \textbf{(eq. 1)}$$

where A_i is an amplitude and τ is a time constant (half-time) of relaxation of fluorescence.

The amplitudes of ΔF vs. voltage (ΔF-V) could be fitted to a Boltzman equation (Manuzzu et al., 1996; Cha et al., 1997; 1998):

$$\Delta F(V) = \Delta Fmin + \frac{(\Delta Fmax - \Delta Fmin)}{1 + \exp[\frac{z\delta F}{RT}(V - V_{0.5})]} \qquad \textbf{(eq. 2)}$$

where ΔFmin and ΔFmax are absolute minimal and maximal amplitudes of ΔF, V is membrane potential, F is the Faraday constant, R is the gas constant, T is the absolute temperature, $V_{0.5}$ (the midpoint voltage) is the membrane potential at 50% of (ΔFmax – ΔFmin), zδ is a steepness factor for the dependence of ΔF on voltage, which (in a simplified case) can be treated as a product of the apparent valence (z) of the fluorescence voltage sensor traversing through the fraction (δ) of the membrane electric field.

To determine apparent $K_{0.5}$ values, fluorescent signals were recorded in response to voltage steps in the absence or presence of different concentrations of organic cations. The difference between ΔF at a given concentration (ΔF_{ligand}) and at saturating concentration ($\Delta F_{ligand(sat)}$) of organic cation was scaled to the maximal difference of fluorescence changes at a given membrane potential, yielding a fractional fluorescence change:

$$\Delta F_{fractional}(ligand) = \frac{\Delta F_{ligand} - \Delta F_{ligand(sat)}}{\Delta F_0 - \Delta F_{ligand(sat)}} \quad \textbf{(eq. 3)}$$

where ΔF_0 represents amplitude of fluorescence changes in the absence of the organic cation. The values of fractional fluorescence changes were plotted against corresponding concentrations of cation and fitted to the Hill equation or to models for one, two or three binding sites.

2.2.2.7. Measurements of Membrane Capacitance

A method of parallel measurements of membrane current and capacitance under TEVC was developed in our laboratory and described earlier (Schmitt and Koepsell, 2002; Schmitt and Koepsell, 2005). The approach is illustrated in Figure 5. Membrane capacitance is calculated from the charges flowing during two symmetrical voltage ramps, one depolarizing and one repolarizing. By this approach, resistive component of the charge transferred during ramps can be eliminated, leaving only the capacitive one (Schmitt and Koepsell, 2002):

$$Cm = Q(capacitive) / \Delta V = 1/2*(Q_A - Q_B) / \Delta V$$

where ΔV is the height of the ramp, and Q_A and Q_B are the current integrals during the two respective ramps.

In these measurements, voltage ramps had durations of 20 ms and heights of 20 mV. Two programs, PULSE and X-CHART (HEKA Electronics, Lambrecht, Germany), were programmed to carry out stimulation, data acquisition, signal averaging, Cm calculation, and to display raw traces and calculated Cm values.

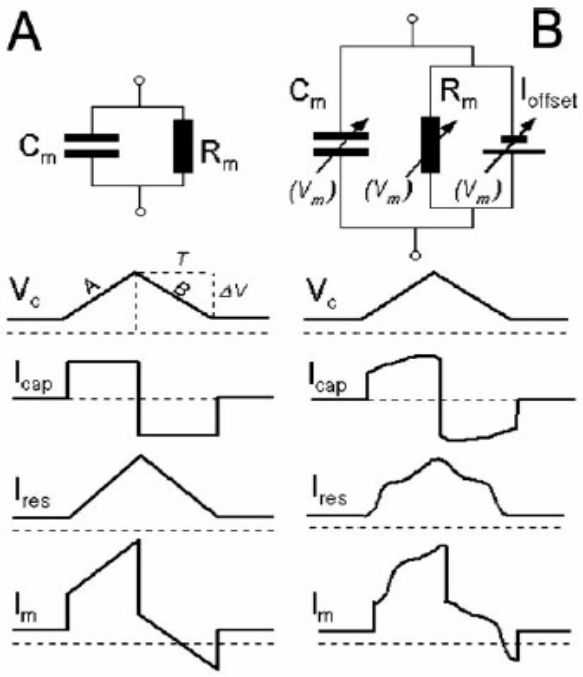

Figure 5. Capacitance measurements using paired voltage ramps (*from Schmitt and Koepsell, 2002*). *Upper panel,* electrical equivalent circuit of hypothetical cells; ***lower panel***, voltage stimulus and corresponding current components. (A) Passive, linear network. Membrane capacitance C_m and resistance R_m can be determined theoretically exact from the current integrals during the ramps A and B, together with the known ramp duration T and ramp height ΔV; (B) Active, nonlinear network. In addition to A, an energy source producing an offset current I_{offset} is present, and the respective values of all elements are functions of membrane potential V_m. If C_m is not constant within the tested voltage range, the calculated C_m represents the corresponding average. V_c, command voltage; I_{cap}, capacitive current component; I_{res}, current across R_m (in A) or across R_m plus I_{offset} (in B); I_m, total membrane current.

2.2.2.8. Tracer Uptake Measurements

For the measurements, 7-10 noninjected oocytes or injected with respective cRNA were placed into the vessel in 190 µl of ORi buffer. Transport was started by addition of 10 µl solution containing 0.1 µCi [^{14}C]TEA or [^{3}H]MPP and allowed to proceed for 15 min at 20-22^{0}C. The concentration of compounds in incubation mixture is indicated in the text. Transport was stopped by rinsing the oocytes three times with ice-cold ORi supplemented with 100 µM quinine, an inhibitor of OCTs (Nagel, 1997). Each oocyte was placed into separate vial and subjected to lysis with 100 µl of 5 % SDS. Afterwards, 1 ml of scintillation cocktail mix Lumasafe^{TM} Plus (Lumac, Netherlands) was added to the vial, and radioactivity of samples was analysed by liquid scintillation counting using Tricarb 1600 (Packard-Bell,

Dreieich, Germany). The amount of transported substrate (in pmol / hour^{-1} per oocyte) was calculated according to the formula

$$\frac{Radioactivity(oocyte)\,[DPM]}{Radioactivity(total)\;\;[DPM]} \times S[\mu M] \times V[\mu L] \times \frac{t[\min]}{60[\min]}$$

where *radioactivity(oocyte)* and *radioactivity(total)* are radioactive counts of the oocyte and incubation mixture, respectively; *S* stands for concentration of substrate, *V* - volume of reaction mixture (typically 200µL) and *t* is time of uptake measurement (typically 15 minutes if not otherwise stated).

Expressed uptake was calculated as the difference between uptake values measured in OCT-expressing oocytes and noninjected oocytes. Alternatively, the difference between uptake values measured in OCT-expressing oocytes in the absence and presence of quinine was calculated in some experiments. Uptake in noninjected oocytes was identical to the uptake of OCT-expressing oocytes measured in the presence of 100 µM quinine. For investigation of concentration-dependence of inhibition of transport, the uptake of [^{14}C]TEA or [^{3}H]MPP at indicated concentrations was measured in the presence of various concentrations of unlabelled TEA, MPP or TBuA. To determine concentration-dependence of the transport, the uptake of [^{14}C]TEA or [^{3}H]MPP at indicated concentrations was measured.

2.2.3. Calculation and Statistics

Generally, the software package GraphPad Prism Version 4.1 (GraphPad Software, San Diego, CA) was used to compute descriptive statistical parameters. Mean values ± S.E. derived from at least three independent experiments are presented. The number of experiments is indicated in the text. Apparent K_M values for tracer cation uptake and $K_{0.5}$ values for cation-induced currents were determined by fitting the Michaelis-Menten equation to the data. $IC_{0.5}$ values for inhibition of tracer cation uptake by nonlabelled cations and $K_{0.5}$ values for TBuA- or choline-induced capacitance changes were calculated by fitting Hill equation to the data. K_d values for the effects of cations on TMR6M-fluorescence of rOCT1 mutant were determined by fitting equations for one site-, two sites-, or three sites-binding models to the data. The software package Clampfit 8.0 (Axon Instruments, Foster City, CA) was employed to calculate descriptive parameters for potential-dependent fluorescence

changes by fitting the data to mono- or biexponential function, and to Boltzmann equation. Two-sided Student´s *t*-test was used to calculate statistical significance of differences between two groups, and ANOVA test with post-hoc Tukey comparison was used when more than two different groups were compared (Motulsky, 2003).

3. Results

Since the cloning of the first member of the SLC22 family, namely the rat organic cation transporter 1 (rOCT1) in 1994 (Gründemann et al., 1994), properties and physiological relevance of the organic cation transporters have been studied intensively. The investigations have demonstrated physiological importance of OCTs and shed some light on the role of OCTs in transport of exogenous organic substances, in particular drugs and toxins, as well as endogenous ones round the body (Wright S., 2005; Koepsell H., 2004; Koepsell et al., 2007). For understanding of transport mechanism of OCTs, a promising approach is biochemical and biophysical investigation of the structure and function which have already revealed some important features of the binding pocket and regulation of transport. However, it is still little known about mechanism of transport in respect to separate steps and underlying conformational changes. In present work, an attempt to detect membrane potential- and substrate-dependent conformation changes of rOCT1 was made. To this end, rOCT1 was studied using a combination of mutational analysis, site-directed chemical labeling with fluorescent dye, combined two-electrode voltage clamp-fluorometry, and tracer flux measurements.

3.1. Construction and characterization of mutants for voltage clamp-fluorometry

3.1.1. Construction and functional characterization of mutants containing introduced cysteine residues (cys-mutants)

The strategy of site-directed chemical labeling requires reaction that is specific for a certain chemical group. Among the amino acids composing natural proteins, only few have side chains with chemical groups meeting this criterion. If such amino acids are present in protein *ab initio* they can be used directly for this purpose. Alternatively, they can be introduced into the sequence that allows labeling at virtually any desired site of the protein. One of the amino acids best suited for that task is cysteine since there is a variety of specific chemical reactions which can be used for modification of sulfhydryls (Karlin A. and Akabas M., 1998). Another advantage of cysteine is that introduction of single residue does not impair secondary structure nor introduces a strong charge; it also has rather moderate hydrophobic properties in comparison to other amino acids used for site-specific labeling (e.g. lysine or amino acids with carboxylic side chain) (Javitch J., 1998; Finkelstein and Pticyn, 2002). Our

strategy employed scanning cysteine mutagenesis of rOCT1 which allows attaching an environmentally sensitive fluorophore tetramethylrhodamine-6-maleimide (TMR6M) to the transporter. The dye TMR6M, covalently attached at a specific place, may form a fluorescence sensor for tracking conformational changes of the protein (Manuzzu et al., 1996; Cha et al., 1998; Candhi and Isacoff, 2005).

It is important to note that mutations were introduced into the rOCT1 mutant where ten of sixteen natural cysteines were replaced by serines, alanines or methionine (C26A, C155A, C417A, C322S, C358A, C418A, C437S, C451M, C470A, C474A (Sturm et al., 2007)) (Fig. 2). For simplicity, this mutant will be referred throughout the text as "10ΔC" and mutations on the basis of 10ΔC will be given in parenthesis with indication of the base construct (i.e., 10ΔC(F483C)). 10ΔC was used to avoid possible complexity or misinterpretations of results rising from the labeling at more than one position − even in the case when labeling of the “natural” cysteines is “silent” in terms of specific fluorescence changes. In some studies presence of background cysteines was considered as noninterfering, relying on the absence of fluorescence changes in response to specific test signal in fluorophore-labeled wildtype, or when it was possible to discriminate fluorescent signals coming obviously from reporters attached at different points (Li et al., 2000; Li and Lester, 2002; Geibel et al., 2003; Dempski et al., 2005). However, one cannot exclude that either interaction between molecules of the dye attached at different places of the same protein molecule, or changed functional properties as result of multi-site labeling would impair the fluorescence signals in comparison to labeling at a single site.

Six natural cysteines (C50, C62, C89, C103, C122, and C143) that are still present in 10ΔC are located within the large extracellular loop between TMH1 and TMH2 (Fig. 2). Replacement of any of them leads to complete inactivation of the transport (Sturm et. all, 2007). Noteworthy, C62 and C103 are conserved in OCTs, while C50, C89, C122, and C143 are maintained throughout the SLC22 family (Koepsell et al., 2003). Based on these observations and experiments testing accessibility of cysteines to thiol-modifing reagents, it was suggested that cysteines of the large extracellular loop build disulfide bridges which are important for correct trafficking and/or functioning of the transporter (Pelis et al., 2006, 2007; Sturm et al., 2007). Hence, even though these cysteines could not be removed, they are most likely not accessible to modification by TMR6M.

Measurements of tetraethylammonium (TEA) or 1-methyl-4-phenylpyridinium (MPP) uptake in *Xenopus laevis* oocytes expressing wildtype rOCT1 or 10ΔC revealed similar values of Michaelis-Menten constant (K_M) and maximal transport velocity (V_{max}) of

10ΔC and wildtype (Table 1). At variance, when oocytes expressing 10ΔC were superfused with 1mM TEA or 10mM choline at membrane potential clamped to −50 mV, roughly 2.4-fold higher maximal currents were observed compared to oocytes expressing wildtype rOCT1 (Table 1). Since tracer flux measurements were performed in unclamped oocytes, membrane potential could be fairly less negative than −50 mV (Weber W., 1999); it is possible that voltage dependences of transport by 10ΔC or wildtype are reasonably different which would also imply changes of reversal potential. However, preliminary survey shows that charge-to-substrate ratio in 10ΔC is higher compared to wildtype; this is most probably due to mutations C451M and/or C322A (B. Schmitt and H. Koepsell, unpublished data). This fact can explain observed discrepancy between electrical and uptake experiments.

Table 1. Functional characterization of the rOCT1, 10ΔC, and 10ΔC(F483C). rOCT1, 10ΔC, or 10ΔC(F483C) were expressed in oocytes, and concentration activation curves of [^{14}C]TEA uptake, [^{3}H]MPP uptake, TEA-induced currents at -50 mV, and choline-induced currents at -50 mV were measured using 8 to 10 different substrate concentrations. V_{max}, I_{max}, K_M, and $K_{0.5}$ values were determined by fitting the Michaelis-Menten equation to the data of individual experiments. Mean values ± S.E. are presented. The number of experiments is given in parentheses.

* $P < 0.05$, *** $P < 0.001$ compared with rOCT1
† $P < 0.05$, ††† $P < 0.001$ compared with 10ΔC
[a] Data from Sturm et al., 2007.

Activity	rOCT1	10ΔC	10ΔC(F483C)
[^{3}H]MPP uptake			
V_{max} (pmol·oocyte^{-1}·h^{-1})	122 ± 30 (5)	133 ± 23 (3)	57 ± 9 (4)
K_M (µM)	3.9 ± 1.1 (3)	2.5 ± 1.0 (3)	3.0 ± 0.7 (3)
[^{14}C]TEA uptake			
V_{max} (pmol·oocyte^{-1}·h^{-1})	503 ± 73 (4)	560 ± 95 (3)	385 ± 68 (4)
K_M (µM)	52 ± 21 (11)	67 ± 8 (3)	143 ± 27 (3)*†
TEA-induced current			
I_{max} (nA)	6.4 ± 2.3 (5)[a]	15.3 ± 1.7 (4)*	9.2 ± 4.1 (3)
$K_{0.5}$ (µM)	30 ± 6 (5)[a]	54 ± 5 (4)	118 ± 8 (3)***†††
Choline-induced current			
I_{max} (nA)	18 ± 13 (46)[a]	43 ± 11 (9)^{*a}	25 ± 3.4 (10)
$K_{0.5}$ (µM)	290 ± 180 (6)[a]	1410 ± 240 (3)^{***a}	1300 ± 160 (10)***

In oocytes expressing rOCT1 or 10ΔC, TEA concentrations required for half-maximal activation of induced currents ($K_{0.5}$(TEA)) were similar to each other and to the values derived from uptake experiments (Table 1). The same is true for MPP which is structurally different to TEA: K_M of MPP-uptake for rOCT1 was nearly the same as for 10ΔC Table 1. However, choline concentration required for half-maximal current ($K_{0.5}$(choline)) in case of 10ΔC was about 5-fold higher compared to wildtype rOCT1 (Table 1). This change of affinity for choline is due to replacements of cysteines 322 and 451 to serine and methionine, respectively (Sturm et al., 2007). Taken together, the data indicate that 10ΔC retains functional properties of rOCT1 with the exception of the affinity for choline.

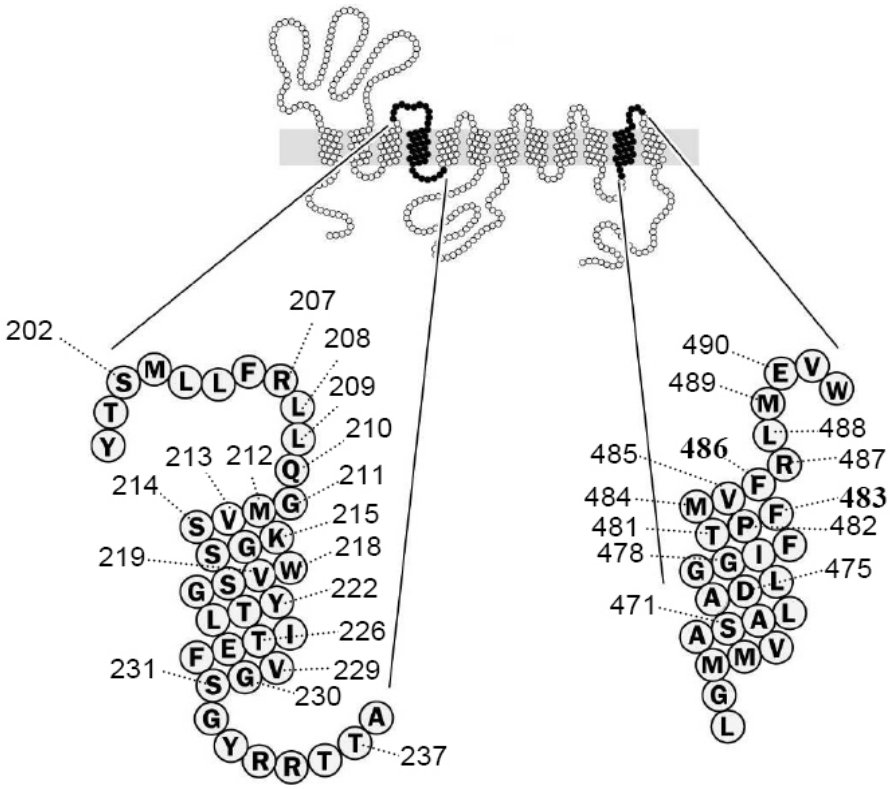

Figure 6. Location of cysteine mutations in 10ΔC. Topology model with amino acid residues that were individually replaced by cysteine, indicated by single-letter code. Endogenous cysteines 470 and 474 of TMH11 were mutated to alanines in 10ΔC.

We generated a set of mutants containing substitutions of single amino acids to cysteines. Mutations were mainly introduced in the parts of the presumed 11th and 4th TMHs which are close to the extracellular surface of the membrane (Fig. 6). These domains are supposed to form a part of the binding pocket since mutational analysis suggested that several

amino acids of the TMHs 4 (W218, Y222, T226) (Popp et al., 2005) and 11 (D475) (Gorboulev et al., 1999) in rOCT1 are involved in binding of organic cations. Moreover, according to presumed structure of rOCT1 (Fig. 3), these two domains line the internal cavity and are surrounded by other transmembrane helices. Therefore, it is quite probable that the chosen parts are undergoing conformational changes when transporter goes through the transport cycle; such changes would be then associated with transitions between different conformations.

Functionality of the individual cysteine substitution mutants expressed in oocytes was tested by uptake measurements of 9 µM [^{14}C]TEA (Fig. 7a). Most of the mutants demonstrated uptake rates of over 50% compared to 10ΔC. Mutations of W218, Y222, and T226, which are involved into substrate binding (Popp et al., 2005), led to significant reduction of activity. Consistent with previous data, mutants 10ΔC(K215C) and 10ΔC(D475C) were virtually inactive. These amino acids are conserved in all OCTs (Koepsell et al., 1998, 2003). Previously it has been shown that mutations K215Q/R and D475N/R in rOCT1 led to inactivation of transport, although these mutations did not impair trafficking and insertion into the membrane. The negative charge at position 475 is required for the transporter since only the mutant rOCT1(D475E) demonstrated transport activity, although the transport rate was markedly reduced and affinities for some substrates was changed significantly (Gorboulev et al., 1999; Popp et al., 2005). Noteworthy, applying the method of paired-ramp membrane capacitance measurements (Schmitt et al., 2002; see also "MATERIALS AND METHODS"), we found that oocytes expressing 10ΔC(D475C) showed choline-induced (10 mM choline) capacitance changes (about 20% of the changes observed with 10ΔC at -50 mV: ~0.25 nF *vs.* ~1.3 nF). However, oocytes expressing the mutant 10ΔC(D475C) did not show current changes upon superfusion with 10 mM choline at -50 mV. Mutant 10ΔC(K215C) was completely inactive (D. Gorbunov and H. Koepsell, unpublished data). Since capacitance changes have been shown to follow binding of substrates to the transporter (Schmitt and Koepsell, 2005), we concluded that the mutant 10ΔC(D475C) can bind substrate although the affinity of the substrate can be changed, as it has been observed for mutant rOCT1(D475E). The lack of transport activity along with preservation of substrate binding suggest that negative charge at position 475 is required for translocation of organic cations through the membrane.

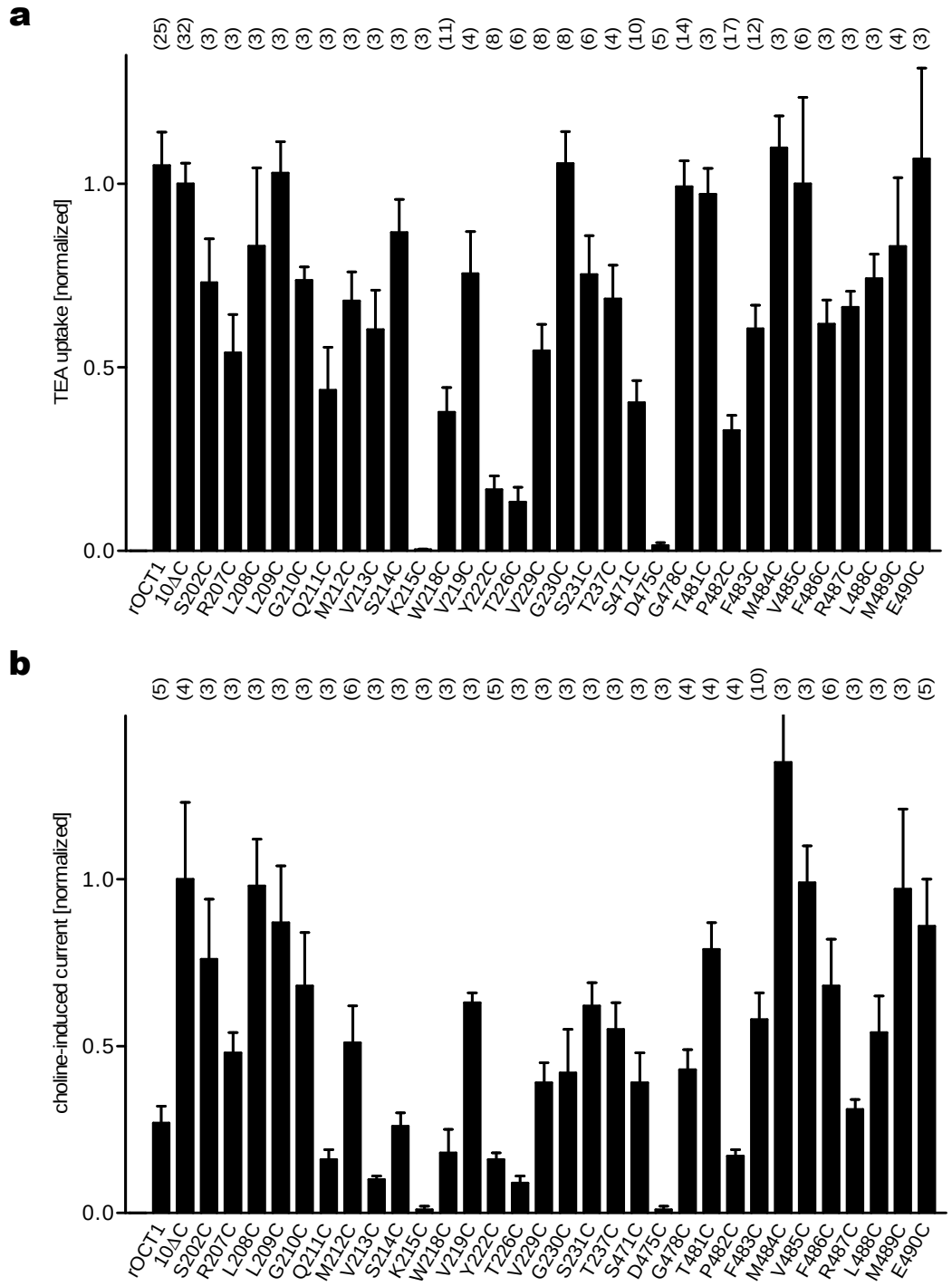

Figure 7. Activity of cysteine-substituted mutants of 10ΔC upon expression in *Xenopus laevis* oocytes. Mutations indicate single amino acid substitutions by cysteine in 10ΔC ***(a)*** Relative uptake of 9 µM [^{14}C]TEA in oocytes expressing the indicated mutants or (***b***) relative current induced by 10 mM choline at -50 mV in TMR6M-treated oocytes expressing the indicated mutants. Mean values ± S.E. are shown. The numbers of independent experiments are given in parenthesis.

3.1.2. Identification of cys-mutants demonstrating fluorescence changes

For scanning of mutants by fluorescence measurements under voltage-clamp conditions, respective cRNAs were injected into individual oocytes. 2 - 4 days later oocytes were labeled by 5 min incubation in Ori containing 5µM TMR6M followed by voltage-clamp as described in "MATERIALS AND METHODS". This procedure should lead to covalent attachment of fluorophore via maleimide to accessible cysteine residues. The treatment resulted in markedly increased background fluorescence of noninjected oocytes that was comparable to fluorescence of oocytes injected with wildtype rOCT1 or mutants. Under voltage clamp to −50mV, noninjected oocytes did not show fluorescence changes after superfusion with 10mM choline, or in response to voltage jumps in buffer with or without choline. Likewise, the OCT ligands MPP, TBuA, and TEA did not induce fluorescence changes (data not shown). These results are in agreement with previous studies performed in other laboratories (Cha et al., 1997, 1998; Loo et al., 1998; Virkki et al., 2006a).

Next, fluorescence signals of oocytes expressing rOCT1 or 10ΔC were examined. TMR6M-treated oocytes expressing respective protein were clamped to −50 mV. Under steady-state conditions (−50 mV), application of 10 mM choline led to generation of inward currents (Fig. 7b), whereas no significant changes of fluorescence signals were observed (data not shown). Also voltage jumps in the absence of substrate or in the presence of 10 mM choline or nontranslocated inhibitor TBuA (100 µM) did not induce changes of background fluorescence signals (data not shown). The lack of fluorescence changes can be either due to lack of the labeling, considering inaccessibility of the natural cysteines, or because attached dye did not sense changes of the environment.

Having confirmed the absence of background fluorescence changes, we checked all cysteine substitution mutants of 10ΔC in a similar manner. Most of the mutants showed considerable currents upon application of 10 mM choline under voltage clamp to -50 mV (Fig. 7b). Interestingly, while for most of the mutants the relative TEA uptake values (normalized to 10ΔC) obtained with nontreated oocytes were similar to the respective relative choline-induced currents obtained with TMR6M-treated oocytes, for substitutions (in 10ΔC) Q211C, V213C, S214C, W218C, G230C, G478C, P482C, and R487C ratios between uptake and current values were significantly decreased (compare panels *a* and *b* on Fig. 7). We established that treatment with TMR6M did not lead to inhibition of choline-induced current by these mutants (data not shown). Difference between effects of mutations on choline-induced currents and TEA-uptakes can be caused by changed substrate specificities.

Alternatively, the mutations may change the stoichiometry between transported positive charge and substrate cation.

At -50 mV, no significant changes of fluorescence were observed when the oocytes expressing any of the mutants were superfused with 10 mM choline or 100µM TBuA (for example, see Fig. 8a). Applying the voltage-jump protocol shown in Figure 8b, we found that only mutant 10ΔC(F483C) showed potential-dependent fluorescence changes (ΔF) in the absence of choline. The fluorescence was decreased under depolarizing voltage jumps and increased under hyperpolarizing jumps (Fig. 8, c and e). Fluorescence intensity returned to baseline when the test pulse was stepped back to the holding potential. The fluorescence level was dependent on the final potential but not on the starting potential (Fig. 9). ΔF varied with the starting potential; however, different starting potentials did not influence fluorescence level at the respective test potential. This indicated that the fluorescence signal represented a memoryless phenomenon.

The observed fluorescence changes were markedly reduced, and dependence on membrane potential was inverted when either substrate choline (10 mM) or inhibitor TBuA (100 µM) was present in the media (Fig. 8, d and e). Mutant 10ΔC(F486C) also showed fluorescence changes in the presence of choline or TBuA that were similar to the respective fluorescence changes of 10ΔC(F483C). At variance to 10ΔC(F483C), with 10ΔC(F486C) no significant potential dependent fluorescence changes were detected in the absence of choline and TBuA (Fig. 8f).

Noteworthy, even prolonged washing out of choline or TBuA did not restore amplitudes of voltage jumps-induced ΔF observed before addition of these ligands. After exposure of an oocyte expressing 10ΔC(F483C) to 10 mM choline or 100µM TBuA for 30 seconds followed by continuous superfusion with ligand-free Ori for 20 minutes, amplitudes of ΔF induced by voltage changes were restored to ~50 - 60 %. Very slow exchange of solutions in the recording chamber could be ruled out since the current induced by choline developed within seconds, and holding current returned to baseline within 15 - 30 seconds after switching solution containing choline to choline-free buffer. In addition, experiments on Na,K-ATPase employing the same machine and the same batches of oocytes did not reveal similar effects (T. Friedrich, personal communications). Bleaching of the fluorophore could not be the reason since repetition of the fluorescence measurements before application of choline (or TBuA) with the same oocyte yielded the same relative voltage jumps-induced ΔF (data not shown).

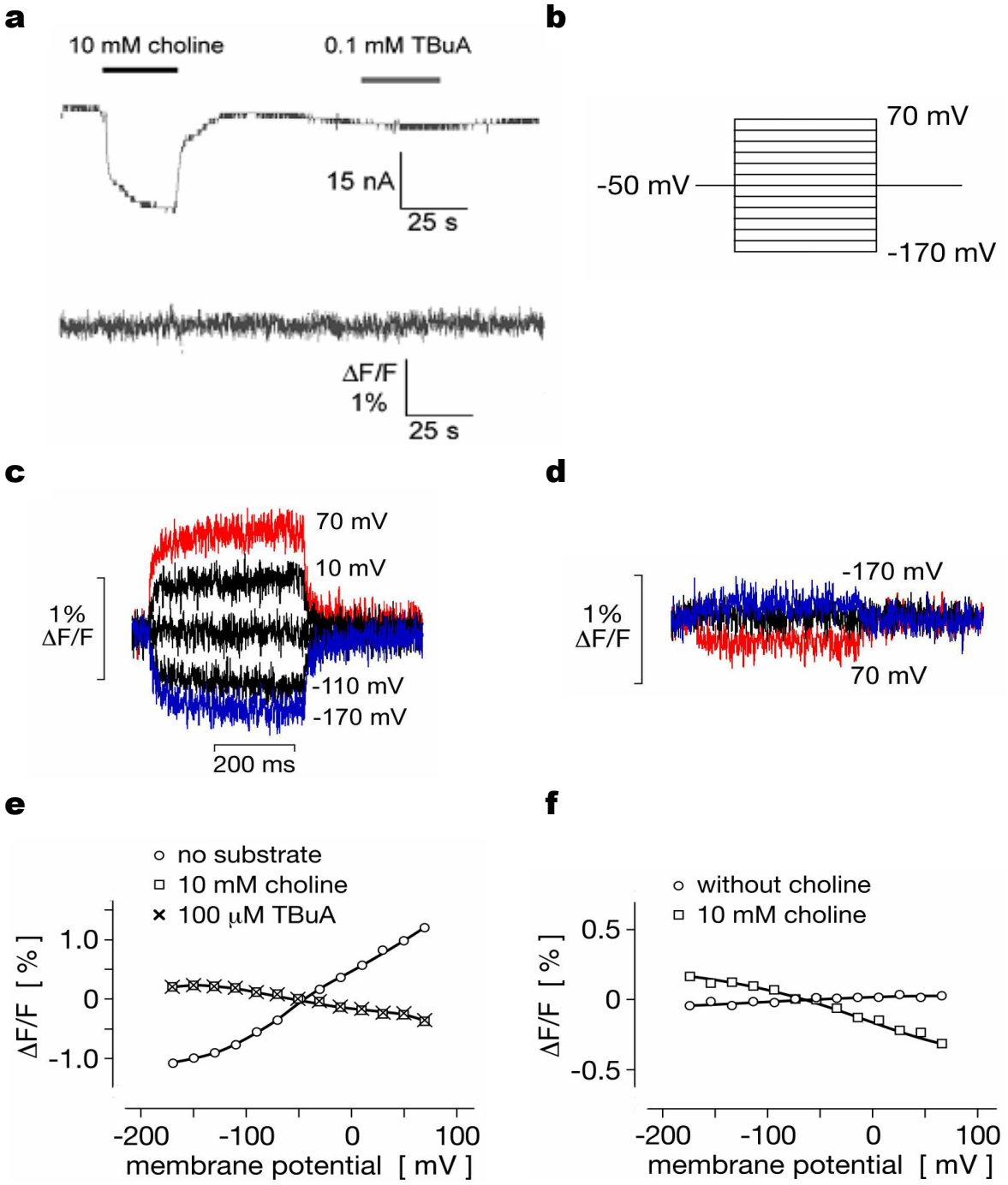

Figure 8. Voltage- and cation-dependent fluorescence changes of TMR6M-labeled mutants 10ΔC(F483) (*a,c,d,e*) and 10Δ(F486C) (*f*). (***a***) Stationary electrical (upper trace) and fluorescence (lower trace) recording at -50 mV in oocyte expressing 10ΔC(F483C). (***b***) Protocol of voltage jumps and (***c***, ***d***) fluorescence recordings in 10ΔC(F483C) in the absence of ligand (***c***) or presence of 10 mM choline (***d***). Fluorescence signals upon jumps to -170 mV or +70 mV are shown in blue and red, respectively. Voltage dependence of amplitudes of fluorescence changes (ΔF-V curves) of 10ΔC(F483C) (***e***) and 10ΔC(F486C) (***f***).

The data imply a specific action of ligands on transporter-associated fluorescence changes. This phenomenon is discussed below. Considering the possibility that voltage-dependent fluorescence changes of TMR6M-labeled transporter could be reduced or diminished once a ligand has been applied, wildtype rOCT1 and all mutants were checked for voltage jumps-induced fluorescence changes before the first application of ligands.

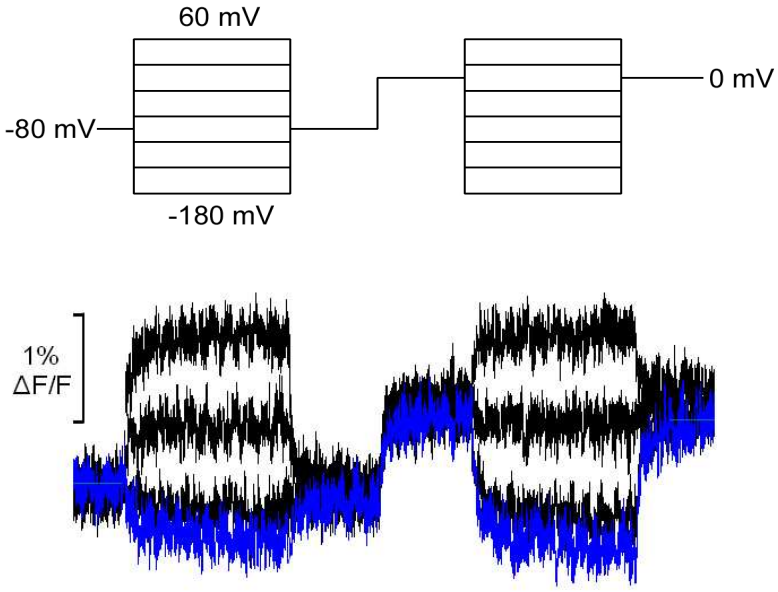

Figure 9. Fluorescence recording in TMR6M-labeled 10ΔC(F483C) upon voltage jumps from different starting potentials. ***Upper panel***, protocol of voltage jumps from a holding potentials of -80 mV or 0 mV to values varying between +60 mV and -180 mV in 40 mV steps. ***Lower panel***, fluorescence traces. Shown are signals corresponding to voltage jumps to +60 mV, -20 mV, or -100 mV (*black traces*), and to -180 mV (*blue trace*).

3.1.3. Organic cation transport and substrate-induced current mediated by the mutant 10ΔC(F483C)

Functional characterization of 10ΔC(F483C)-mediated transport was performed using typical model substrates of OCTs choline, TEA and MPP in tracer flux or in electrical experiments (Koepsell et al., 2007).

In oocytes expressing 10ΔC(F483C), for TEA uptake a K_M value of 143 ± 27 µM, and for TEA-induced inward current at -50 mV $K_{0.5}$ of 118 ± 8 µM were determined (Table 1 and Fig. 10b). These values were about 2-times higher compared with rOCT1(10ΔC) or wildtype (Table 1). In contrast, the K_M value for MPP uptake by 10ΔC(F483C) was 3 ± 0.7 µM and was not different to K_M values of 10ΔC or wildtype rOCT1 (Table 1 and Fig. 10a). In

addition, the values of $K_{0.5}$ for choline-induced inward currents for 10ΔC(F483C) were nearly the same as for 10ΔC (Table 1). It is consistent with previous finding that mutation D475E in TMH 11 markedly increased the affinity to tetraalkylammonium compounds, whereas affinity to MPP was not changed (Gorboulev et al., 1999). A minor decrease of K_M and $K_{0.5}$ only for TEA, despite considerable difference between phenylalanine and cysteine in terms of size and physicochemical properties, suggests that amino acid at position 483 is not involved in the binding of substrates.

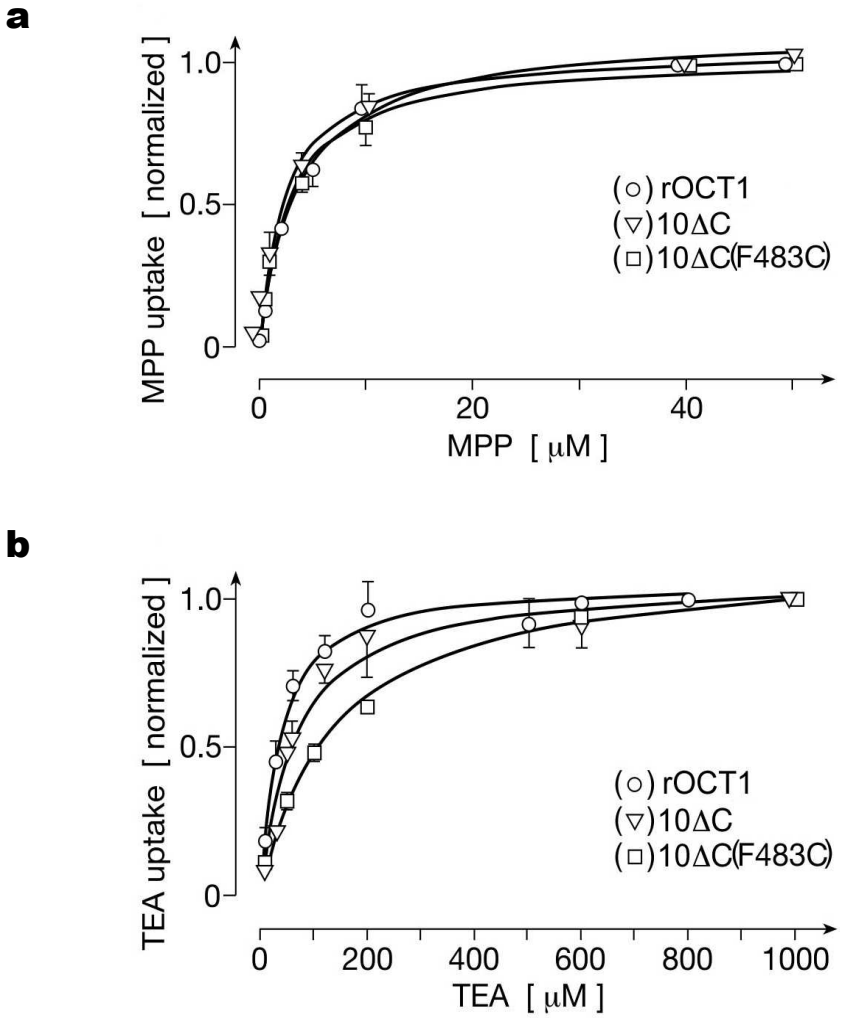

Figure 10. Concentration dependence of MPP- and TEA-uptake by rOCT1, 10ΔC, and 10ΔC(F483C). Wildtype rOCT1, 10ΔC, or 10ΔC(F483C) were expressed in oocytes, and concentration activation curves of [^{3}H]MPP uptake (***a***) or [^{14}C]TEA uptake (***b***) were measured. Uptake values were normalized within a single experiment, each point is a mean value of 3 independent experiments ± S.E. Data were fitted to Michaelis-Menten equation.

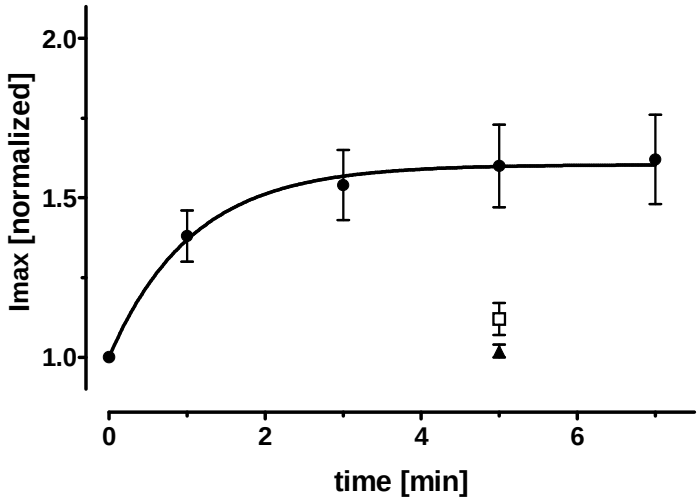

Figure 11. Activation of choline-induced current mediated by 10ΔC(F483C) after treatment with TMR6M. Oocytes expressing 10ΔC(F483C) were clamped to -50 mV, and 10 mM choline-induced current (Imax) was measured after incubation with 100 µM TMR6M followed by washing out of unbound dye from the recording chamber (*filled circles*). Abscissa is the cumulative incubation time. Values were normalized within a single experiment; each point is a mean of 3 experiments ± S.E. Activation of current mediated by 10ΔC after incubation with 100 µM TMR6M for 5 min (*filled triangle*, mean of 3 experiments ± S.E.), or by 10ΔC(F483C) after incubation with 5 µM TMR6M for 5 min (*open square*, mean of 7 experiments ± S.E.) is shown for comparison.

We checked whether labeling of 10ΔC(F483C) by TMR6M alters transporter function. Oocytes expressing 10ΔC(F483C) were clamped to -50 mV and incubated with 5 µM TMR6M for 5 min, or with 100 µM TMR6M for 1 to 7 min. After indicated time, oocytes were washed and the inward currents induced by superfusion with 10 mM choline were measured. Whereas treatment with 5 µM TMR6M did not change choline-induced current significantly, treatment with 100 µM TMR6M increased a current in a time-dependent manner reaching maximal effect after 5 min (maximal activation factor was 1.64 ± 0.14, n=3) (Fig. 11). No effect of treatment with 100 µM TMR6M on currents induced by 10 mM choline was observed in oocytes expressing 10ΔC (Fig. 11). For the mutant 10ΔC(F483C), the value of $K_{0.5}$(choline) was not significantly changed when the oocytes were incubated for 5 min with 100 µM TMRM (nontreated 1.3 ± 0.16 mM, after treatment 1.8 ± 0.18 mM; $P>0.05$ by Student's *t* test for difference). The data indicate that under the labeling conditions used for fluorescence measurements, only a part of the expressed 10ΔC(F483C) molecules is labeled. However, we have noticed that treatment of 10ΔC(F483C)-expressing oocytes with 100 µM TMR6M largely increased background fluorescence without relative increase of specific

fluorescence changes (data not shown). Therefore, the procedure of 5 min treatment with 5 µM TMR6M was chosen for fluorometric measurements with the mutant 10ΔC(F483C).

3.2. Fluorometric measurements of TMR6M-labeled 10ΔC(F483C)

The observed fluorescence changes of the TMR6M attached to 10ΔC(F483C) or 10ΔC(F486C) are due to changes in the local surroundings of the dye. These in turn can reflect conformation changes of the transporter, considering that local changes are linked to global ones (Gandhi and Isacoff, 2005). 10ΔC(F483C) showed fluorescence changes in response to voltage jumps both in the absence and in the presence of substrate, thus demonstrating intrinsic ability of the transporter to sense membrane potential.

rOCT1 mediates transport under a wide range of membrane potentials varying between −150 mV and +50mV (Nagel et al., 1997; Arndt et al., 2001). Therefore, we assume that under tested potentials transporter can occupy conformational states which are relevant to physiological conditions.

3.2.1. Kinetics of voltage-dependent fluorescence changes of 10ΔC(F483C) in the absence of ligands

Oocytes expressing the mutant were labeled by incubation with 5 µM TMR6M and clamped to -50 mV. After a period at −50 mV holding potential, the cells were subjected to voltage test pulses varying usually between +70 and −170 mV in 20 mV steps (“ON” pulses) followed by a step back to −50 mV (“OFF” pulses).

We analyzed the time course of the fluorescence changes. The “ON” fluorescence signals could be successfully fitted by a sum of two exponentials (eq. 1 in MATERIALS AND METHODS, section 2.2.2.6). An example of the fitting is shown in theFigure 12. Biexponential fit was significantly better than monoexponential one ($P<0.001$, F-test). The "fast" time constant τ_{fast} ranged between 7 and 17 ms, the "slow" one τ_{slow} ranged between 73 and 122 ms (Fig. 12). The relaxation time constants were independent of voltage. No significant difference between relaxation time constants after switching to depolarized or hyperpolyrized potentials could be detected (one-way ANOVA with post hoc Tukey test for difference between values).

The “OFF” fluorescence signals also consisted of fast and slow components. The time constants of the “OFF” signals were independent of the test potential (Fig. 12).

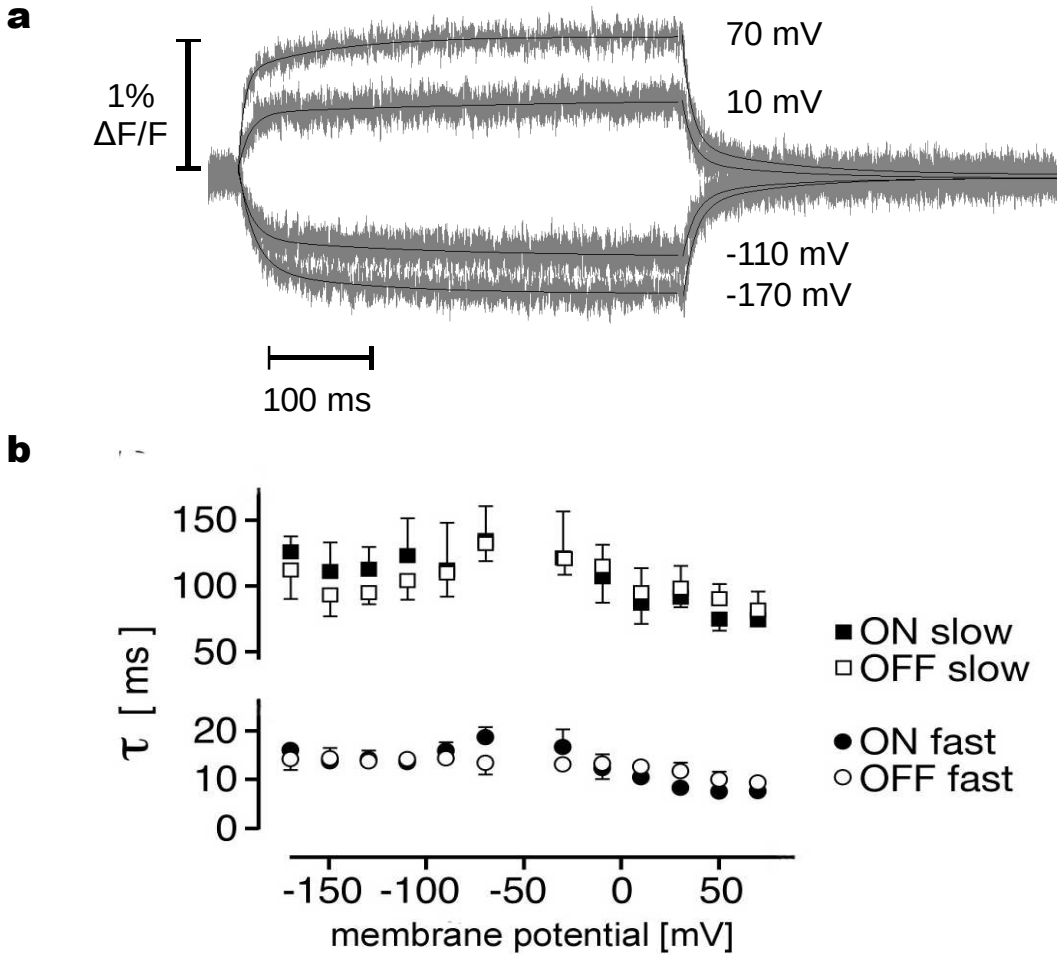

Figure 12. Kinetics of voltage jumps-induced fluorescence changes in 10ΔC(F483C)-TMR6M in the absence of substrate. Protocol of voltage jumps is the same as in Figure 8. (***a***) Fitting of fluorescence signals to sum of two exponentials. Shown are fluorescence signals upon jumps from holding potential of -50 mV to indicated test potentials. *Solid lines* represent curve fitting. (***b***) Voltage dependence of time constants. Mean values ± S.E. of 10 experiments are presented. *Filled symbols* represent the ON where membrane potential was stepped from -50 mV to different test potentials. *Open symbols* represent the time constants of the relaxations of the OFF when membrane potential was returned from test potential to -50 mV.

Figure 13 shows voltage dependence of amplitudes of fluorescence changes ΔF for mutant 10ΔC(F483C) in response to voltage jumps. Amplitudes of total fluorescence changes ΔF_{total} could be determined from the fluorescence averaged over last 50 ms of a jump. Alternatively, they could be derived from biexponential fits to the data. Both approaches gave same results demonstrating that the fluorescence reached stable value during the voltage pulse

(Fig. 13: *open squares* represent ΔF obtained by averaging (ΔF_{total}), *filled circles* represent ΔF derived from biexponential fit (ΔF_{total_fit})). Plotting amplitudes of fluorescence changes against the membrane potential resulted in the ΔF-V curves. In the cases of ΔF_{total} and ΔF_{fast} (Fig. 13, *open circles*), ΔF-V curves approached saturation under hyperpolarized and depolarized potentials wherease ΔF_{slow}-V curve did not show obvious saturation (Fig. 13).

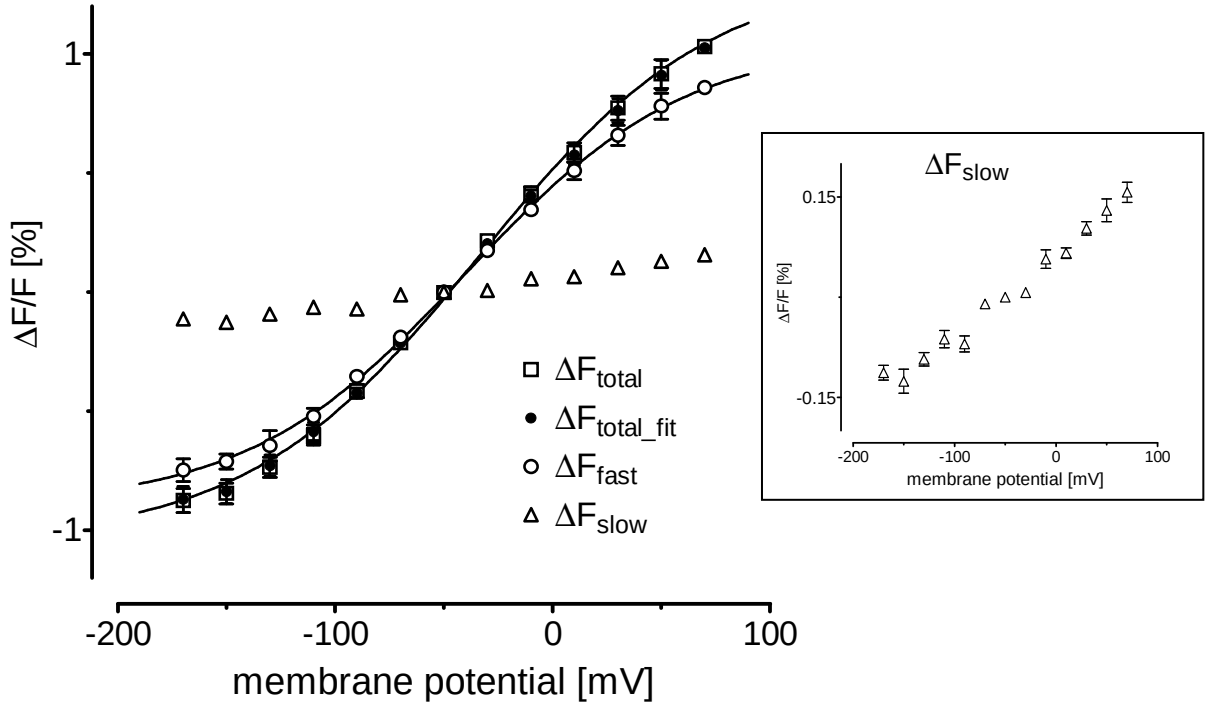

Figure 13. Voltage dependence of components of voltage jumps-induced fluorescence changes in 10ΔC(F483C)-TMR6M. ΔF_{total} was determined as average fluorescence over last 50 ms of voltage pulse; ΔF_{total_fit}, ΔF_{fast} and ΔF_{slow} were derived from exponential fit to the fluorescence signals. Mean values ± S.E. of 10 experiments are presented. ***Inlet*** shows ΔF_{slow} plotted on a different scale. Data were fitted to Boltzmann equation (solid lines).

Sigmoidal dependence of the ΔF_{fast} on voltage could be adequately described with the Boltzmann relation (eq.2 in MATERIALS AND METHODS, section 2.2.2.6) giving a value of the midpoint voltage $V_{0.5}$ as −38 ± 5 mV (n = 10). For ΔF_{total} , $V_{0.5}$ was calculated as −33 ± 7 mV (n=10). $V_{0.5}$ of ΔF_{slow}, could not be estimated satisfactory because of the low amplitudes and lack of saturation at depolarized potentials.

The data indicate that ΔF_{fast} and ΔF_{slow} reflect different phenomena. The main component of the total fluorescence changes, ΔF_{fast} might represent potential-dependent

conformation change of the transporter. ΔF_{slow} has a little input into total fluorescence changes; it demonstrates weaker potential dependence and occurs on a slower time scale. This suggests that ΔF_{slow} might represent a secondary structural change.

3.2.2. Voltage-dependent fluorescence changes of 10ΔC(F483C) in the presence of ligands

3.2.2.1. Determination of apparent affinities to organic cations using fluorescence measurements

Once the substrate is present, all states of the transport cycle become available, resulting in a redistribution of the protein between these states. Thus, addition of substrate can lead to alteration of fluorescence signal, which was indeed observed at the saturating concentrations of substrate choline (10mM) or nontranslocated inhibitor TBuA (100µM): under these conditions voltage jump-induced fluorescence changes were markedly reduced along with inversion of voltage dependence (Fig. 8c,d,e). It is remarkable that amplitudes of voltage jump-induced fluorescence changes at saturating concentrations of 100 µM TBuA or 10 mM choline were very similar. It suggests that binding of the inhibitor does not “lock” transporter in a particular conformation but allows a conformational switch between at least two ligand-bound states as in the case of bound choline. Considering membrane impermeability of TBuA, it also suggests that decrease of observed fluorescence changes reflect mainly binding of a ligand to transporter on extracellular side of the membrane rather than binding-transport events.

To study the effect of ligands on voltage-dependent fluorescence changes more systematically, we examined the concentration dependence. Included in the Figure 14 is an example of voltage jump-induced fluorescence changes from continuous recordings on oocytes expressing the 10ΔC(F483C) mutant at different concentrations of TBuA varying from 0.1 nM to 200 µM. After solution exchanges to the stated concentrations of a ligand, voltage step protocols were applied in which, starting from a holding potential of -50 mV, oocytes were clamped to potentials between +50 mV and -150 mV.

Voltage dependencies of amplitudes of fluorescence changes at different concentrations of TBuA or choline are shown in Figure 15a. Interestingly, presence of small concentrations of ligands (0.1 nM TBuA or 0.1 µM choline) decreased ΔF. This suggests that ligands can effectively interact with the transporter even at concentrations considerably lower than $K_{0.5}$ values determined from transport measurements.

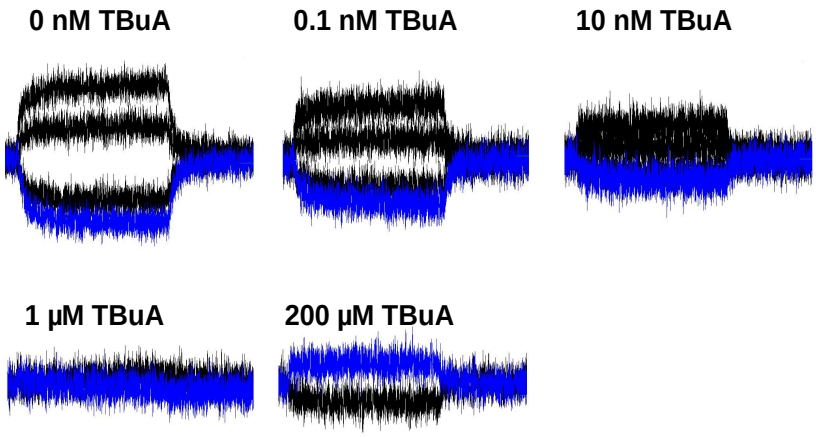

Figure 14. Voltage jumps-induced fluorescence responses in 10ΔC(F483C)-TMR6M at different concentrations of TBuA. An example of original fluorescence traces at different concentrations of TBuA. Shown are signals corresponding to jumps from holding potential of -50 mV to test potentials of +50 mV, -10 mV, or -110 mV (*black traces*), and -170 mV (*blue trace*). For 200 µM TBuA, only traces corresponding to jumps to +50 mV (*black*) and -170 mV (*blue*) are shown.

Changes of amplitudes of voltage jumps-induced fluorescence changes caused by addition of a ligand reflect redistribution of conformational states at a given membrane potential as a consequence of ligand binding. Therefore, an effect of ligands on fluorescence can be used to determine ligands affinities. Since we do not know whether our measurements follow simple transition between bound and unbound states, or more steps are involved (e.g. conformational rearrangements of the transporter with bound ligand (TBuA or choline) or dissociation of ligand (e.g. choline) on intracellular side), the constants obtained so far should be referred as apparent affinity constants. To derive these values, a fractional fluorescence changes $\Delta F_{fractional}$ induced by a ligand at a given membrane potential were plotted against substrate concentrations. $\Delta F_{fractional}$ were determined as the difference between amplitudes of fluorescence changes at a given concentration (ΔF_{ligand}) and at saturating concentration ($\Delta F_{ligand(sat)}$) of a ligand, scaled to the maximal difference of fluorescence changes ($\Delta F_0 - \Delta F_{ligand(sat)}$) at a given membrane potential (see eq. 3 in MATERIALS AND METHODS, section 2.2.2.6). Since bleaching of the fluorophore did not allow to conduct experiments upon long illumination, fluorescence changes were measured in response to voltage jumps from holding potential of -50 mV to +50 mV and -150 mV. In addition to choline and TBuA,

substrates TEA and MPP have been chosen since these are also typical model ligands of rOCT1 (Koepsell et al., 2007).

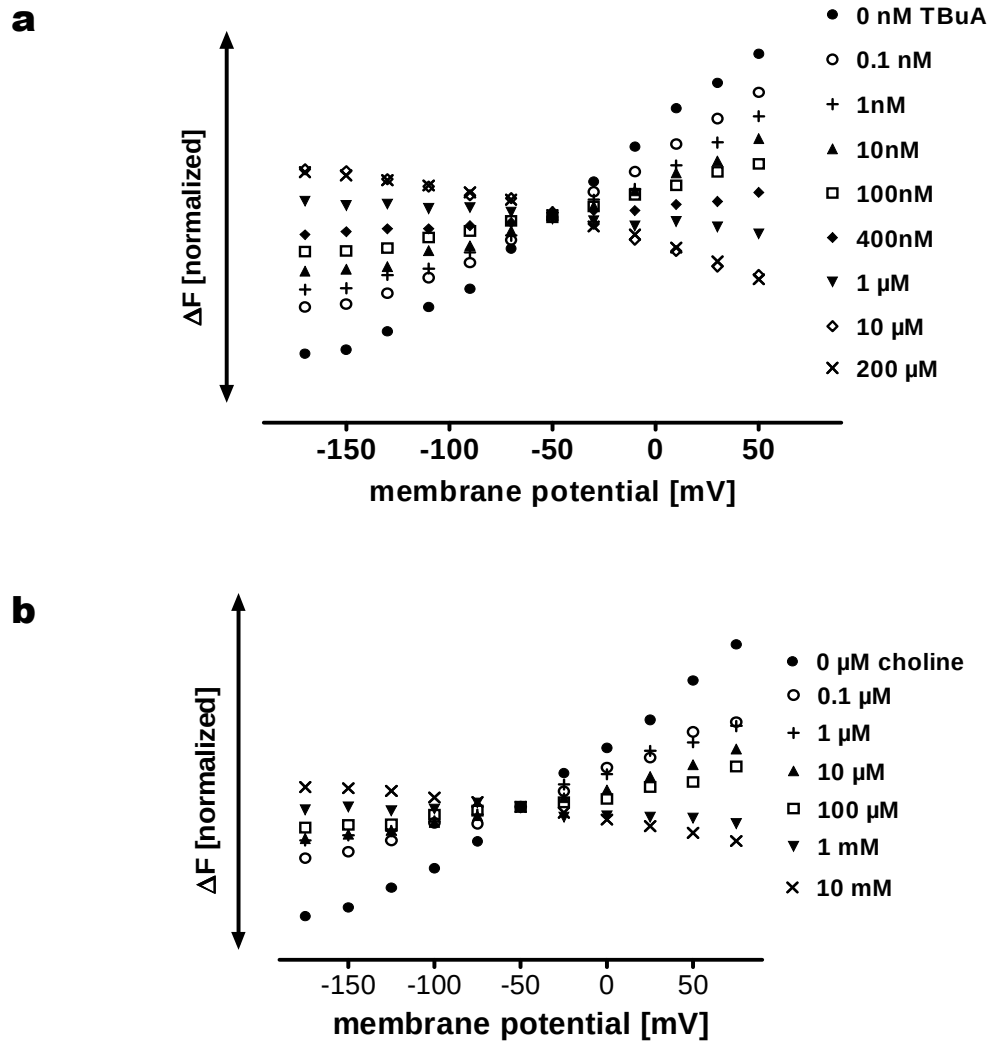

Figure 15. Voltage dependence of fluorescence amplitudes at different concentrations of TBuA (*a*) or choline (*b*) for 10ΔC(F483C)-TMR6M. Mean values of 4 (in ***a***) or 3 (in ***b***) experiments are presented; for simplicity of presentation S.E. are omitted.

Plot of choline-dependent amplitudes of voltage jumps-induced fluorescence changes versus voltage is shown in Figure 16a. The data could be fitted to a two-site model significantly better than to a one-site model (P<0.001 by F-test). Thus, two different affinities, $K_{d(high\text{-}aff)}$ and $K_{d(low\text{-}aff)}$, could be clearly distinguished (Table 2). Similarly, high- and low-affinity binding sites could be determined for TEA and MPP (Table 2 and Fig. 16, b and c). Notably, for all individual experiments as well as for the averaged data, fitting to a two-site model was significantly better than to a one-site model (P < 0.001 by F-test) (Fig. 16).

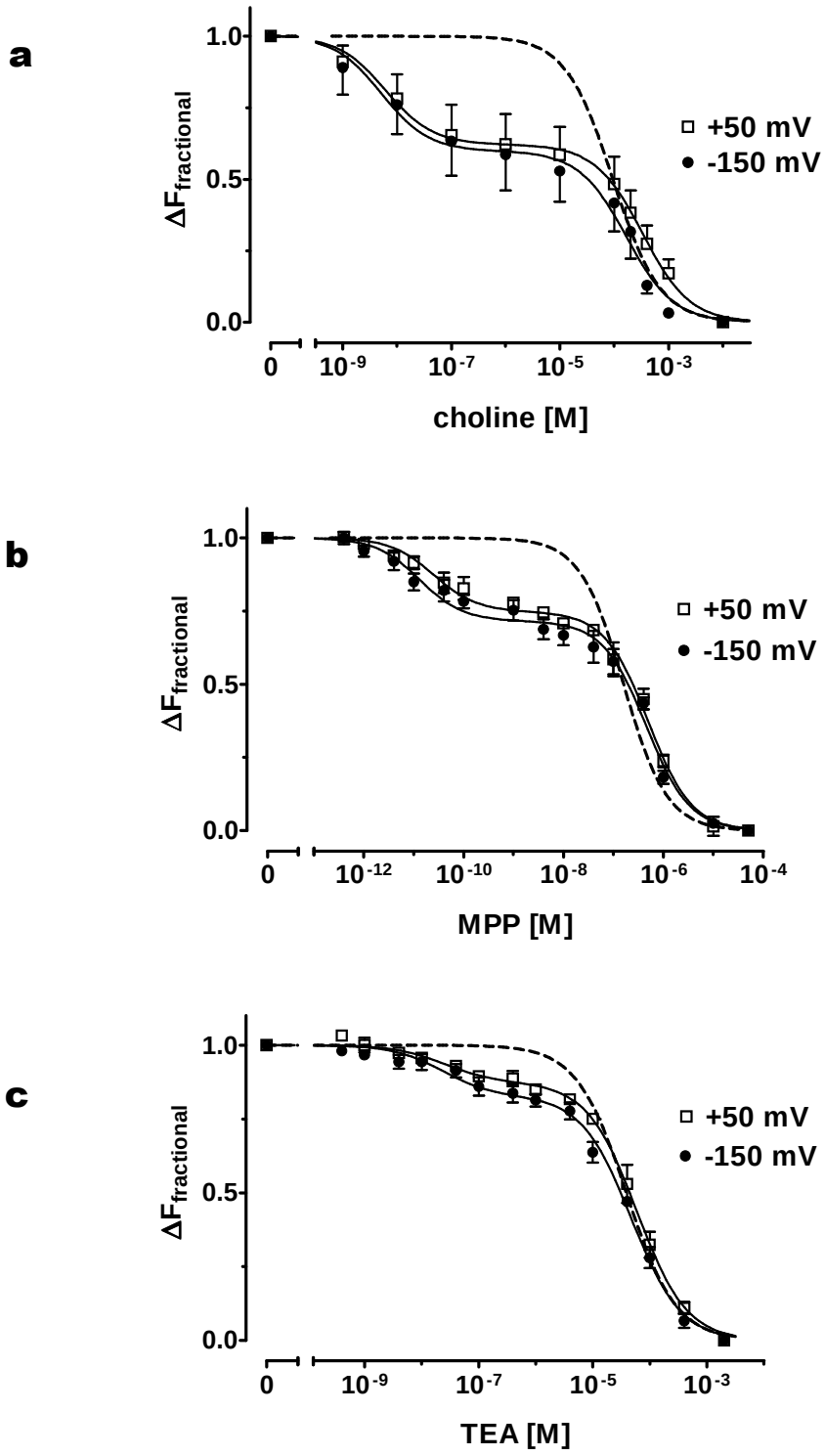

Figure 16. Determination of two binding affinities for translocated substrates by fluorometric measurements in 10ΔC(F483C)-TMR6M. (**a**) Choline-, (**b**) MPP-, or (**c**) TEA-dependent amplitudes of voltage jumps-induced (from starting potential of -50 mV to test potentials of +50 mV or -150 mV) fluorescence changes were normalized as described in text. Each point is a mean value ± S.E. of 4 experiments. Fitting to a two-site model (*solid lines*) is shown. Fitting to a one-site model (*broken line*) is shown for ΔF induced by voltage jumps to +50 mV.

Table 2. K_d values of 10ΔC(F483C) determined by fluorescence measurements.
Mean values ± S.E. of four independent experiments are presented.

	K_d at -150 mV	K_d at +50 mV	Ratio $\frac{K_{d(low\text{-}aff)}(+50\ mV)}{K_{d(low\text{-}aff)}(-150\ mV)}$
choline	site 1: 8 ± 4 nM site 2: 0.26 ± 0.07 mM	site 1: 21 ± 11 nM site 2: 0.43 ± 0.07 mM	1.65
TEA	site 1: 26 ± 10 nM site 2: 49 ± 15 µM	site 1: 41 ± 18 nM site 2: 77 ± 13 µM	1.57
MPP	site 1: 23 ± 10 pM site 2: 0.85 ± 0.09 µM	site 1: 33 ± 13 pM site 2: 1.03 ± 0.08 µM	1.21
TBuA	site 1: 2±1 pM site 2: 0.35±0.07 nM site 3: 0.26±0.05 µM	site 1: 2±1 pM site 2: 0.65±0.3 nM site 3: 0.35±0.1 µM	1.35

The values of $K_{d(low\text{-}aff)}$ determined by fluorescence measurements are 3-4 times lower than the K_M or $K_{0.5}$ values determined by uptake or current measurements, respectively (compare Table 1 and Table 2). This suggests that the low-affinity constants K_d of the effect of substrates on fluorescence changes are due to substrate binding to the same site that is involved into transport. The difference can be due to the following reason. K_M values derived from transport measurements represent combination of kinetic constants of all steps of the transport cycle, whereas substrate effect on voltage-dependent fluorescence reflects mainly binding of a ligand to the transporter.

Concentration dependence of the effect of TBuA on the potential-dependent ΔF is shown in Figure 17. A two-site model yielded much better fit than a one-site model; however, fitting to a three-site model improved the goodness of fit significantly ($P<0.01$ by F-test for comparison of three-site vs. two-site models). For each individual experiment, fitting to a three-site model was also significantly better than to a two-site model ($P < 0.01$ by F-test). The half-maximal concentrations of TBuA at the three sites are shown in Table 2.

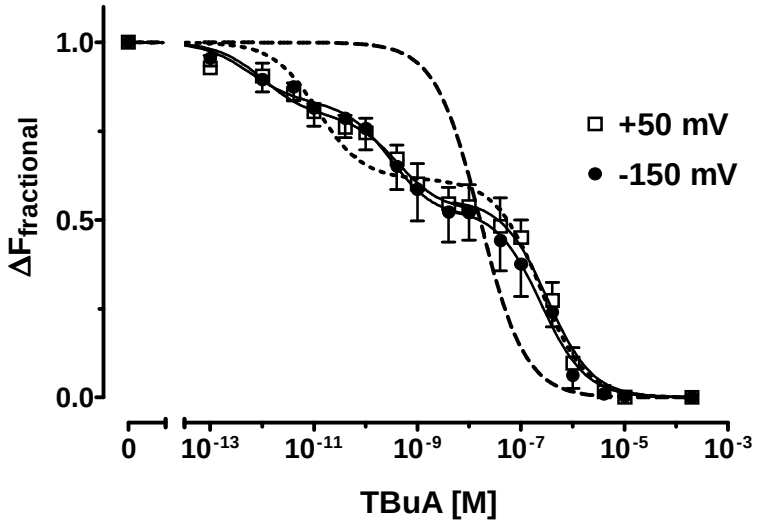

Figure 17. Determination of three binding affinities for inhibitor TBuA by fluorometric measurements in 10ΔC(F483C)-TMR6M. TBuA-dependent amplitudes of voltage jumps-induced (from starting potential of -50 mV to tets potentials of +50 mV or -150 mV) fluorescence changes were normalized as described in text. Each point is a mean value ± S.E. of 4 experiments. Fitting to a three-site model (*solid line*) is shown. Fitting to one-site (broken line) or two-site (dotted line) models is shown for ΔF induced by voltage jumps to +50 mV.

Interestingly, for all ligands neither high- nor low-affinity apparent constants show significant voltage dependence (P>0.05 by Student's *t* test for comparison of respective K_d values for −150 mV and +50 mV), although values for depolarized potential were constantly higher than for hyperpolarized potential (Table 2). At variance, $K_{0.5}$ values of choline- or TEA-induced currents mediated by rOCT1 were found to be about 3.5-times less at −90 mV compared to −10 mV: for choline, 130 and 500 µM, respectively; for TEA, 15 and 49 µM, respectively (Busch et al., 1996). Similar voltage dependence of K_M or K_i values was found for rOCT2 (Budimann et al., 2000; Volk et al., 2003). Assuming that fluorescence measurements reflect mainly binding of ligands on extracellular side of the membrane (see beginning of this section), the data suggest that binding to the outward-open transporter does not contribute, or make only partial contribution, into potential dependence of $K_{0.5}$ values.

3.2.2.2. Kinetics of fluorescence changes in the presence of ligands

The time courses of ΔF at different concentrations of ligands could be analyzed in the same way as in the absence of ligands. Figure 18 shows relaxation time constants derived from bi- or monoexponential fitting to the data. For 0.1 nM TBuA fast and slow components

could be isolated; τ_{fast} and τ_{slow} were similar to the respective time constants for the absence of substrate and varied between 7 ÷ 19 ms and 84 ÷ 108 ms (Figure 18b,d,e). With increase of TBuA concentration, the slow component disappeared: at 1 or 10 nM TBuA fitting to monoexponential equation produced satisfactory fits with time constants varying between 10-29 ms in each case (Figure 18c,f). At 200 µM TBuA, ΔF induced by voltage jumps to most positive or negative potentials could be fitted to monoexponential equation giving τ of 14 ± 6 ms (for jump from -50mV to +50 mV) and 21 ± 11 ms (for jump from -50 mV to -170 mV) (not shown). At concentrations 0.1 − 1µM TBuA, ΔF were too small precluding from correct determination of time constants. For a particular concentration of TBuA, the time constants of fluorescence changes did not show statistically significant voltage dependence (one-way ANOVA with post hoc Tukey test for difference between values) (Figure 18).

Figure 19 shows plots of amplitudes of fluorescence changes against voltage (ΔF-V curves) at 0 and 0.1 nM TBuA. In the absence of TBuA fitting to Boltzmann equation yielded values of $V_{0.5}$ as −32 ± 7 mV for ΔF_{total} and −37 ± 4 mV for ΔF_{fast} (n = 4). Presence of 0.1 nM TBuA shifted $V_{0.5}$ for both ΔF_{total} and ΔF_{fast} to −4 ± 9 mV and −12 ± 10 mV, respectively (n = 4). $V_{0.5}$ values in the absence and presence of TBuA were significantly different ($P < 0.05$ by Student's *t* test). Amplitudes of slow components in 0.1 nM TBuA were also decreased concurrently with the decrease of ΔF_{fast} that, along with the lack of saturation under positive potentials, precluded from fitting to Boltzmann equation.

Voltage dependence of amplitudes of fluorescence changes at different concentrations of TBuA is shown in Figure 15a. ΔF−V curves saturated under hyperpolarized potentials similarly to the ΔF-V curve in the absence of TBuA. At variance, under depolarized potentials ΔF-V curves did not saturate in the presence of TBuA that did not allow to determine $V_{0.5}$ values. However, such voltage dependence suggests that $V_{0.5}$ are shifted to depolarized potentials in comparison to $V_{0.5}$ determined in the absence of TBuA, although we cannot estimate whether there is further shift of ΔF-V curves at TBuA concentrations ≥1 nM in comparison to ΔF-V curve at 0.1 nM TBuA.

Similar results were obtained for fluorescence changes in the presence of translocated substrate choline. Figure 15b shows an overlay of ΔF−V plots for different concentrations of choline. ΔF−V curves could not be fitted to Boltzmann equation because of lack of saturation at positive potentials. The data indicate that choline induced a positive shift of $V_{0.5}$ of ΔF−V curves similarly to TBuA.

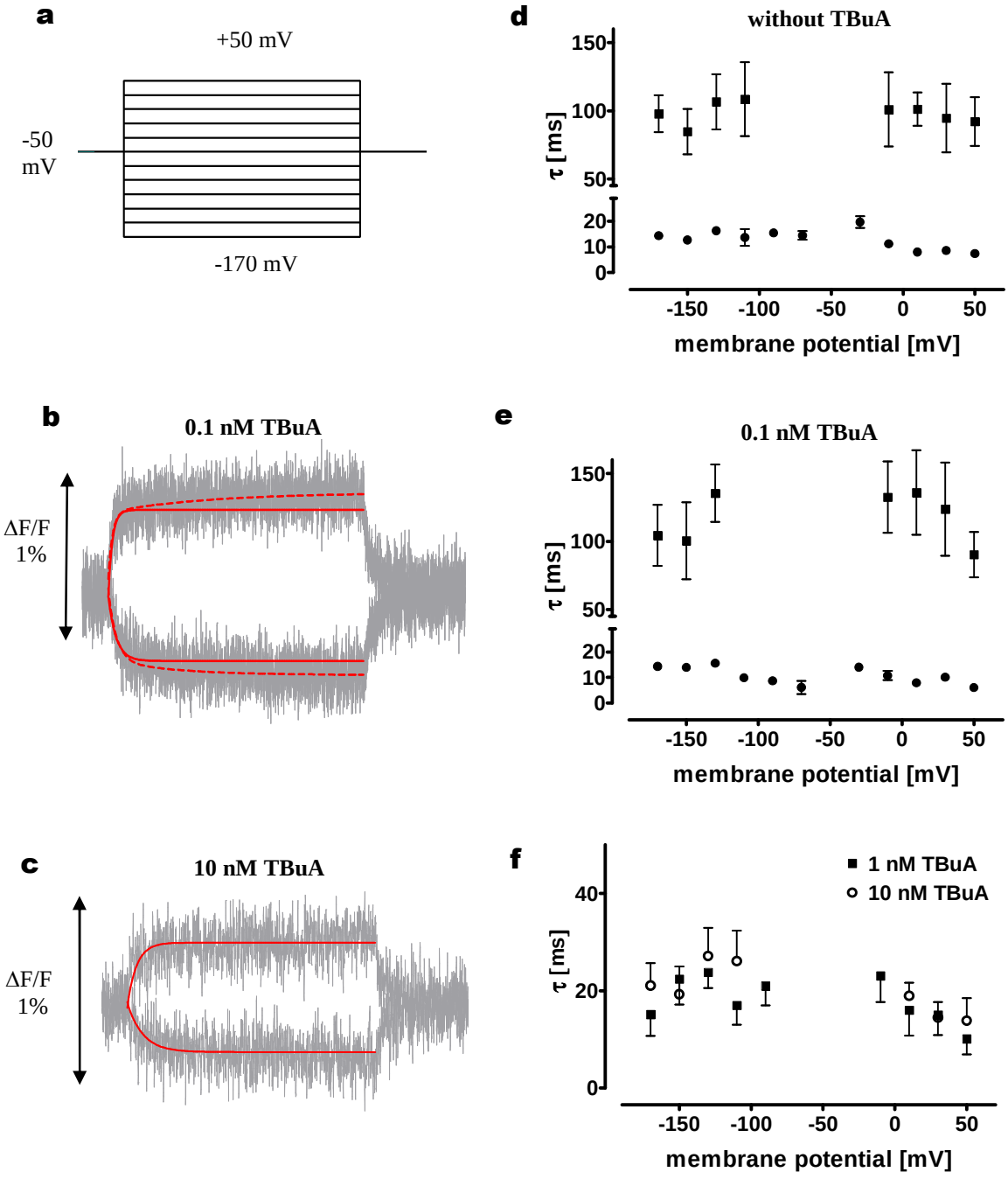

Figure 18. Kinetics of voltage jumps-induced fluorescence changes in 10ΔC(F483C)-TMR6M in the presence and absence of TBuA. Fluorescence signals are from the same cell as in Fig. 14. (***a***) Protocol of voltage jumps. (***b,c***) Fluorescence changes in the presence of TBuA. Shown are signals upon jumps to +50 mV or -150 mV. Data were fitted to biexponential (*broken line* in ***b***) or monoexponential (*solid line* in ***c***) function. Parameters of the fast component obtained from the fit to biexponential function were used for simulation of monoexonential function (*solid line* in ***b***). (***d,e,f***) Time constants of relaxations of fluorescence changes in the absence (***d***) and presence of 0.1 nM TBuA (***e***), 1 nM or 10 nM TBuA (***f***). Mean values ± S.E. of 4 experiments are presented.

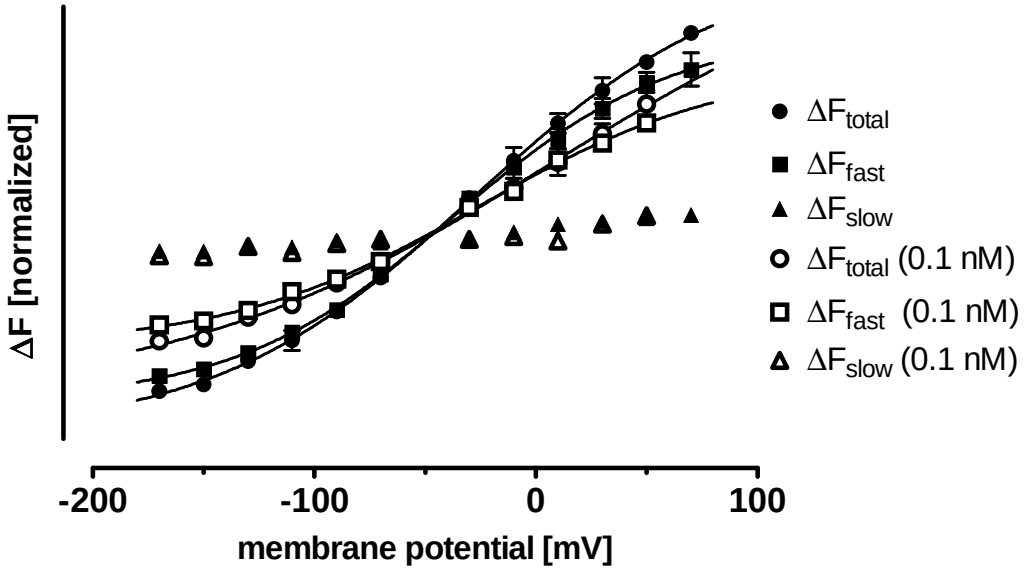

Figure 19. Voltage dependence of voltage jumps-induced fluorescence changes in 10ΔC(F483C)-TMR6M in the presence and absence of TBuA. ΔF-V curves for components of fluorescence changes in the absence (*filled symbols*) or presence of 0.1 nM TBuA (*open symbols*). Mean values ± S.E. of 4 experiments are presented. Data were fitted to Boltzmann equation (*solid lines*).

For tested concentrations of choline, only fast component of voltage jumps-induced fluorescence changes could be isolated. Values of time constants varied between 9 ÷ 27 ms for 0.1 µM or 1 µM choline (data not shown). Similarly to ΔF at 200 µM TBuA, time constants of ΔF at 10 mM choline were estimated being in the range of 10-40 ms (data not shown). Time constants of ΔF at a given concentration of choline did not show significant voltage dependence (one-way ANOVA with post hoc Tukey test for difference between values).

High-affinity binding sites for TBuA determined by fluorescent measurements were saturated at TBuA concentrations around 10 nM. Similarly, high-affinity binding site for choline was saturated at concentrations around 100 nM choline (Table 2, Fig. 16 and 17). This correlates with disappearance of the slow component of voltage jump-induced fluorescence changes in the presence of ligands. The data suggest that transporter with ligand bound at high-affinity site(s) can switch between two conformations in a voltage-dependent manner. The shift of $V_{0.5}$ of ΔF to depolarized potentials in the presence of small concentrations of ligands suggests that binding of ligand to high-affinity site(s) stabilizes certain conformation of the protein under physiological membrane potentials. Since hyperpolarization induced

increase of fluorescence and depolarization induced decrease of fluorescence in the absence as well as in the presence of low concentrations of ligands, and temporal characteristics of the respective changes were similar under these conditions, it suggests a similarity of fast transitions of empty transporter and transporter with ligand bound at high-affinity site(s).

3.3. Characterization of TBuA interaction with mutants on the basis of 10ΔC

3.3.1. Analysis of TBuA binding to 10ΔC(F483C) by measurements of membrane capacitance

To investigate binding of TBuA to transporter, the method of online membrane capacitance measurements was used. This method allows to follow interaction of ligands with transporter without measuring transport, and was successfully applied for analysis of binding of translocated as well as nontranslocated ligands to rOCT1 and rOCT2 (Schmitt and Koepsell, 2002, 2005; Sturm et al., 2007). It was shown that specific capacitance changes in rOCT1- or rOCT2-expressing *Xenopus* oocytes could be induced by charged or noncharged as well as transported or nontransported ligands. It was concluded that substrate-induced ΔCm reflects electrogenic conformational change of the protein upon binding rather than transport of a ligand (Schmitt and Koepsell, 2005).

Ligand-induced capacitance changes in rOCT1 are significantly lower than in 10ΔC that did not allow measurements of concentration dependence (Sturm et al., 2007). Therefore, TBuA-induced changes of membrane capacitance were measured in oocytes expressing 10ΔC or 10ΔC(F483C) that were clamped to -50 mV. Figure 20 shows concentration dependence of amplitudes of capacitance changes. For both mutants, small but significant ΔCm could be observed upon superfusion with buffer containing 5 nM TBuA (10ΔC, 0.11 ± 0.03 nF; 10ΔC(F483C), 0.19 ± 0.11 nF; n=4 for each). These changes were significantly higher than artificial changes induced by switching between zero TBuA solutions (Fig. 20) or induced by ligands in noninjected oocytes (Schmitt and Koepsell, 2005). These data indicate an existence of high-affinity binding site(s) for TBuA with K_d < 5 nM in both mutants. However, the capacitance measurements were not sensitive enough to determine K_d values for this(these) site(s). For both mutants, a second TBuA binding site with a K_d value around 1 µM could be resolved (10ΔC, 0.95 ± 0.11 µM; 10ΔC(F483C), 1.06 ± 0.37 µM; n=4 for each). These values are similar to the low-affinity K_d values determined by fluorescence measurements (around

0.3 µM, Table 2). Thus, the data support the presence of high- and low-affinity binding sites for TBuA.

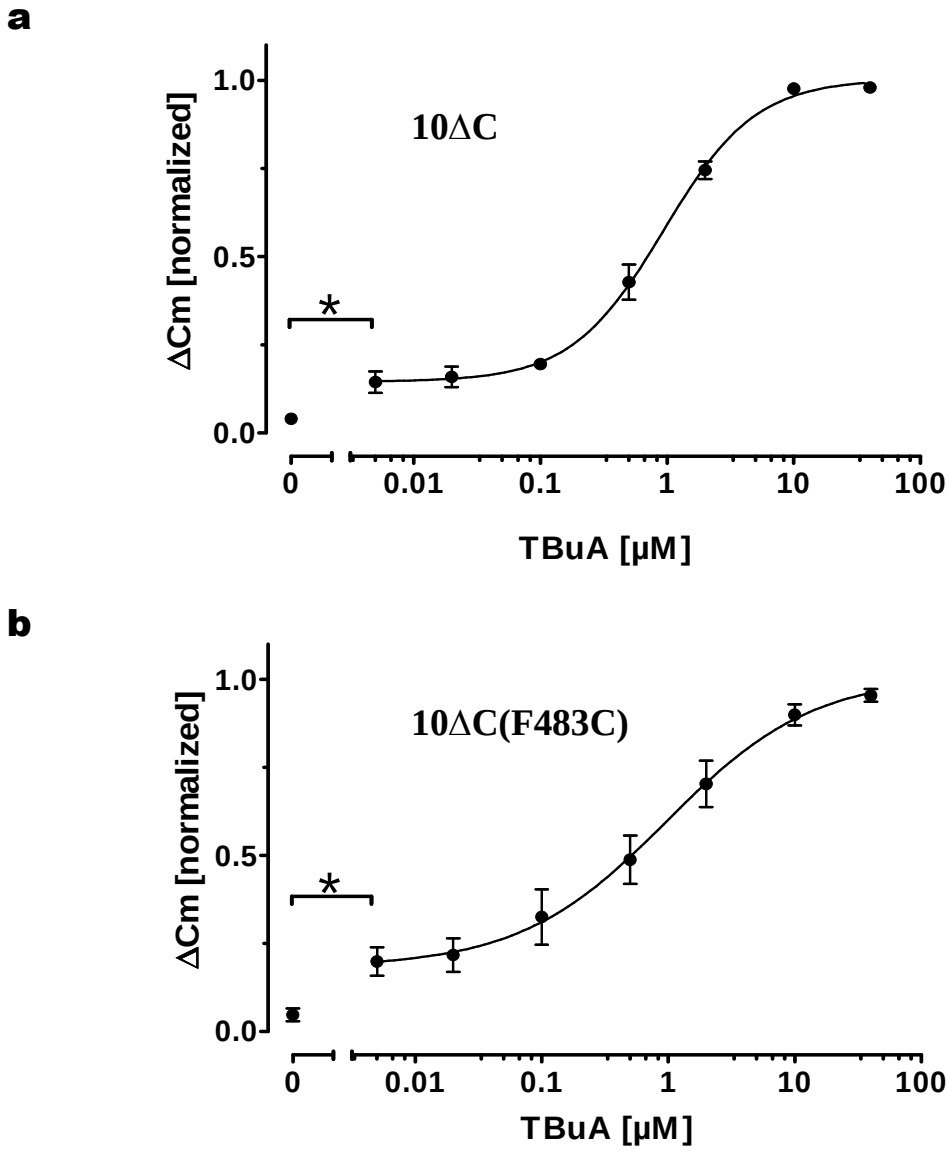

Figure 20. Concentration dependence of TBuA-induced capacitance changes. Oocytes expressing 10ΔC (***a***) or 10ΔC(F483C) (***b***) were clamped to -50 mV. Membrane capacitance was monitored upon exchange of Ori buffer with Ori (zero TBuA concentration) or with Ori containing different concentrations of TBuA. Capacitance changes ΔCm were normalized within a single experiment to a maximal saturation value derived from fitting of data (excluding value corresponding to zero TBuA concentration) to a Hill equation. Mean values ± S.E. of 4 experiments are presented. *, $P < 0.05$ (Student's *t* test)

3.3.2. Inhibition by TBuA of MPP or TEA uptake by 10ΔC(F483C)

To measure affinity of nontransported ligands, an inhibition study can be performed alternatively to binding measurements. We investigated the effect of cysteine replacement of F483 on the inhibition of MPP and TEA uptake by TBuA. 10ΔC(F483C) was expressed in oocytes and uptake of 2.5 nM [^{3}H]MPP was determined in the presence of various concentrations of TBuA (Fig. 21a, *open squares*). MPP concentration used for uptake measurements is 1000 times lower than the K_M for MPP; thus, competitive interactions at the transport site can be neglected. The inhibition curve could be satisfactorily fitted to a single-site inhibition model. An IC_{50} value of 22 ± 4.5 nM (n = 5) was obtained. Similar value of 24 ± 1.3 nM (n = 2) was determined in oocytes expressing 10ΔC(F483C) that were incubated for 5 min with 100 µM TMR6M (Fig. 21a, *closed circles*). Noteworthy, values 15 to 20 times higher were obtained for 10ΔC (340 ± 70 nM; n = 3; Fig. 21a, *open triangles*) and with wildtype rOCT1 (460 ± 100 nM; n = 3; Fig. 21a, *open circles*). To determine whether the high-affinity inhibition of 10ΔC(F483C) by TBuA is dependent on the substrate, the concentration dependence for inhibition of TEA uptake by 10ΔC(F483C) was measured in comparison to 10ΔC and wildtype rOCT1 (Fig. 21b). The measurements were performed with 9 µM [^{14}C]TEA, the concentration which is at least 5 times below the K_M values. For TBuA inhibition of TEA uptake, similar IC_{50} values were determined as for TBuA inhibition of MPP uptake (10ΔC(F483C), 11.3 ± 1.3 nM, n = 3; 10ΔC, 280 ± 70 nM, n = 3; rOCT1, 620 ± 40 nM, n = 3).

The IC_{50} values for inhibition of 10ΔC and rOCT1 by TBuA were close to each other and to the K_d value of TBuA binding to 10ΔC obtained by capacitance measurements, whereas the IC_{50} values for inhibition of 10ΔC(F483C) were significantly less than corresponding values for 10ΔC or rOCT1, as well as K_d of TBuA binding at low affinity site identified by capacitance measurements (1.06 ± 0.37 µM) or fluorescence measurements (around 0.3 µM). At the same time, the IC_{50} values were significantly higher than K_d of high-affinity sites identified by fluorescence measurements (site 1, 2 pM; site 2, 0.35 ÷ 0.65 nM). A possible explanation is that binding of TBuA at high-affinity binding site(s) of 10ΔC(F483C) induces an allosteric interaction between this site and low-affinity transport site for MPP or TEA that leads to blocking of transport. Since concentrations of MPP (2.5 nM) or TEA (9µM) used for transport measurements are saturating for high-affinity binding sites of MPP (around 30 pM) or TEA (around 30 nM), there may be a competition (although not necessarily pure competitive) of TBuA with MPP or TEA for high-affinity binding site(s), which leads to increase of the apparent inhibitory constant.

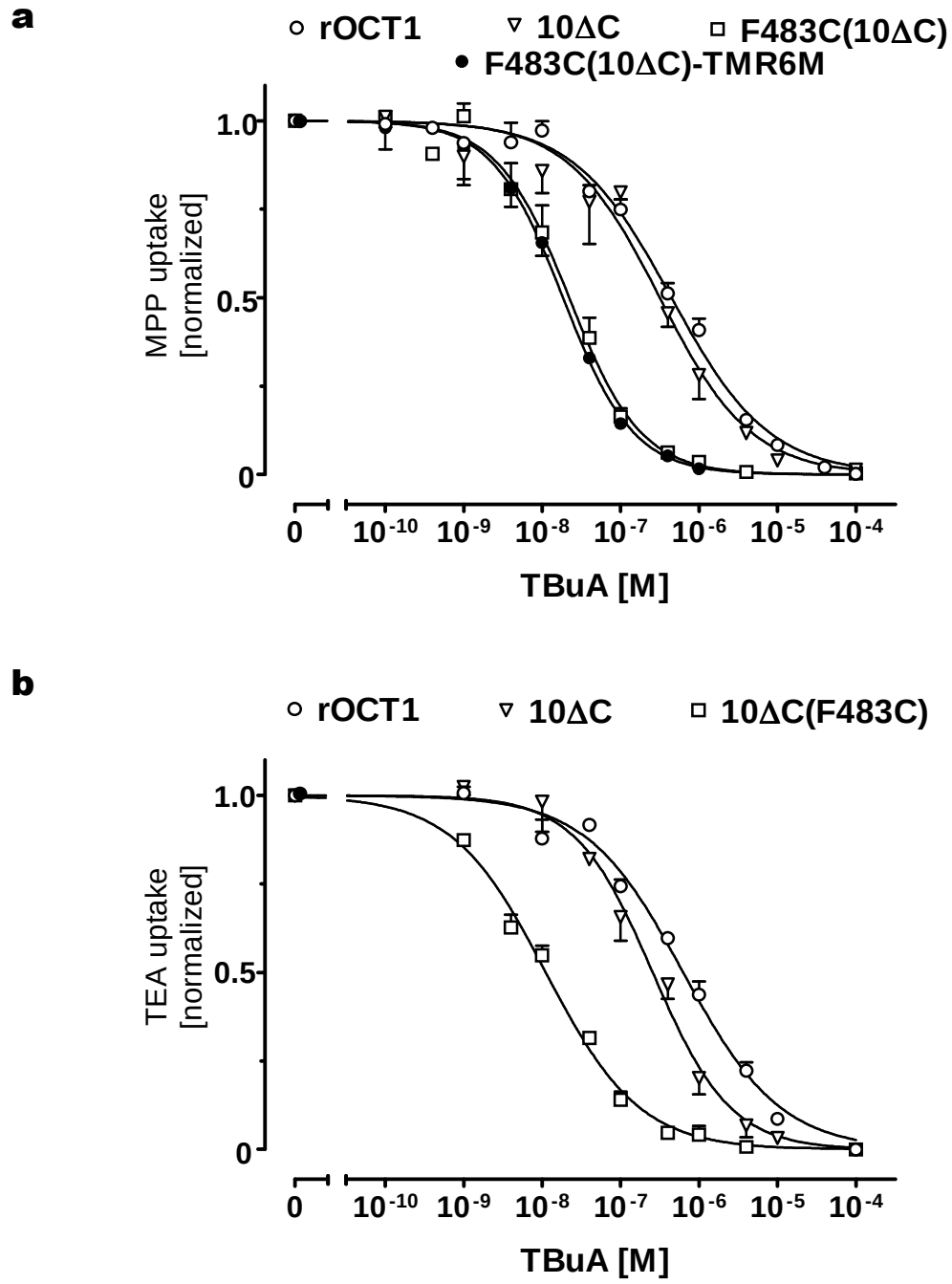

Figure 21. TBuA-mediated high-affinity inhibition of cation uptake by 10ΔC(F483C). rOCT1, 10ΔC, or 10ΔC(F483C) were expressed in oocytes. In one experimental series, 10ΔC(F483C) was labeled by incubating the oocytes for 5 min with 100 µMTMR6M [10ΔC(F483C)-TMR6M)]. Uptake of 2.5 nM [^{3}H]MPP (***a***) or 9 µM [^{14}C]TEA (***b***) was measured in the presence of various concentrations of TBuA. Mean values ± S.E. of three to five or of two [10ΔC(F483C)-TMR6M)] individual experiments are shown. The data were fitted to a Hill equation.

We tested whether MPP at concentrations in the range of the K_M value for MPP uptake (~3 µM; Table 1) competes for high-affinity inhibition of MPP uptake by TBuA in oocytes expressing 10ΔC(F483C) (Fig. 22). The concentration dependence of TBuA

inhibition using MPP concentrations of 2.5 nM, 2 µM, and 40 µM was measured. The obtained IC_{50} values increased with increasing concentrations of MPP (2.5 nM MPP, 22 ± 1 nM; 2 µM MPP, 40 ± 5 nM; 40 µM MPP, 296 ± 21 nM). Assuming competitive inhibition and a K_M value for MPP of 3 µM, similar *Ki* values were calculated (2.5 nM MPP, 22 ± 1 nM; 2 µM MPP, 23 ± 3 nM; 40 µM MPP, 20 ± 1 nM; n = 3 each). These data suggest competition between the high-affinity inhibitory site of TBuA and the low-affinity transport site of MPP.

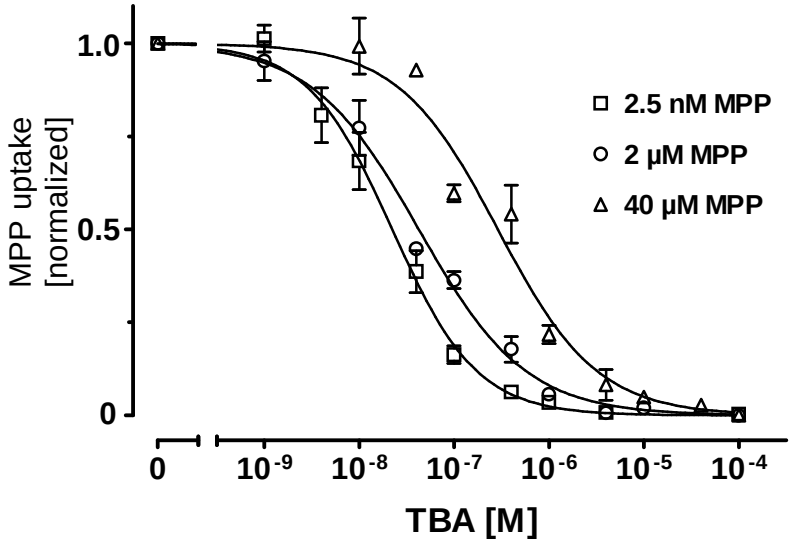

Figure 22. Competition between the high-affinity TBuA inhibition site and the low-affinity MPP transport site in 10ΔC(F483C). Inhibition by TBuA of [^{3}H]MPP uptake in oocytes expressing 10ΔC(F483C) was measured using different MPP concentrations. Mean values ± S.E. of 3 experiments are presented. Data were fitted to a Hill equation.

3.3.3. Effect of mutations in TMHs 2 and 11 on inhibition of MPP uptake by TBuA

Presence of an allosteric interaction between high- and low-affinity binding sites introduced (or intensified) by mutation F483C assumes an impaired interaction between different parts or domains of the protein. Previously described model structure of rOCT1 with an inward-facing substrate binding pocket (Popp et al., 2005) suggests that F483 is located outside the substrate binding pocket in the region which may be involved in contact between TMHs 2 and 11 (Fig. 23). It is possible that the F483C exchange disturbs the interaction between these TMHs and that binding of TBuA to a high-affinity binding site in distant substrate binding region can block a transport-related conformational changes in the destabilized 10ΔC(F483C) mutant but not in 10ΔC or in rOCT1. Interestingly, according to

the model, two conserved amino acid residues in the TMH 2 (W147 and D150) and two conserved residues in the TMH 11 (F483 and F486) are located in close proximity; three of four amino acids are aromatic and can be involved into aromatic interactions.

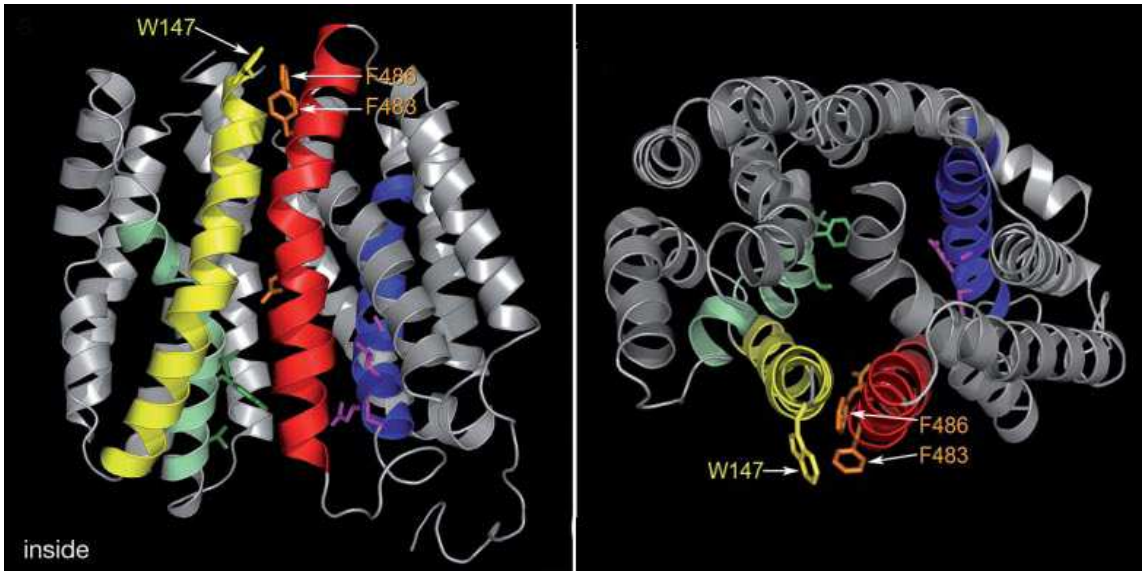

Figure 23. Presumed contact area between TMHs 2 and 11. Ribbon representation of a model structure of rOCT1. TMH 2 is coloured in yellow, and TMH 11 in red. ***Left panel***, view parallel to membrane; ***right panel***, view from extracellular side. Arrows point to aromatic amino acids of TMH 2 (W147) and 11 (F483, F486).

To test the hypothesis of the involvement of TMHs 2 and 11 into contact, amino acids W147, D150 and F486 were substituted for cysteines in 10ΔC, and effect of single mutations on the inhibition of MPP uptake by TBuA was assessed. Figure 24a shows inhibition curves obtained for the mutants. After exchange D150C, the affinity for inhibition of MPP uptake by TBuA was not changed (IC_{50} of 0.31 ± 0.09 µM; n = 3). However, when W147 was replaced by cysteine, the affinity for TBuA inhibition of MPP uptake was increased to approximately the same value (IC_{50} of 16 ± 3.5 nM; n = 3) as in the case of 10ΔC(F483C) (IC_{50} of 22 ± 4.5 nM; n = 5). Similar IC_{50} value was obtained when W147 was substituted to serine (18 ± 1 nM, n = 3). Remarkably, the same affinity for inhibition of MPP uptake by TBuA was obtained when F486 was replaced by cysteine (IC_{50} of 23 ± 4.0 nM, n = 3). Taking together, virtually the same increase in affinity for TBuA inhibition of MPP uptake compared with 10ΔC was obtained when any of three aromatic amino acids within the predicted contact area between two TMHs was replaced by cysteine. It strongly supports the initial hypothesis that binding and /or transport of ligands involves interaction between the TMHs 2 and 11.

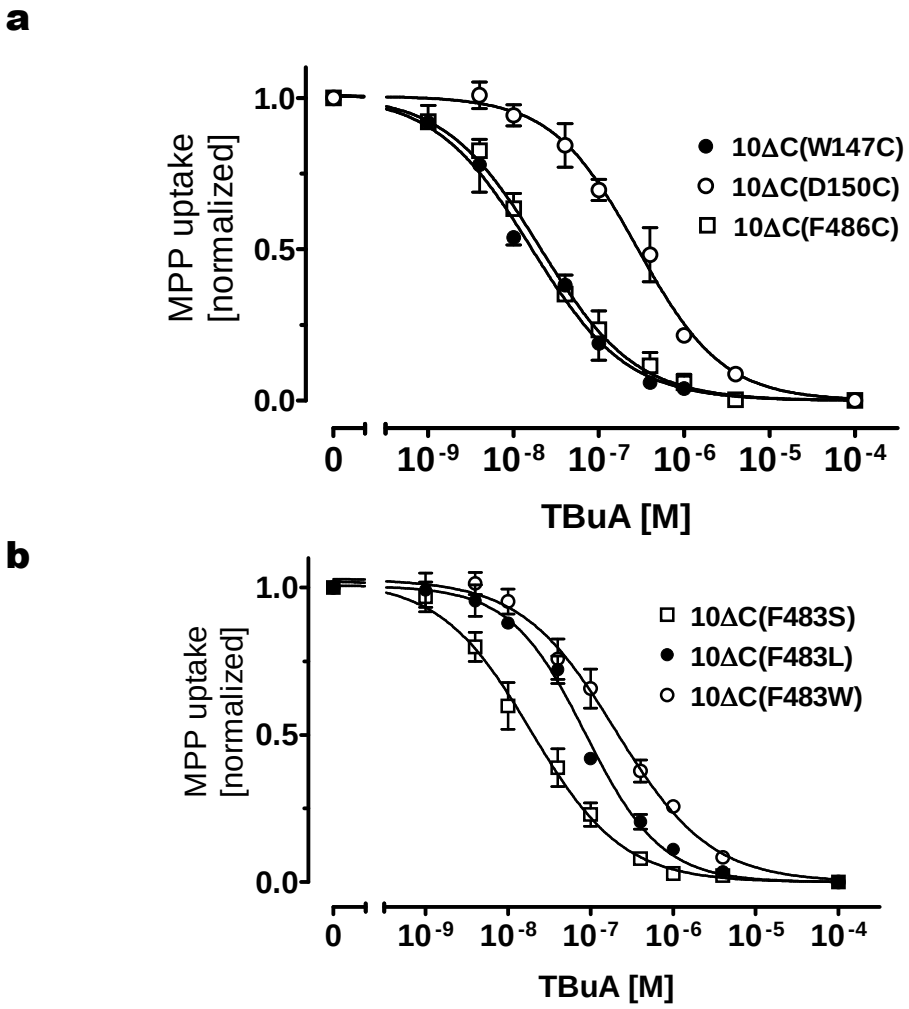

Figure 24. Inhibition of MPP uptake by TBuA in mutants of 10ΔC with exchanged amino acids within TMHs 2 and 11. Mutants of 10ΔC containing single cysteine substitution (***a***) or single amino acid exchange of F483 to serine, leucine or tryptophan (***b***) were expressed in oocytes. Uptake of 2.5 nM [^{3}H]MPP was measured in the presence of various concentrations of TBuA. Mean values ± S.E. of three individual experiments are presented. The data were fitted to a Hill equation.

To test the importance of structural properties of amino acid at position 483, inhibition of MPP uptake by TBuA was measured when F483 was replaced by serine, leucine, or tryptophan (Fig. 24b). For mutant 10ΔC(F483S), a similar IC_{50} value (28 ± 7 nM; n = 3) was obtained for inhibition of MPP uptake by TBuA as for 10ΔC(F483C). This suggests that serine and cysteine disturb the hydrophobic interaction between the TMH 2 and 11 in a similar manner. However, after replacement of F483 by leucine, the IC_{50} of TBuA for inhibition of MPP-uptake was decreased only 4-fold (IC_{50} = 84 ± 9 nM; n = 3). The inhibition by TBuA remained unchanged when F483 was replaced by bulkier but aromatic tryptophan (IC_{50} = 230 ± 60 nM; n = 3). It suggests that a tryptophan in position 483 mediates a

sufficiently strong hydrophobic interaction with the TMH 2 similar to a phenylalanine, whereas leucine is only partially effective.

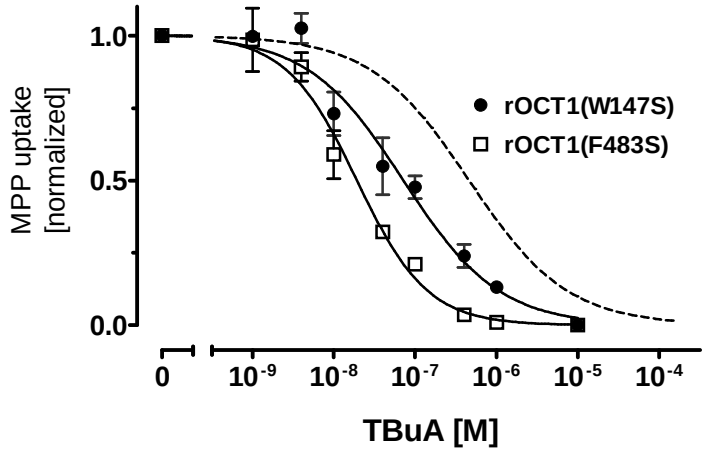

Figure 25. Inhibition of MPP uptake by TBuA in mutants of rOCT1 with exchanged amino acids within TMHs 2 and 11. Mutants of rOCT1 containing single amino acid substitution to serine were expressed in oocytes. Uptake of 2.5 nM [^{3}H]MPP was measured in the presence of various concentrations of TBuA. Mean values ± S.E. of three individual experiments are presented. The data were fitted to a Hill equation. *Broken line* represents inhibition curve obtained for rOCT1.

Although 10ΔC demonstrated same low-affinity inhibition by TBuA as wildtype rOCT1, it could not be excluded that high-affinity inhibition after single mutations in 10ΔC may be induced by multiple mutations in comparison to wildtype rOCT1. Therefore, it was necessary to check whether the affinity increase of TBuA to inhibit MPP uptake observed after replacement of F483 or W147 in 10ΔC by serine could be observed when these mutations were introduced into wildtype rOCT1. Figure 25 shows dose-response curves obtained for the inhibition of [^{3}H]MPP (2.5 nM) uptake by TBuA in oocytes expressing wildtype rOCT1, rOCT1(F483S), or rOCT1(W147S). Similar to respective mutations introduced into 10ΔC, both mutations in rOCT1 led to a significant increase in affinity (IC_{50} values: rOCT1, 460 ± 60 nM; rOCT1(F483S), 19 ± 4 nM; and rOCT1(W147S), 71 ± 9 nM; n = 3 for each). Although the affinity of rOCT1(W147S) was lower compared with 10ΔC(W147S) or rOCT1(F483S), these data indicate that the increase of TBuA inhibition efficiency for MPP-uptake observed after mutations of F483 or W147 in 10ΔC, represents intrinsic properties of rOCT1.

4. Discussion

The data obtained in this study demonstrate conformational changes in rOCT1 which are associated with transport. To detect conformational changes, an environment-sensitive fluorescent dye tetramethylrhodamine-6-maleimide (TMR6M) was attached at a specific point of the transporter molecule, and fluorescence changes were recorded in response to changes of membrane potential and substrate concentration.

Changes of TMR6M-fluorescence intensity reflect changes of physico-chemical properties of the local environment of the dye and thus reflect local movements (Cha and Bezanilla., 1997, 1998; Gandhi and Isacoff, 2005). Reasoning that overall conformational changes of a protein are coordinated movements of domains, monitoring of local changes can be used for tracking of conformational changes, although limitations of such approach should be considered (Gandhi et al., 2000; Gandhi and Isacoff, 2005).

4.1. Fluorescence labeling of rOCT1 and mutants

We have introduced 22 single cysteine substitutions in the extracellular ends of TMHs 4, 11, and corresponding flanking extracellular loops which can also be part of the respective TMHs (Fig. 6) (Popp et al., 2005; Zhang et al., 2005). These TMHs are thought to be part of a binding pocket (see INTRODUCTION, Fig. 3); thus, we expected that they could undergo specific conformational changes which could be tracked after site-specific covalent attachement of TMR6M.

Labeling of the transporter with TMR6M at positions 483 and 486 in TMH 11 resulted in formation of a fluorescent sensor fluorescence intencity of which has changed in a substrate- and voltage-dependent manner. Other cysteine susbtitutions in TMH4 and TMH 11, as well as natural cysteines of wildtype rOCT1 (this study) and W147C in TMH2 (T. Friedrich, personal communication), did not show fluorescence changes after treatment with TMR6M. This may have several reasons. First, TMR6M-labeling may be essentially limited or not possible at some positions because of the inaccessibility of the introduced cysteines to the fluorophore. Second, covalent modification may lead to inactivation of transporter disabling conformational changes. However, nearly all mutants were active after treatment with TMR6M (with exception of substitutions K215C and D475C which inactivate the transporter), although extents of labeling have not been established. Finally, it is possible that

environmental conditions (e.g., hydrophobicity) of the bound TMR6M are not changing during conformational transitions of the transporter. Thus, the absence of fluorescence changes does not exclude that the part of the protein containing TMR6M-labeled cysteine moves during transport.

4.2. Conformational changes of TMR6M-labeled transporter in the absence of organic cations

Fluorescence changes observed for the mutant 10ΔC(F483C) demonstrate that transporter can undergo conformational changes in a voltage-dependent manner. Voltage dependence of fluorescence changes can be described by Boltzmann equation which suggests that transporter can occupy two principal states in the absence of a ligand. Hyper- or depolarization drives the transporter into one corresponding state; however, at resting membrane potential, one state does not essentially prevail over another.

The observed voltage dependence of conformation changes in the absence of organic cations can be due to voltage-dependent binding and debinding of an inorganic ion(s) or conformational changes associated with mobile charge of the protein (Läuger and Jauch, 1986; Mager et al., 1998; Bezanilla, 2008). In the first case, time constants of fluorescence relaxations would demonstrate a strong dependence on membrane potential (Li et al., 2000; Loo et al., 2005; Virkki et al., 2006), whereas time constants of relaxations associated with mobile charge are independent of voltage (Ghanda et al., 2002; 2004). These data suggest that rOCT1 exhibits a conformational flexibility associated with intrinsic mobile charge, i.e. that some mobile domain(s) of the transporter carries a net charge. Fluorescence measurements do not allow to determine whether the mobile charge is positive or negative, since the physical nature of quenching of rhodamine dyes is not dependent on behaviour of the charge in an electrical field (Cha and Bezanilla, 1997, 1998). Speculating that cation selectivity of rOCT1 may be governed by a negative charge within the permeation pathway, the same charge can be invoked to explain an electrogenic conformational change, as it was suggested for ligand-induced electrogenic conformation change in rOCT2 (Schmitt and Koepsell, 2005).

Experimental data obtained for OCTs point to an alternating-access mechanism as the one employed by these transporters (see INTRODUCTION, section 1.3). This is in agreement with data suggesting an alternating-access as a common mechanism for transporters of the MFS superfamily (Guan and Kaback, 2005; Low et al., 2008). In this term, transporter switches between inward- and outward-open conformations. It looks plausible that

the conformational change in the absence of ligands is indeed transition between these two conformations. The rate of this transition, characterized by fast fluorescence changes, is in the range of 40-100 s^{-1} which is in agreement with estimated turnover number of rOCT1 reconstituted in proteoliposomes (>20 s^{-1}, Keller et al., 2005). The slow component of fluorescence changes occurred on much slower time scale (τ ~ 0.1 s) and with low amplitudes. Although the possibility that the slow fluorescence changes characterize another conformation change of the transporter cannot be ruled out, it is likely that they are due to interaction of the fluorophore with a nearby part of the protein. Vanishing of the slow component in the presence of low concentration of ligands (at concentrations saturating high-affinity binding site(s) but not low affinity transport site, see below) supports the last scenario. In this case, binding at high-affinity site may spatially constrain the mobility of TMH 11 (or its extracellullar part with attached TMR6M) or of nearby protein domain. However, without determination of the physical mechanism of change of the fluorescence intensity (change of the quantum yield due to interaction with quencher, or reorientation of the fluorophore, or spectral shift of the excitation) (Cha and Bezanilla, 1997, 1998), this question cannot be solved unambiguously.

4.3. Conformational changes of TMR6M-labeled transporter in the presence of organic cations

Using effects of the organic cations on potential-dependent fluorescence changes of TMR6M-labeled 10ΔC(F483C) as a readout for ligand binding, we were able to demonstrate presence of high- an low-affinity binding site in 10ΔC(F483C). It looks probable that low-affinity binding constants determined by fluorescence measurements reflect binding to the site associated with transport of substrates. This is suggested by the similarity of the low-affinity constants to K_M values determined by transport- or current measurements, or to K_d value for TBuA determined by capacitance measurements. The presence of high-affinity binding in rOCT1, which is not associated with translocation of the substrate, is a novel finding which is discussed latter.

Noteworthy, considerations of fluorescence changes in the absence of ligands are also valid for the situation when ligands at low concentrations are present. Binding of choline or TBuA at high-affinity site(s) shifts $V_{0.5}$ values of ΔF-V curves to depolarized potentials suggesting stabilization of one particular conformation at physiological potentials. Physiological significance of this phenomenon is not clear, but one can speculate that

stabilization of a certain conformation of the transporter may influence an efficiency of interaction of substrates at the low-affinity binding site associated with transport.

While choline is a substrate of OCTs that can be translocated across the membrane, TBuA was shown not to be transported by rOCT1 (Arndt et al., 2001) and not to induce current in 10ΔC or 10ΔC(F483C) injected *Xenopus* oocytes. Since TBuA is a competitive inhibitor for most substrates of rOCT1 (Gorboulev et al., 1999; Dresser et al., 2002, and this study), one can conclude that TBuA can bind within the binding pocket in the outward-open conformation; this is true at least for the low-affinity binding of TBuA. Similarity of fluorescence changes of 10ΔC(F483C) in the presence of saturating concentrations of choline or TBuA suggests that (*i*) transporter with bound TBuA is not locked in one conformation but can switch between at least two states; and (*ii*) these states are associated with translocation of organic cations across the membrane. Interestingly, molecular dynamics simulations of LacY (Holyoake and Sansom, 2007) and measurements of interhelical distances in LacY at periplasmic or cytoplasmic site of the membrane (Majumdar et al., 2007; Smirnova et al., 2007) showed that transporter with bound ligand can occupy a stable intermediate conformation with internal cleft closed on both sides of the membrane. Similar compact conformation was also suggested by electron crystallography study of MdfA, a multidrug transporter from MFS (Sigal et al., 2007). This “closed” state resembles the “occluded” conformation of crystallized EmrD (Yin et al., 2006), another multidrug transporter from MFS. Considering these data, one can suggest that TBuA bound inside the binding pocket does not prevent closing of cleft on extracellular side.

Interestingly, voltage-dependent fluorescence changes of TMR6M at positions 483 or 486 are different in the absence of ligands but not in the presence of saturating concentrations of ligands. In the absence of ligands 10ΔC(F483C) but not 10ΔC(F486C) showed fluorescence changes, whereas in the presence of saturating concentrations of ligands fluorescence changes were similar for both mutants. It suggests that TMR6M at position 486 is exposed to a constant environment upon conformational changes of empty transporter, whereas conformational changes of loaded transporter induce similar changes of TMR6M-environment at both positions. Thus, conformations of TMH11 upon conformational changes of empty or loaded transporter are not completely identical, a conclusion which appears intuitive but is not obvious from analysis of fluorescence changes of a single mutant, since fluorescence changes under saturating concentrations of ligand (i.e., under transport mode) can be contributed from multiple states of the transport cycle. Althoug available data suggest that general fold of MFS transporters in the bound state is similar to empty state, different

bending or winding of transmembrane helices cannot be excluded (Holyoake and Sansom, 2007; Lemieux M., 2007).

4.4. High- and low-affinity binding sites of rOCT1

Different ligands induced similar effect on voltage jumps-induced fluorescence changes, although with different efficiency. Lower values of K_d at high-affinity sites as well as at low-affinity sites were detected for bulkier MPP and TBuA than for choline and TEA. It is noteworthy that the affinities of the high- and low-affinity sites are highly different for different ligands: for example, K_d values for TBuA are ~2 pM, ~0.5 nM, and ~0.3 µM, while K_d values for choline are ~10 nM and ~0.3 mM.

To avoid artifacts by TMR6M labeling of endogenous cysteines in rOCT1, we performed the fluorescence measurements by introducing cysteine residues in mutant 10ΔC in which all cysteines, with the exception of those in the large extracellular loop, were removed. In principle, it cannot be excluded that the affinities for cations were influenced by the mutations or by the labeling of C483 with TMR6M. However, for the following reasons it is highly probable that wild-type rOCT1 contains similar high-affinity binding sites. First, it seems highly improbable that new high- affinity binding site(s) is(are) generated by removal of endogenous cysteine residues and/or replacement of amino acid residues with cysteines followed by labeling with TMR6M. Specific conservative mutations may increase the affinity of a pre-existing binding site (Gorboulev et al., 2005; Popp et al., 2005); however, multiple mutations are not supposed to form binding sites that do not exist in the wild-type transporter. Second, by inhibition experiments, we detected a high-affinity TBuA binding site with the same affinity in 10ΔC(F483C), TMR6M-labeled 10ΔC(F483C), 10ΔC(F483S), 10ΔC(W147C), rOCT1(F483S), and rOCT1(W147S). In the last two cases, perturbation of the structure is reduced to a single amino acid substitution. Third, capacitance measurements in *Xenopus* oocytes expressing *10*ΔC or 10ΔC(F483C) also suggest the existence of a high-affinity TBuA binding site with a K_d < 5 nM. The existence of a high-affinity MPP binding site of human organic cation transporter OCT1, with a K_d of ~6 pM, has been demonstrated by replacement liquid chromatography for the solubilized and immobilized transporter (Moaddel et al., 2005). Notably, this value of K_d is close to the value of high-affinity K_d obtained in this study for 10ΔC(F483C) (~30 pM, Table 2). Finally, recent study on interactions of hOCT1, hOCT2, and hOCT3 with antiviral nucleoside drugs clearly demonstrated biphasic inhibition of MPP uptake by 2',3'-dideoxy-3'-thiacytidine: IC_{50} values

for high- and low-affinity inhibition were determined in the range of 10 − 20 pM and 1 − 5 mM, respectively (G. Menuesa and H. Koepsell, unpublished data).

So far, high-affinity binding has been shown for model ligands of OCTs or drug, among which only choline is a physiological organic cation. Whether high-affinity binding site is relevant for other ligands of OCTs, is not known. Nevertheless, since high-affinity binding constant of choline is ~15 nM, a concentration which can be considerably lower than the concentration of choline in body fluids (Klein et al., 1993), it suggests that high-affinity site(s) of transporter in the plasma membrane of cells is(are) occupied most of the time .

Our observations open interesting perspectives concerning evolutionary development of high-affinity binding sites in rOCT1, their physiological importance, and putative biomedical implications. Polyspecific transporters that excrete xenobiotics may have been evolved to protect organisms from xenobiotics in the environment. Transporters for endogenous compounds such as choline or monoamine neurotransmitters may have achieved the capability for polyspecific substrate recognition by developing a binding region that contains interaction sites for various compounds. The existence of a polyspecific binding region in organic cation transporters was suggested by single point mutations that led to affinity changes for individual cations (Gorboulev et al., 1999, 2005; Popp et al., 2005; Zhang et al., 2005), by model analysis of OCTs (Popp et al., 2005; Zhang et al., 2005; C. Volk, V. Gorboulev, and H. Koepsell, unpublished data), and by results presented in this study.

While it can easily be imagined that the substrate binding region of organic cation transporters serves as collector for organic cations with different chemical structures, it is not obvious how the binding of cations at various sites may lead to cation translocation. It is possible that translocation is facilitated only when a low-affinity cation binding site is occupied. Measurements of the concentration dependence of [^{3}H]MPP uptake at low MPP concentrations (1 pM to 100 nM MPP in human embryonic kidney 293 cells stably transfected with rOCT1) could not resolve high-affinity transport suggesting that high-affinity cation binding in rOCT1 may not be able to induce translocation (H. Koepsell, unpublished data). However, since the translocation probably includes a large conformational change in which a binding pocket containing different binding sites switches between an outward- and inward-facing orientations, cations bound to high-affinity binding site may be translocated together with cations at a low-affinity site. Considering slow dissociation rate of substrate in the case of the high-affinity binding, it is unlikely that transport can be operated via high-affinity site. On the other hand, structural changes within the binding pocket during transition from the outward to inward facing orientation may facilitate intracellular release of substrates

(Volk et al., 2003). However, structural changes which can induce considerable change of affinity would require sufficient energy that seems irrelevant to uniport mechanism of transport driven by electrochemical potential of substrate.

4.5. Perturbation of interaction between TMHs 2 and 11 by mutations in a presumed contact region

Transport of organic cations may be inhibited in several ways. In addition to competition between two transported cations at the low-affinity transport site, cations bound to low- or high-affinity sites may block the transport mechanism. For example, a bulky cation bound to the low-affinity transport site may not be able to pass a pore-like structure (Schmitt and Koepsell, 2005), or it may directly block the transport. Another possibility is that binding of a bulky cation to a high-affinity site blocks a transport-relevant conformational change. Such a mechanism may include subtle allosteric structural changes that may cause dramatic effects on transport.

This study provides an example how destabilization of the tertiary structure of rOCT1 at a model-predicted interaction area between the TMH 2 and 11 allows or alters an allosteric effect after binding of TBuA to a high-affinity site. Whereas TBuA does not induce high-affinity inhibition of MPP or TEA transport by wild-type rOCT1 or 10ΔC, cation transport can be blocked already at very low TBuA concentrations upon replacement of F483, F486, or W147 at the modeled contact area between the TMHs 2 and 11 by small hydrophilic amino acids. It can be hypothesized that this contact area is important for the stabilization of the native conformation of rOCT1 since proteins containing double mutations in this area (W147S/F483S, W147C/F483C, and W147C/F486C) did not reach the plasma membrane upon expression in *Xenopus* oocytes (D. Gorbunov, V. Gorboulev, and H. Koepsell, unpublished data). The observed functional effects of the single point mutations in the modeled contact area allow several conclusions. First, the predicted interaction between the TMH 2 and 11 is critically involved in transport-related conformational changes of rOCT1. The functional importance of this contact region demonstrated in this work supports the proposed tertiary structure model of rOCT1. Second, destabilizing mutants at transport-relevant interaction points between TMHs may be used to detect and characterize high-affinity cation binding sites by inhibition experiments. Third, instead of changing transport of model cations, a transformation of a high-affinity noninhibitory binding site to a high-affinity inhibition site may occur due to mutations in organic cation transporters. Such mutations can

be localized at transport-relevant interaction points between different TMHs or other parts of the transporters that are involved in transport-relevant structural changes. Thus, small concentrations of cationic drugs in the body that do not change the function of wild-type transporters may block transport in patients carrying such mutations in OCT transporters.

In summary, we have shown that OCT1 undergoes conformational changes in voltage-dependent manner, which may represent a switch between inward- and outward-facing conformations of the binding pocket. We have also shown that OCT1 contains high-affinity cation sites in addition to low-affinity transport sites. Cation binding to high-affinity sites may not disturb low-affinity cation transport in wild-type OCT1. However, mutations of amino acids in transport relevant key positions, which can be distinct from the cation binding region, may transform noninhibitory high-affinity binding sites to high-affinity inhibition sites and thereby cause adverse drug reactions in patients.

5. Summary

5.1. Summary

Polyspecific organic cation transporters (OCTs) of the SLC22 family mediate downhill transport of organic cations and play an essential role in excretion and distribution of endogenous organic cations and for the uptake, elimination and distribution of cationic drugs and toxins. Although physiological and pharmacological significance of OCTs is widely accepted, many questions concerning structure and transport mechanism still remain open.

To investigate conformational changes of the rat OCT1 during transport cycle, voltage-clamp fluorometry was performed with a cysteine-deprived mutant in which phenylalanine 483 in transmembrane helix (TMH) 11 close to the extracellular surface was replaced by cysteine and covalently labeled with tetramethylrhodamine-6-maleimide. Potential-dependent fluorescence changes were observed that were sensitive to the presence of substrates choline, tetraethylammonium (TEA), 1-methyl-4-phenylpyridinium (MPP), and of the nontransported inhibitor tetrabutylammonium (TBuA). The data suggest that the transporter undergoes conformational changes in voltage- and substrate-dependent manner which are compatible with alternating access mechanism. Using potential-dependent fluorescence changes as readout, one high-affinity binding site per substrate and two high-affinity binding sites for TBuA were identified in addition to the previously described single interaction sites. Coexisting high-affinity cation binding sites in organic cation transporters may collect xenobiotics and drugs; however, translocation of organic cations across the membrane may only be induced when a low-affinity cation binding site is loaded. Whereas high-affinity binding of TBuA has no effect on cation uptake by wildtype rat OCT1, replacement by cysteine or serine of amino acids W147, F483, and F486 located in a modeled contact region between TMH2 and TMH11 outside the binding pocket leads to inhibition of MPP or TEA uptake. Thus, mutations of amino acids in transport relevant key positions, which can be distinct from the cation binding region, may transform noninhibitory high-affinity binding sites to high-affinity inhibition sites and thereby cause adverse drug reactions in patients.

5.2. Zusammenfassung

Polyspezifische Transporter für organische Kationen (OCTs) der SLC22 Familie transportieren organische Kationen entlang des elektrochemischen Gradienten und spielen eine entscheidende Rolle bei der Ausscheidung und Gewebeverteilung von endogenen organischen Kationen und bei der Aufnahme, Ausscheidung und Verteilung von kationischen Medikamenten und Toxinen. Obwohl die physiologische und pharmakologische Bedeutung von Transportern für organische Kationen allgemein anerkannt ist, bleiben viele Fragen bezüglich der Struktur und des Transportmechanismus dieser Transporter noch offen.

Um Konformationsänderungen von rOCT1 während des Transportzyklus zu untersuchen, wurde die „Voltage-clamp-Fluorometrie“ angewandt, bei der in einer cysteinarmen rOCT1 Mutante Phenylalanin 483 in der Transmembranhelix (TMH) 11 nahe an der extrazellulären Seite der Membran durch Cystein ersetzt und mit Tetramethylrhodamin-6-maleimid kovalent markiert wurde. Dabei wurden spannungsabhängige Fluoreszenzänderungen beobachtet, die durch die Anwesenheit der Substrate - Cholin, Tetraethylammonium (TEA), 1-Methyl-4-phenylpyridinium (MPP) - und des nichttransportierten Hemmstoffes Tetrabutylammonium (TBuA) moduliert wurden. Die gewonnenen Daten deuten darauf hin, dass der Transporter Konformationsänderungen durchläuft, die spannungs- und substratabhängig sind, was mit dem „alternating access“ Mechanismus vereinbar ist.

Die Analyse der spannungsabhängigen Fluoreszenzänderungen zeigte die Existenz je einer hochaffinen Bindungsstelle für Substrate und zweier hochaffinen Bindungsstellen für TBuA zusätzlich zu den früher identifizierten Bindungsstellen. Multiple hochaffine Kationenbindungsstellen in OCTs können Xenobiotika und Arzneimittel anreichern, aber die Translokation von organischen Kationen über die Membran kann erst dann erfolgen, wenn die niederaffine Bindungsstelle besetzt ist.

Während die hochaffine Bindung von TBuA an den Wildtyp rOCT1 keine Wirkung auf die Aufnahme von Kationen hat, führt der Austausch der Aminosäuren W147, F483 und F486, die anhangs des Modells in der Kontaktregion zwischen TMH 2 und TMH 11 außerhalb der Bindungstasche lokalisiert sind, durch Cystein oder Serin zur Hemmung der MPP- und TEA-Aufnahme. Die Mutation der Aminosäuren in den für den Transport entscheidenden Positionen, die sich nicht unbedingt in der Kationenbindungstasche befinden, kann also eine nichtinhibitorische hochaffine Bindungsstelle in eine inhibitorische hochaffine Bindungsstelle umwandeln und dadurch unerwartete Effekte bei der Therapie mit verschiedenen Arzneimitteln hervorrufen.

6. Abbreviations

ΔF	fluorescence change
BES	N,N-Bis-(2-hydroxyethyl)-2-ethansulfonic acid
Ci	Curie (3.7×10^{10} Bequerel)
Cpm	counts per minute
DNA	deoxyribonucleic acid
DNase	deoxyribonuclease
DMSO	dimethylsulfoxide
EtOH	ethanol
Fig.	Figure
MFS	N,N-bis[2-Hydroxyethyl]-2-aminoethansulfonic acid
MOPS	3-Morpholino-2-Hydroxypropanesulfonic acid
MPP	1-Methyl-4-phenylpyridinium
mRNA	messenger ribonucleic acid
OAT	organic anion transporter
OCT	organic cation transporter
OCTN	organic cation/carnitine transporter
PAH	para-aminohippuric acid
PCR	polymerase chain reaction
RNA	ribonucleic acid
RNase	ribonuklease
rpm	rounds per minute
S.E.	standard error
Tab.	Table
TBuA	tetrabuthylammonium
TEA	tetraethylammonium
TEVC	two-electrodes voltage clamp
TMA	tetramethylammonium
TMH	transmembrane helix
TMR6M	tetramethylrhodamine-6-maleimide
TPeA	tetrapenthylammonium
(v/v)	volume per volume
(w/v)	weight per volume

prefixes:

h	human
m	mouse
r	rat
rb	rb

7. Acknowledgements

First of all, I am very grateful to Prof. Dr. Hermann Koepsell for giving me the opportunity to work in his laboratory, for many fruitful discussions we have had, and for supervising my scientific work. I also want to thank Prof. Dr. Rainer Hedrich for his co-supervision.

I am thankful to Dr. Valentin Gorboulev who has generously provided me with the constructs for expression of rOCT1 and mutants. I also appreciate keenly his openness for discussion and general help from my first days in Germany.

A part of the work was performed at MPI for Biophysics in Frankfurt (Main) in collaboration with Prof. Dr. Ernest Bamberg and Dr. Thomas Friedrich whom I want to thank for providing me with this opportunity. I am grateful to Dr. Thomas Friedrich for teaching me voltage clamp-fluorometry measurements.

I would like to acknowledge Dr. Bernhard Schmitt for teaching me the basics of electrophysiology, for his help and valuable advices.

A special thanks goes to Irina Schatz for the great technical assistance in synthesis of constructs.

I am very thankful to Alina Filatova who made a lot of corrections to convert early drafts into readable text.

I would like to thank people from the groups of Prof. Koepsell and Prof. Bamberg who worked together with me and to whom I always could turn for discussion and help.

8. List of Publications

1. Schmitt B., Gorbunov D. (equal co-author), Schlachtbauer P., Mueller T., and Koepsell H. Charge-to-substrate ratio during organic cation uptake by rat OCT2 varies with substrate, voltage and inorganic ions. *Submitted*.
2. Gorbunov D., Gorboulev V., Shatskaya N., Mueller T., Bamberg E., Friedrich T., and Koepsell H. High-affinity Cation Binding to Transporter OCT1 Induces Movement of Helix 11 and Blocks Transport after Mutations in a Modelled Interaction Domain between Two Helices. *Mol Pharmacol* (2008) 73(1): 50-61.
3. Sturm A., Gorboulev V., Gorbunov D., Keller T., Volk C.,Schmitt B., Schlachtbauer P., Grummich O., Ciarimboli G., , Schlatter E., and Koepsell H. Identification of cysteines in rat organic cation transporters rOCT1 (C322, C451) and rOCT2 (C451) critical for transport activity and substrate affinity. *Am Jour Physiol Ren Physiol* (2007) 293(3): F767-79.
4. Karataeva N., Gorbunov D., Prokudin I., Buneva V., Kulminskaya A., Neustroev K., and Nevinsky G. Human milk antibodies with polysaccharide kinase activity. *Immun Lett* (2006) 103(1): 58-67.
5. Gorbunov D., Karataeva N., Buneva V., and Nevinsky G. Lipid kinase activity of antibodies from milk of clinically healthy human mothers. *Biochim Biophys Acta* (2005) 1735(3): 153-166.
6. Popp C., Gorboulev V., Mueller T., Gorbunov D., Shatskaya N., and Koepsell H. Amino acids critical for substrate affinity of rat organic cation transporter 1 line the substrate binding region in a model derived from the tertiary structure of lactose permease. *Mol Pharmacol* (2005) 67(5): 1600-1611.
7. Kerb R., Brinkmann U., Chatskaia N., Gorbunov D., Gorboulev V., Mornhinweg E., Keil A., Eichelbaum M., and Koepsell H. Identification of genetic variations of the human organic cation transporter hOCT1 and their functional consequences. *Pharmacogenetics* (2002)12(8): 591-595.
8. Gorbunov D., Semenov D., Shipitsin M., Kit Y., Kanyshkova T., Buneva V., and Nevinsky G. Phosphorylation of minor lipids of human milk tightly bound to secretory immunoglobulin A. *Russ Jour Immun* (2000) 5(3): 267-278.

9. Curriculum Vitae

Name:	Dmitry Gorbunov
Date of Birth:	November 18, 1976
Place of Birth:	Tokmak (Rep. of Kyrgyzstan, UdSSR)
Nationality:	Russian

Education:

Sept. 1994 – June 1999	Novosibirsk State University, Novosibirsk, Russia Graduate student at the Faculty of Natural Sciences, Biology Department Specialization “Molecular Biology and Biochemistry”
Sept. 1997 – June 1999	Novosibirsk Institute of Bioorganic Chemistry, Novosibirsk, Russia Diploma student at the Laboratory of Reparation Enzymes
Sept. 1999 – Feb. 2002	Novosibirsk Institute of Bioorganic Chemistry Postgraduate student, scientific co-worker
March 2002 – March 2008	Institute of Anatomy and Cell Biology, University of Wuerzburg, Wuerzburg, Germany PhD student, scientific co-worker

10. References

Aleboyeh M., Takeda M., Onozato M., Tojo A., Noshiro R., Hasannejad H., Inatomi H., Narikawa S., Huang X., Khamdang S., Anzai N., and H. Endou. 2003. Expression of human organic anion transporter in the choroid plexus and their interactions with neurotransmitter metabolites. *Jour Pharmacol Sci*. 93: 430-436.

Alnouti Y., Petrick J., and C. Klaassen. 2006. Tissue distribution and ontogeny of organic cation transporters in mice. *Drug Metab Dispos*. 34: 477–482.

Amphoux A., Vialou V., Drescher E., Brüss M., La Cour C., Rochat C., Millan M., Giros B., Bönisch H., and S. Gautron. 2006. Differential pharmacological in vitro properties of organic cation transporters and regional distribution in rat brain. *Neuropharmacology*. 50: 941–952.

Anzai N., Jutabha P., Enomoto A., Yokoyama H., Nonoguchi H., Hirata T., Shiraya K., He X., Cha S., Takeda M., Miyazaki H., Sakata T., Tomita K., Igarashi T., Kanai Y., and H. Endou. 2005. Functional characterization of rat organic anion transporter 5 (Slc22a19) at the apical membrane of renal proximal tubules. *Jour Pharmacol Exp Ther*. 315: 534–544.

Anzai N., Kanai Y., and H. Endou. 2006. Organic anion transporter family: current knowledge. *Jour Pharmacol Sci*. 100: 411–426.

Arndt P., Volk C., Gorboulev V., Budiman T., Popp C., Ulzheimer- Teuber I., Akhoundova A., Koppatz S., Bamberg E., Nagel G., and H. Koepsell. 2001. Interaction of cations, anions, and weak base quinine with rat renal cation transporter rOCT2 compared with rOCT1. *Am Jour Physiol Renal Physiol*. 281: F454– F468.

Augustine L., Markelewicz Jr R., Boekelheide K., and N. Cherrington. 2005. Xenobiotic and endobiotic transporter mRNA expression in the blood-testis barrier. *Drug Metab Dispos*. 33: 182–189.

Babu E., Takeda M., Narikawa S., Kobayashi Y., Enomoto A., Tojo A., Cha S., Sekine T., Sakthisekaran D., and H. Endou. 2002. Role of human organic anion transporter 4 in the transport of ochratoxin A. *Biochim Biophys Acta*.1590: 64-75.

Bahn A., Prawitt D., Buttler D., Reid G., Enklaar T., Wolff N., Ebbinghaus C., HillemannA., Schulten H., Gunawan B., Fazesi L., Zabel B., and G. Burckhardt. 2000. Genomic structure and in vivo expression of the human organic anion transporter 1 (hOAT1) gene. Biochem Biophys Res Commun. 275: 623–630.

Bahn A., Ebbinghaus C., Ebbinghaus D., Ponimaskin E., Fuzesi L., Burckhardt G., and Y. Hagos. 2004. Expression studies and functional characterization of renal human organic anion transporter 1 isoforms. *Drug Metab Dispos*. 32: 424-430.

Bahn A., Ljubojevic M., Lorenz H., Schultz C., Ghebremedhin E., Ugele B., Sabolic I., Burckhardt G., and Y. Hagos. 2005. Murine renal organic anion transporters mOAT1 and mOAT3 facilitate the transport of neuroactive tryptophan metabolites. *Am Jour Physiol Cell Physiol.* 289: C1075-C1084.

Barendt W., and S. Wright. 2002. The human organic cation transporter (hOCT2) recognizes the degree of substrate ionization. *Jour Biol Chem.* 277(25): 22491–22496.

Bednarczyk D., Ekins S., Wikel J., and S. Wright. 2003. Influence of molecular structure on substrate binding to the human organic cation transporter, hOCT1. *Mol Pharmacol*. 63: 489–498.

Bezanilla F. 2008. How membrane proteins sense voltage. *Nat Rev Mol Cell Biol*. 9(4): 323-32.

Burckhardt G., and N. Wolff. 2000. Structure of renal organic anion and cation transporters. *Am Jour Physiol Renal Physiol.* 278: F853–F866.

Busch A., Quester S., Ulzheimer J., Waldegger S., Gorboulev V., Arndt P., Lang F., and H. Koepsell. 1996. Electrogenic properties and substrate specificity of the polyspecific rat cation transporter rOCT1. *Jour Biol Chem*. 271: 32599-32604.

Busch A., Karbach U., Miska D., Gorboulev V., Akhoundova A., Volk C., Arndt P., Ulzheimer J., Sonders M., Baumann C., Waldegger S., Lang F., and H. Koepsell. 1998. Human neurons express the polyspecific cation transporter hOCT2, which translocatesmonoamine neurotransmitters, amantadine, and memantine. *Mol Pharmacol.* 54: 342–352.

Cha A., and F. Bezanilla. 1997. Characterizing voltage-dependent conformational changes in the Shaker K1 channel with fluorescence. *Neuron*. 19: 1127–1140.

Cha A., and F. Bezanilla. 1998. Structural Implications of Fluorescence Quenching in the Shaker K1 Channel. Jour Gen Physiol. 112: 391–408.

Cha A., Zerangue N., Kavanaugh M., and F. Bezanilla. 1998. Fluorescence techniques for studying cloned channels and transporters expressed in Xenopus oocytes. *Methods Enzymol*. 296: 566-578.

Cha S., Sekine T., Fukushima J., Kanai Y., Kobayashi Y., Goya T., H. Endou. 2001. Identification and characterization of human organic anion transporter 3 expressing predominantly in the kidney. *Mol Pharmacol*. 59: 1277–1286.

Chen J., Li Z., Pan H., Murphy D., Tamir H., Koepsell H., and M. Gershon. 2001. Maintenance of serotonin in the intestinal mucosa and ganglia of mice that lack the high-affinity serotonin transporter: abnormal intestinal motility and the expression of cation transporters. *Jour Neurosci*. 21: 6348–6361

Choudhuri S., Cherrington N., Li N., and C. Klaassen. 2003. Constitutive expression of various xenobiotic and endobiotic transporter mRNAs in the choroid plexus of rats. Drug *Metab Dispos*. 31: 1337–1345.

Ciarimboli G., and E. Schlatter. 2005. Regulation of organic cation transport. *Eur Jour Physiol*. 449: 423–441.

M. J. Dresser, A. T. Gray, and K. M. Giacomini. 2000. Kinetic and selectivity differences between rodent, rabbit, and human organic cation transporters (OCT1). *Jour Pharmacol Exp Ther*. 292: 1146–1152.

Duran J., Peral M., Calonge M., and A. Ilundain. 2005. OCTN3: A Na^+-independent L-carnitine transporter in enterocytes basolateral membrane. *Jour Cell Physiol*. 202: 929–935.

Enomoto A., Kimura A., Chairoungdua A., Shigeta Y., Jutabha P., Cha S., Hosoyamada S., Takeda M., Sekine T., Igarashi T., Matsuo H., Kikuchi Y., Oda T., Ichida K., Hosoya T., Shimotaka K., Niwa T., Kanai Y., and H. Endou. 2002a. Molecular identification of a renal urate-anion exchanger that regulates blood urate levels. *Nature*. 417: 447-452.

Enomoto A., Takeda M., Shimoda M., Narikawa S., Kobayashi Y., Yamamoto T., Sekine T., Cha S., Niwa T., and H. Endou. 2002b. Interaction of human organic anion transporters 2 and 4 with organic anion transport inhibitors. *Jour Pharmacol Exp Ther*. 301: 797-802.

Enomoto A., Wempe M., Tsuchida H., Shin H., Cha S., Anzai N., Goto A., Sakamoto A., Niwa T., Kanai Y., Anders M., and H. Endou. 2002. Molecular identification of a novel carnitine transporter specific to human testis: Insights into the mechanism of carnitine recognition. *Jour Biol Chem*. 277(39): 36262-36271.

Eraly S., Hamilton B., and S. Nigam. 2003. Organic anion and cation transporters occur in pairs of similar and similarly expressed genes. *Biochem Biophys Res Commun*. 300: 333–342.

Eraly S., Monte J., and S. Nigam. 2004. Novel slc22 transporter homologs in fly, worm, and human clarify the phylogeny of organic anion and cation transporters. *Physiol Genomics*. 18: 12–24.

Finkelstein A., and O. Pticyn. 2002. in *Protein Physics*, (pp. 13-135). Academic Press.

Gandhi C., Loots E., and E. Isacoff. (2000) Reconstructing voltage sensor-pore interaction from a fluorescence scan of a voltage-gated KC channel. *Neuron* 27: 585–595.

Gandhi C., and E. Isacoff. Shedding light on membrane proteins. 2005. *TRENDS in Neurosciences*. 28(9): 472-479.

Geibel, S., Kaplan, J., Bamberg, E., and T. Friedrich. 2003. Conformational dynamics of the NaK-ATPase probed by voltage clamp fluorometry. *Proc Nat Acad Sci*. 100(3): 964-969.

Gong S., Lu X., Xu Y., Swiderski C., Jordan C., and J. Moscow. 2002. Identification of OCT6 as a novel organic cation transporter preferentially expressed in hematopoietic cells and leukemias. *Exp Hematol.* 30: 1162–1169.

Gorboulev V., Ulzheimer J., Akhoundova A., Ulzheimer-Teuber I., Karbach U., Quester S., Baumann C., Lang F., Busch A., and H. Koepsell. 1997. Cloning and characterization of two human polyspecific organic cation transporters. *DNA Cell Biol.* 16: 871–881.

Gründemann D., Gorboulev V., Gambaryan S., Veyhl M., and H. Koepsell. 1994. Drug excretion mediated by a new prototype of polyspecific transporter. *Nature.* 372: 549–552.

Gründemann D., Schechinger B., Rappold G., and E. Schömig. 1998. Molecular identification of the corticosteronesensitive extraneuronal catecholamine transporter. *Nature Neuroscience.* 1: 349–351.

Gründemann D., Harlfinger S., Golz S., Geerts A., Lazar A., Berkels R., Jung N., Rubbert A., and E. Schömig. 2005. Discovery of the ergothioneine transporter. *Proc Natl Acad Sci.* 102: 5256–5261.

Haag C., Berkels R., Gründemann D., Lazar A., Taubert D., and E. Schömig. 2004. The localisation of the extraneuronal monoamine transporter (EMT) in rat brain. *Jour Neurochem*. 88: 291–297.

Hayer-Zillgen M., Brüss M., and H. Bönisch. 2002. Expression and pharmacological profile of the human organic cation transporters hOCT1, hOCT2 and hOCT3. *Brit Jour Pharmacol*. 136: 829–836.

Ho S., Hunt H., Horton R., Pullen J., and L. Pease. 1989. Site-directed mutagenesis by overlap extension using the polymerase chain reaction. *Gene*. 77: 51-59.

Hong M., Tanaka K., Pan Z., Ma J., and You G. 2007. Determination of the external loops and the cellular orientation of the N- and the C-termini of the human organic anion transporter hOAT1. *Biochem Jour.* 401(2): 515–520.

Hosoyamada M., Ichida K., Enomoto A., Hosoya T., and H. Endou. 2004. Function and localization of urate transporter 1 in mouse kidney. *Jour Am Soc Nephrol.* 15: 261-268.

Huang Y., Lemieux M., Song J., Auer M., D. Wang. 2003. Structure and mechanism of the glycerol-3-phosphate transporter from *Escherichia coli*. *Science*. 301(5633) :616-620.

Inazu M., Takeda H., and T. Matsumiya. 2003. Expression and functional characterization of the extraneuronal monoamine transporter in normal human astrocytes. *Jour Neurochem.* 84: 43–52.

Inazu M., Takeda H., Maehara K., Miyashita K., Tomoda A., and T. Matsumiya. 2006. Functional expression of the organic cation/carnitine transporter 2 in rat astrocytes. *Jour Neurochem.* 97: 424–434.

Jacobsson J., Haitina T., Lindblom J., and R. Fredriksson. 2007. Identification of six putative human transporters with structural similarity to the drug transporter SLC22 family. *Genomics.* 90(5): 595-609.

Javitch A. 1998. Probing structure of neurotransmitter transporters by substituted-cysteine accessibility method. *Methods Enzymol*. 296: 331-346.

Karbach U., Kricke J., Meyer-Wentrup F., Gorboulev V., Volk C., Loffing-Cueni D., Kaissling B., Bachmann S., and H. Koepsell. 2000. Localization of organic cation transporters OCT1 and OCT2 in rat kidney. *Am Jour Physiol Renal Physiol*. 279: F679–F687.

Karlin A., and M. Akabas. 1998. Substituted-cysteine accessibility method. *Methods Enzymol*. 293: 123-145.

Kekuda R., Prasad P., Wu X., Wang H., Fei Y., H. Leibach F., and V. Ganapathy. 1998. Cloning and functional characterization of a potential-sensitive, polyspecific organic cation transporter (OCT3) most abundantly expressed in placenta. *Jour Biol Chem.* 273: 15971–15979.

Keller T., Elfeber M., Gorboulev V., Reiländer H., and H. Koepsell. 2005. Purification and functional reconstitution of the rat organic cation transporter OCT1. *Biochemistry.* 44(36): 12253-12263.

Keller T., Schwarz D., Bernhard F., Dötsch V., Hunte C., Gorboulev V., and H. Koepsell. 2008. Cell free expression and functional reconstitution of eukaryotic drug transporters. *Biochemistry.* 47(15): 4552-4564.

Kimura H., Takeda M., Narikawa S., Enomoto A., Ichida K., and H. Endou. 2002. Human organic anion transporters and human organic cation transporters mediate renal transport of prostaglandins. *Jour Pharmacol Exp Ther.* 301: 293-298

Klein J., Gonzalez R., Köppen A., and K. Löffelholz. 1993. Free choline and choline metabolites in rat brain and body fluids: sensitive determination and implications for choline supply to the brain. *Neurochem Int*. 22(3): 293-300.

Kobayashi Y., Ohshiro N., Sakai R., Ohbayashi M., Kohyama N., and T. Yamamoto. 2005. Transport mechanism and substrate specificity of human organic anion transporter 2 (hOAT2[SLC22A7]). *Jour Pharm Pharmacol*. 57: 573-578.

Koepsell H., Schmitt B., and V. Gorboulev. 2003. Organic cation transporters. *Rev Physiol Biochem Pharmacol*. 150: 36–90.

Koepsell H. 2004. Polyspecific organic cation transporters: their functions and interactions with drugs. *TRENDS in Pharmacological Sciences*. 25(7): 375-381.

Koepsell H., and H. Endou. 2004. The SLC22 drug transporter family. 2004. *Eur Jour Physiol*. 447: 666–676

Koepsell H., Lips K., and C. Volk. 2007. Polyspecific organic cation transporters: structure, function, physiological roles, and biopharmaceutical implications. *Pharmaceutical Research*. 24(7): 1227-1251.

Kojima R., Sekine T., Kawachi M., Cha S., Suzuki Y., and H. Endou. 2002. Immunolocalization of multispecific organic anion transporters, OAT1, OAT2, and OAT3, in rat kidney. *Jour Am Soc Nephrol*. 13: 848-857.

Kristufek D., Rudorfer W., Pifl C., and S. Huck. 2002. Organic cation transporter mRNA and function in the rat superior cervical ganglion. *Jour Physiol.* 543: 117–134.

Kummer W., Wiegand S., Akinci S., Wessler I., Schinkel A., Wess J., Koepsell H., Haberberger R., and Lips K. 2006. Role of acetylcholine and polyspecific cation transporters in serotonin- induced bronchoconstriction in the mouse. *Respir Res.* 7: 65.

Kusuhara H., Sekine T., Utsunomiya-Tate N., Tsuda M., Kojima R., Cha S., Sugiyama Y., Kanai Y., and H. Endou. 1999. Molecular cloning and characterization of a new multispecific organic anion transporter from rat brain. *Jour Biol Chem.* 274: 13675-13680

Kuze K., Graves P., Leahy A., Wilson P., Stuhlmann H., and G. You. 1999. Heterologous expression and functional characterization of a mouse renal organic anion transporter in mammalian cells. *Jour Biol Chem.* 274: 1519-1524.

Läuger P., and P. Jauch. 1986. Microscopic description of voltage effects on ion-driven cotransport systems. Jour Membr Biol. 91: 275-284.

Lemieux M.J. 2007. Eukaryotic major facilitator superfamily transporter modeling based on the prokaryotic GlpT crystal structure. *Mol Memb Biol.* 24(5-6): 333-341.

Li M., Farley R., and H. Lester. 2000. An intermediate state of the γ-aminobutyric acid transporter GAT1 revealed by simultaneous voltage clamp and fluorescence. *Jour Gen Physiol*. 115: 491-508.

Li M., and H. Lester. 2002. Early Fluorescence Signals Detect Transitions at Mammalian Serotonin Transporters. *Biophys Jour.* 83: 206–218.

Lips K., Volk C., Schmitt B., Pfeil U., Arndt P., Miska D., Ermert L., Kummer W., and H. Koepsell. 2005. Polyspecific cation transporters mediate luminal release of acetylcholine from bronchial epithelium. *Am Jour Respir Cell Mol Biol.* 33: 79–88.

Lips K., Wunsch J., Zarghooni S., Bschleipfer T., Schukowski K., Weidner W., Wessler I., Schwantes U., Koepsell H., and W. Kummer. 2007. Acetylcholine and molecular components of its synthesis and release machinery in the urothelium. *Eur. Urol*. 51(4): 1042-1053.

Ljubojevic M., Balen D., Breljak D., Kusan M., Anzai N., Bahn A., Burckhardt G., and I. Sabolic. 2007. Renal expression of organic anion transporter OAT2 in rats and mice is regulated by sex hormones. *Am Jour Physiol Renal Physiol.* 292(1): F361-372.

Mager S., Cao Y., and H. Lester. 1998. Measurements of transient currents from neurotransmitter transporter expressed in Xenopus oocytes. Meth Enzym. 296: 551-566.

Maniatis G., Ramirez F., Cann A., Marks P., and A. Bank. 1976. Translation and stability of human globin mRNA in Xenopus Oocytes. *Journal of Clinical Investigations*. 58: 1419-1427.

Mannuzzu L., Moronne M., and E. Isacoff. 1996. Direct physical measure of conformational rearrangement underlying potassium channel gating. *Science*. 271(5246): 213-216.

Moaddel R., Ravichandran S., Bighi F., Yamaguchi R., and I. Wainer. 2007. Pharmacophore modelling of stereoselective binding to the human organic cation transporter (hOCT1). *Br Jour Pharmacol*. 151(8): 1305-1314.

Motohashi H., Sakurai Y., Saito H., Masuda S., Urakami Y., Goto M., Fukatsu A., Ogawa O., and K. Inui. 2002. Gene expression levels and immunolocalization of organic ion transporters in human kidney. *Jour Am Soc Nephrol*. 13: 866-874.

Müller J., Lips K., Metzner L., Neubert R., Koepsell H., and M. Brandsch. 2005. Drug specificity and intestinal membrane localization of human organic cation transporters (OCT). *Biochem Pharmacol*. 70: 1851–1860.

Meyer-Wentrup F., Karbach U., Gorboulev V., Arndt P., and H. Koepsell. 1998. Membrane localization of the electrogenic cation transporter rOCT1 in rat liver. *Biochem Biophys Res Commun*. 248: 673–678.

Motulsky H.J. 2003. in *Prism4 Statistics Guide – Statistical analyses for laboratory and clinical researchers*, pp. 40-88. GraphPad Software Inc., San Diego, CA, (www.graphpad.com)

Nagel G., Volk C., Friedrich T., Ulzheimer J., Bamberg E., and H. Koepsell. 1997. A reevaluation of substrate specificity of the rat cation transporter rOCT1. *Jour Biol Chem*. 272(51): 31953–31956.

Nigam S., Bush K., V. Bhatnagar. 2007. Drug and toxicant handling by the OAT organic anion transporters in the kidney and other tissues. *Nat Clin Pract Nephrol.* 3(8): 443-8.

Okuda M., Saito H., Urakami Y., Takano M., and K. Inui. 1996. cDNA cloning and functional expression of a novel rat kidney organic cation transporter, OCT2. *Biochem Biophys Res Commun.* 224: 500–507.

Okuda M., Urakami Y., Saito H., and K. Inui. 1999. Molecular mechanisms of organic cation transport in OCT2-expressing Xenopus oocytes. *Biochim Biophys Acta.* 1417: 224–231.

Pao S., Paulsen I., and M. Saier Jr. 1998. Major facilitator superfamily. *Microbiol Mol Biol Rev.* 62: 1–34.

Pelis R., Suhre W., Wright S.. Functional influence of N-glycosylation in OCT2-mediated tetraethylammonium transport. 2006a. *Am Jour Physiol Renal Physiol*. 290(5): F1118-26

Pelis R., Zhang X., Dangprapai Y., and S. Wright. 2006b. Cysteine accessibility in the hydrophilic cleft of human organic cation transporter 2. *Jour Biol Chem*. 281: 35272-35280.

Pelis R., Dangprapai Y., Wunz T., and S. Wright. 2007. Inorganic mercury interacts with cysteine residues (C451 and C474) of hOCT2 to reduce its transport activity. *Am J Physiol Renal Physiol*. 292(5): F1583-1591.

Peltekova V., Wintle R., Rubin L., Amos C., Huang Q., Gu X., Newman B., Van Oene M., Cescon D., Greenberg G., Griffiths A., George-Hyslop P., and K. Siminovitch. 2004. Functional variants of OCTN cation transporter genes are associated with Crohn disease. *Nature Genetics.* 36: 471–475.

Perry J., Dembla-Rajpal N., Hall L., and J. Pritchard. 2006. A Three-dimensional model of human organic anion transporter 1: aromatic amino acids required for substrate transport. *Jour Biol Chem*. 281(49): 38071-38079.

Rizwan A., Krick W., G. Burckhardt. 2007. The chloride dependence of the human organic anion transporter 1 (hOAT1) is blunted by mutation of a single amino acid. *Jour Biol Chem*. 282(18): 13402-13209.

Rizwan A., and G. Burckhardt. 2007. Organic anion transporters of the SLC22 Family: biopharmaceutical, physiological, and pathological roles. *Pharmaceutical Research*. 24(3): 450-470.

Saier M., Jr. 2000. A functional-phylogenetic classification system for transmembrane solute transporters. *Microbiol Mol Biol Rev.* 64(2): 354–411.

Sata R., Ohtani H., Tsujimoto M., Murakami H., Koyabu N., Nakamura T., Uchiumi T., Kuwano M., Nagata H., Tsukimori K., Nakano H., and Y. Sawada. 2005. Functional analysis of organic cation transporter 3 expressed in human placenta. *Jour Pharmacol Exp Ther*. 315: 888–895.

Schinkel A., and J. Jonker. 2003. Mammalian drug efflux transporters of the ATP binding cassette (ABC) family: an overview. *Adv Drug Deliv Rev.* 55: 3–29.

Schmitt B., and H. Koepsell. 2002. An improved method for real-time monitoring of membrane capacitance in Xenopus laevis oocytes. *Biophys Jour*. 82: 1345–1357.

Schmitt B., and H. Koepsell. 2005. Alkali cation binding and permeation in the rat organic cation transporter rOCT2. *Jour Biol Chem.* 280(26): 24481–24490.

Schneider E., Machavoine F., Pleau J., Bertron A., Thurmond R., Ohtsu H., Watanabe T., Schinkel A., and M. Dy. 2005. Organic cation transporter 3 modulates murine basophil functions by controlling intracellular histamine levels. *Jour Exp Med*. 202: 387–393.

Schömig E., Lazar A., and D. Gründemann. 2006. Extraneuronal monoamine transporter and organic cation transporters 1 and 2: a review of transport efficiency. *Handb Exp Pharmacol.* 175:151-80.

Seithel A., Karlsson J., Hilgendorf C., Björquist A., and A. Ungell. 2006. Variability in mRNA expression of ABC- and SLC transportersin human intestinal cells: comparison between human segments and Caco-2 cells. *Eur Jour Pharm Sci*. 28: 291–299.

Sekine T., Watanabe N., Hosoyamada M., Kanai Y., and H. Endou. 1997. Expression cloning and characterization of a novel multispecific organic anion transporter. *Jour Biol Chem.* 272: 18526-18529.

Sekine T., Cha S., Tsuda M., Apiwattanakul N., Nakajima N., Kanai Y., and H. Endou. 1998. Identification of multispecific organic anion transporter 2 expressed predominantly in the liver. *FEBS Lett*. 429: 179-182.

Sekine T., Miyazaki H., and H. Endou. 2006. Molecular physiology of renal organic anion transporters. *Am Jour Physiol Renal Physiol*. 290(2): F251-F261.

Shang T., Uihlein A., van Asten J., Kalyanaraman B., and C. Hillard. 2003. 1-Methyl-4-phenylpyridinium accumulates in cerebellar granule neurons via organic cation transporter 3. *Jour Neurochem.* 85: 358–367.

Sigal N., Lewinson O., Wolf S., and E. Bibi. 2007. E. coli multidrug transporter MdfA is a monomer. Biochemistry. 46(17): 5200-5208.

Slitt A., Cherrington N., Hartley D., Leazer T., and C. Klaassen. 2002. Tissue distribution and renal developmental changes in rat organic cation transporter mRNA levels. *Drug Metab Dispos*. 30: 212–219.

Stauffer D., and A. Karlin. 1994. Electrostatic potential of the acetylcholine binding sites in the nicotinic receptor probed by reactions of binding-site cysteines with charged methanethiosulfonates. *Biochemistry.* 33(22): 6840-6849.

Sturm A., Gorboulev V., Gorbunov D., Keller T., Volk C., Schmitt B., Schlachtbauer P., Ciarimboli G., and H. Koepsell. 2007. Identification of cysteines in rat organic cation transporters rOCT1 (C322, C451) and rOCT2 (C451) critical for transport activity and substrate affinity. *Am Jour Physiol Renal Physiol*. 293: F767-F779.

Suhre W., Ekins S., Chang C., Swaan P., and S. Wright. 2005. Molecular determinants of substrate/inhibitor binding to the human and rabbit renal organic cation transporters hOCT2 and rbOCT2. *Mol Pharmacol*. 67:1067–1077.

Sugawara-Yokoo M., Urakami Y., Koyama H., Fujikura K., Masuda S., Saito H., Naruse T., Inui K., and K. Takata. 2000. Differential localization of organic cation transporters rOCT1 and rOCT2 in the basolateral membrane of rat kidney proximal tubules. *Histochem Cell Biol.* 114: 175–180.

Sun W., Wu R., van Poelje P., and M. Erion. Isolation of a family of organic anion transporters from human liver and kidney. 2001. *Biochem Biophys Res Commun.* 283: 417–422.

Sweet D., Miller D., and J. Pritchard. 2001. Ventricular choline transport: a role for organic cation transporter 2 expressed in choroid plexus. *Jour Biol Chem.* 276: 41611–41619.

Sweet D., Chan L., Walden R., Yang X., Miller D., and J. Pritchard. 2003. Organic anion transporter 3 [Slc22a8] is a dicarboxylate exchanger indirectly coupled to the Na^+ gradient. *Am Jour Physiol Renal Physiol*. 284: F763-F769.

Tamai I., Yabuuchi H., Nezu J., Sai Y., Oku A., Shimane M., and A. Tsuji. 1997. Cloning and characterization of a novel human pH-dependent organic cation transporter, OCTN1. *FEBS Lett.* 419: 107–111.

Tamai I., Ohashi R., Nezu J., Yabuuchi H., Oku A., Shimane M., Sai Y., and A. Tsuji. 1998. Molecular and functional identification of sodium ion-dependent, high affinity human carnitine transporter OCTN2. *Jour Biol Chem.* 273(32): 20378–20382.

Tamai I., Ohashi R., Nezu J., Sai Y., Kobayashi D., Oku A., Shimane M., and A. Tsuji. 2000. Molecular and functional characterization of organic cation/carnitine transporter family in mice. *Jour Biol Chem*. 275(51): 40064-40072.

Tamai I., China K., Sai Y., Kobayashi D.,. Nezu J., Kawahara E., and A. Tsuji. 2001. Na^+-coupled transport of L-carnitine via high-affinity carnitine transporter OCTN2 and its subcellular localization in kidney. *Biochim Biophys Acta*. 1512: 273–28.

Tamai I., Nakanishi T., Kobayashi D., China K., Kosugi Y., Nezu J., Sai Y., and A. Tsuji. 2004. Involvement of OCTN1 (SLC22A4) in pH-dependent transport of organic cations. *Mol. Pharacol.* 1: 57–66.

Tanaka K., Xu W., Zhou F., and G. You. 2004. Role of glycosylation in the organic anion transporter OAT1. *Jour Biol Chem*. 279(15): 14961–14966.

Taubert D., Grimberg G., Stenzel W., and E. Schömig E. 2007. Identification of the endogenous key substrates of the human organic cation transporter OCT2 and their implication in function of dopaminergic neurons. PLoS ONE 2(4): e385. doi:10.1371/journal.pone.0000385.

Taylor M., and D. Smith. 1985. Quantitative changes in protein synthesis during oogenesis in Xenopus laevis. *Developmental Biology*. 110: 230-237.

Taylor M., Johnson A., and D. Smith. 1985. Growing Xenopus oocytes have spare translational capacity. *Proc Nat Acad Sci*. 82: 6586-6589.

Terada T., Shimada Y., Pan X., Kishimoto K., Sakurai T., Doi R., Onodera H., Katsura T., Imamura M., and K. Inui. 2005. Expression profiles of various transporters for oligopeptides, amino acids and organic ions along the human digestive tract. *Biochem Pharmacol*. 70: 1756–1763.

Ugele B., St-Pierre M., Pihusch M., Bahn A., and P. Hantschmann. 2003. Characterization and identification of steroid sulfate transporters in human placenta. *Am Jour Physiol Endocrinol Metab.* 284: E390-E398.

Urakami Y., Akazawa M., Saito H., Okuda M., Inui K. 2002. cDNA cloning, functional characterization, and tissue distribution of an alternatively spliced variant of organic cation transporter hOCT2 predominantly expressed in the human kidney. *Jour Am Soc Nephrol.* 13: 1703–1710.

Vardy E., Arkin I., Gottschalk K., Kaback H., and S. Schuldiner. 2004. Structural conservation in the major facilitator superfamily as revealed by comparative modeling. *Protein Sci*. 13: 1832–1840.

Vialou V., Amphoux A., Zwart R., Giros B., and S. Gautron. 2004. Organic cation transporter 3 (Slc22a3) is implicated in salt intake regulation. *Jour Neurosci*. 24: 2846–2851.

Wagner C., Friedrich B., Setiawan I., Lang F., and S. Bröer. 2000. The use of xenopus laevis oocytes for the functional characterization of heterologously expressed membrane proteins. *Cellular Physiology and Biochemistry*. 10: 1-12.

Wallace D. 1987. Large- and small-scale phenol extractions. *Methods Enzymol.* 152: 33-41.

Webber W. 1999. Ion currents of *Xenopus laevis* oocytes: state of the art. *Biochim Biophys Acta.* 1421: 213-233.

Wolff N., Thies K., Kuhnke N., Reid G., Fiedrich B., Lang F., and G. Burckhard. 2003. Protein kinase C activation downregulates human organic anion transporter 1-mediated transport through carrier internalization. *Jour Am Soc Nephrol*. 14: 1959–1968.

Wright S., and Dantzler W. 2004. Molecular and cellular physiology of renal organic cation and anion transport. *Physiol Rev.* 84: 987–1049.

Wright S. 2005. Role of organic cation transporters in the renal handling of therapeutic agents and xenobiotics. *Toxicology and Applied Pharmacology.* 204: 309– 319.

Wu X., Prasad P., Leibach F., and V. Ganapathy. 1998a. cDNA sequence, transport function, and genomic organization of human OCTN2, a new member of the organic cation transporter family. *Biochem Biophys Res Commun*. 246: 589–595.

Wu X., Kekuda R., Huang W., Fei Y., Leibach F., Chen J., Conway S., and V. Ganapathy. 1998b. Identity of the organic cation transporter OCT3 as the extraneuronal monoamine transporter (uptake2) and evidence for the expression of the transporter in the brain. *Jour Biol Chem.* 273: 32776–32786

Wu X., Huang W., Ganapathy M., Wang H., Kekuda R., Conway S., Leibach F., and V. Ganapathy. 2000. Structure, function, and regional distribution of the organic cation transporter OCT3 in the kidney. *Am Jour Physiol Renal Physiol*. 279: F449–F458.

Xuan W., Lamhonwah A., Librach C., Jarvi K., and I. Tein. 2003. Characterization of organic cation/carnitine transporter family in human sperm. *Biochem Biophys Res Commun.* 306: 121– 128.

Zhang L., Dresser M., Chun J., Babbitt P., and K. Giacomini. 1997. Cloning and functional characterization of a rat renal organic cation transporter isoform (rOCT1A). *Jour Biol Chem.* 272: 16548–16554.

Zhang X., Shirahatti N., Mahadevan D., and S Wright. 2005. A conserved glutamate residue in transmembrane helix 10 influences substrate specificity of rabbit OCT2 (SLC22A2). *Jour Biol Chem.* 280(41): 34813–34822.

Yakushiji K., Kai S., Yamauchi M., Kuwajima M., Osada Y., and K. Toshimori. 2006. Expression and distribution of OCTN2 in mouse epididymis and its association with obstructive azoospermia in juvenile visceral steatosis mice. *Int Jour Urol*. 13: 420–426.

Yin Y., He X., Szewczyk P., Nguyen T., and G. Chang. 2006. Structure of the multidrug transporter EmrD from *Escherichia coli*. *Science*. 312: 741-744.

Youngblood G., and D. Sweet. 2004. Identification and functional assessment of the novel murine organic anion transporter Oat5 (Slc22a19) expressed in kidney. *Am Jour Physiol Renal Physiol*. 287: F236–F244.

Zhang L., Dresser M., Gray A., Yost S., Terashita S., and K. Giacomini. 1997. Cloning and functional expression of a human liver organic cation transporter. *Mol Pharmacol*. 51: 913–921.

Zhou F., Xu W., Hong M., Pan Z., Sinko P., Ma J., and G. You. 2005. The role of N-linked glycosylation in protein folding, membrane targeting, and substrate binding of human organic anion transporter hOAT4. *Mol Pharmacol.* 67(3): 868–876.

Zhou F., and G. You. 2007. Molecular Insights into the structure-function relationship of organic anion transporters OATs. *Pharmaceutical Research*. 24(1): 28-36.

Zwart R., Verhaagh S., Buitelaar M., Popp-Snijders C., and D. Barlow. 2001. Impaired activity of the extraneuronal monoamine transporter system known as uptake-2 in Orct3/Slc22a3-deficient mice. *Mol Cell Biol.* 21(13): 4188-4196